Bulletin
of
The Geological Society of America

VOLUME 70 January 1959 NUMBER 1

CONTENTS

Pages

Athabasca formation of western Canada. By William Carruthers Gussow 1-18

Analytical and experimental study of simple geologic structures. By Allan R. Sanford 19-52

Hydrothermal alteration in the Front Range mineral belt, Colorado. By Félix González Bonorino 53-90

Geometry of superposed folding. By L. E. Weiss 91-106

Short Notes

Faulted Rundle (Mississippian) section at Crowsnest Pass, Alberta, Canada. By Samuel J. Nelson 107-110

Age of the samarskite of Kishengarh, Rajasthan, India. By U. Aswathanarayana 111-114

Subscription $15.00 per year.

Printing Office: Mt. Royal & Guilford Aves., Baltimore 2, Md.

Communications for publications should be addressed to The Geological Society of America, Dr. H. R. Aldrich, Secretary, 419 West 117 Street, New York, N. Y.

Please give notice of change of address 4 weeks in advance. Claims for nonreceipt of the Bulletin of a given month must be sent to the Secretary of the Society before the end of the second succeeding month.

Second-class Postage paid at Baltimore, Md.
Accepted for mailing at special rate of postage provided for in Section 1103
Act of October 3, 1917, authorized on July 8, 1918.

PAPERS IN PRESS FOR FORTHCOMING ISSUES

LATE DEVONIAN UNCONFORMITY IN CENTRAL UTAH. By J. Keith Rigby

DETERMINATION OF CRUSTAL STRUCTURE FROM PHASE VELOCITY OF RAYLEIGH WAVES. By Maurice Ewing and Frank Press

GEOPHYSICAL INVESTIGATION OF THE CONTINENTAL MARGIN BETWEEN CAPE HENRY, VIRGINIA, AND JACKSONVILLE, FLORIDA. By J. B. Hersey *et al.*

TURBIDITY-CURRENT DEPOSITS IN SAN PEDRO AND SANTA MONICA BASINS OFF SOUTHERN CALIFORNIA. By Donn S. Gorsline and K. O. Emery

ROLE OF FLUID PRESSURE IN MECHANICS OF OVERTHRUST FAULTING

I. Mechanics of fluid-filled porous solids and its application to overthrust faulting. By M. King Hubbert and William W. Rubey

II. Overthrust belt in geosynclinal area of western Wyoming in light of fluid-pressure hypothesis. By William W. Rubey and M. King Hubbert

(Separates of this paper will be available at $1.25 per copy. Send orders and remittance to The Geological Society of America, 419 West 117 St., New York 27, N. Y.

BULLETIN OF THE GEOLOGICAL SOCIETY OF AMERICA
VOL. 70, PP. 1-18, 7 FIGS. JANUARY 1959

2037
8818

ATHABASCA FORMATION OF WESTERN CANADA

BY WILLIAM CARRUTHERS GUSSOW

ABSTRACT

Geological reports over the past 50 years have so confused the age designation of the Athabasca formation that logic has been abandoned even in the face of new evidence that the current Precambrian designation is untenable.

The absolute age of the Athabasca formation cannot be fixed without fossil evidence. Herein, it is tentatively assigned to the Middle Devonian? or Late Cambrian? on the basis of structural relationships and lithologic characteristics, with full awareness of the risk involved in such a practice. The name Martin Lake series is here introduced for the ancient folded and faulted sedimentary-volcanic rocks of the Martin Lake area, which have been erroneously correlated with the Athabasca formation. Recent dating indicates that they are late Early Precambrian and are much older than the "Late Proterozoic" to which they have been assigned.

This is an example of the need for a revision of the Precambrian time classification and the abandonment of terms such as Proterozoic, Algonkian, and Archean, which are carry-overs from the old concept of a twofold subdivision of the Precambrian—now known to be at least five to six times as long as the fossil record.

CONTENTS

TEXT

	Page
Introduction	1
Acknowledgments	3
Regional setting	3
Investigations since 1917	5
Martin Lake series and Athabasca formation redefined	7
Martin Lake series	7
Athabasca formation	10
Sub-Athabasca unconformity	12
Diabase dikes	13
Correlation of the Athabasca formation	13
General statement	13
Basal Cambrian	13
Basal Ordovician	15
Basal Devonian	15
Conclusions	17
Economic geology	17
References cited	17

ILLUSTRATIONS

Figure	Page
1. Index map, Lake Athabasca area	2
2. Map of the east end of Lake Athabasca and Fond du Lac	3
3. Distribution of Athabasca formation and Martin Lake series and outcrop area of Trout Lake dolomite	4
4. Geology of Martin Lake series type area	8
5. North Shore distribution of Athabasca formation and Martin Lake series	9
6. Photogeologic map of Trout Lake area, Saskatchewan	11
7. Cross sections showing structural relationships of Athabasca formation, Martin Lake series, and Middle Devonian of the Interior Plains; and the Precambrian basement complex	14

TABLE

	Page
1. Tentative revised table of formations for northern Saskatchewan	16

INTRODUCTION

The extensive flat-lying sandstone along the south shore of Lake Athabasca[1] (Fig. 1) was first described by McConnell (1893). He referred to it as the "Athabasca Sandstone" and designated it as Cambrian. Dowling and Tyrrell (*in* Tyrrell, 1897) concurred with McConnell's age classification but correlated the Athabasca sandstone with the Keweenawan, which at that time was also considered to be Cambrian. In 1914, McInnes placed the Athabasca sandstone

[1] Athabasca is both the original and the recently revised spelling; Athabaska is now obsolete.

in the Upper Huronian. However, in 1915, when his map was published, the Athabasca sandstone was indicated as Keweenawan(?) and considered to be Precambrian(?). Camsell (1915) and Alcock (1915; 1917) followed McInnes and placed the Athabasca sandstone in the Keweenawan(?). Since then it has been referred to the Precambrian, not, however, without question. J. B. Mawdsley (1949) and Blake (1956) attempted to determine its age but were unable to find fossils, so it retained its Precambrian designation.

Reasons for this Precambrian classification are the apparent absence of fossils from the Athabasca formation and the miscorrelation of these flat-lying sandstones with a thick series of tightly folded and deformed Precambrian sandstones and volcanic rocks in the area of Beaverlodge Lake, and the correlation of these with "Proterozoic" rocks at Great Slave Lake, Dubawnt Lake, and Baker Lake (Fig. 1). To avoid further ambiguity, the Precambrian conglomerate-sandstone-volcanic rock series in the Beaverlodge area is here renamed the

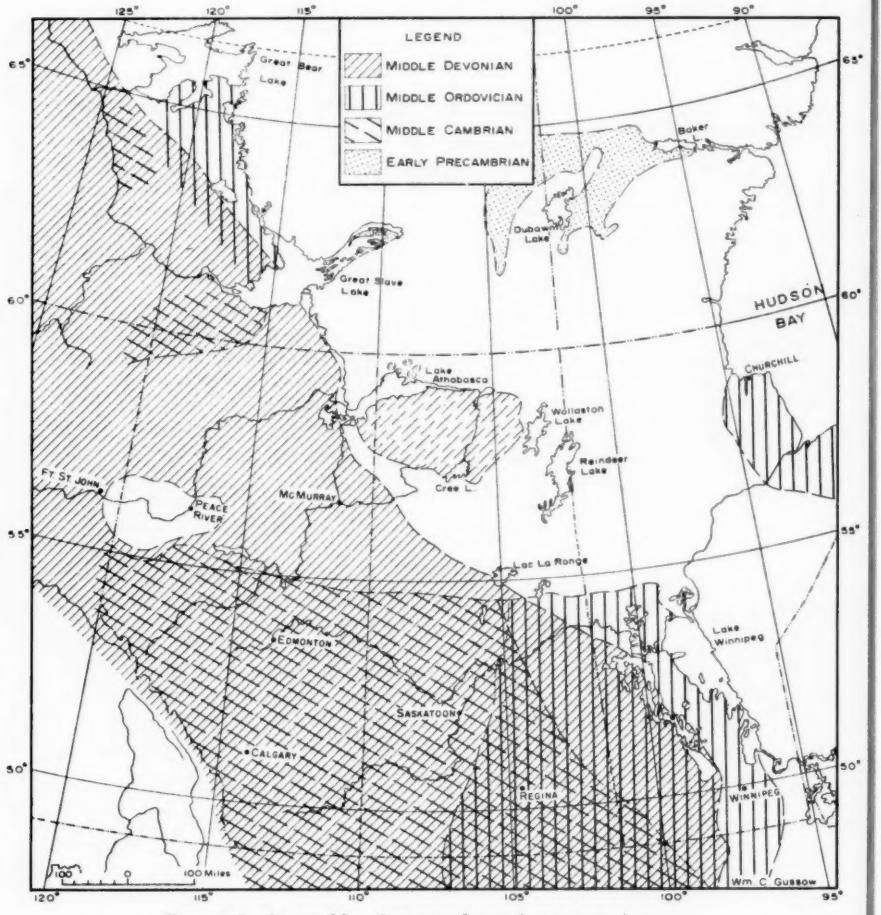

FIGURE 1.—INDEX MAP SHOWING LAKE ATHABASCA AREA

Regional distribution of the Athabasca formation and the Cambrian, Ordovician, and Middle Devonian basal sandstones is indicated. Map base traced from Geological Survey of Canada Map 1045A. Geology compiled from published and unpublished sources.

Martin Lake series after the type locality at Martin Lake. The name Athabasca formation is retained for the flat-lying strata south of Lake Athabasca, which were originally named the "Athabasca Sandstone" by McConnell.

preciation is also expressed to R. T. D. Wickenden, C. K. Bell, B. C. MacDonald, J. S. Kermeen, and K. D. Hannigan for their interest. Grateful acknowledgment is made to J. B. Mawdsley for arranging for the loan of aerial photographs of the Trout Lake area. J. B. Mawdsley and P. S. Warren kindly read the manuscript and offered valuable suggestions. Editorial comments by F. J. Alcock and J. C. Sproule are gratefully acknowledged.

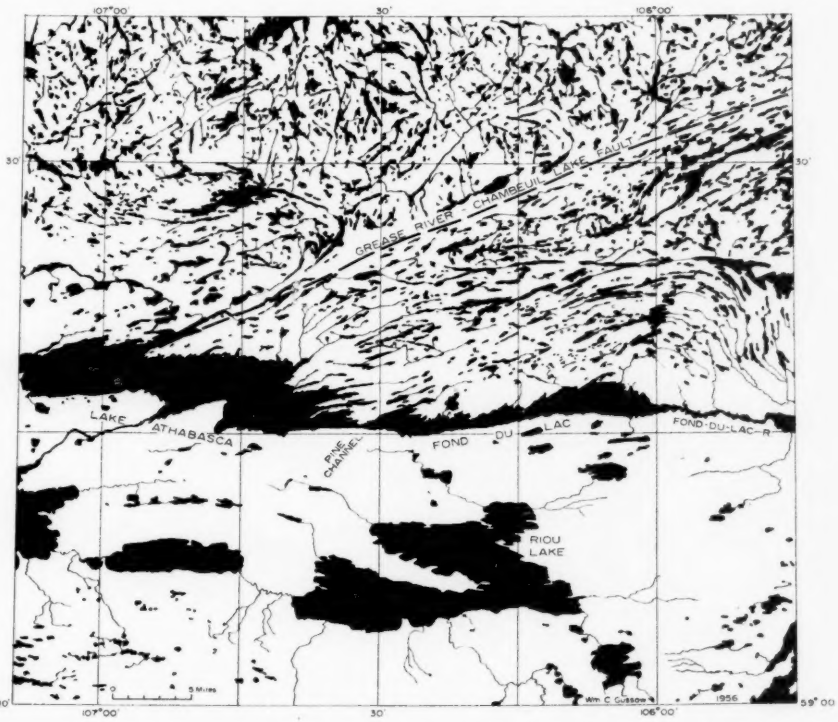

FIGURE 2.—MAP OF THE EAST END OF LAKE ATHABASCA AND FOND DU LAC

Map shows the contrasting topography of the folded Precambrian of the north shore and the flat-lying Athabasca formation of the south shore. Traced from Geological Survey of Canada Maps 364A and 365A (Alcock, 1936).

The present author questions the Precambrian age of the Athabasca formation and attempts to re-evaluate the published data. The results of this study were presented in the discussion of a paper by I. C. Brown and G. M. Wright in a symposium on "The Proterozoic in Canada" (Gill, 1957). A short preliminary outline by Gussow was published in 1957.

ACKNOWLEDGMENTS

The writer expresses his sincere thanks to D. A. W. Blake and Mrs. Blake for making available unpublished photographs, original field notes, and thin sections of rock samples.

REGIONAL SETTING

The original Athabasca sandstone area is bounded on the north by Lake Athabasca, Fond du Lac, Fond-du-Lac River, and Black Lake. The first base maps of the region made from aerial photographs show that the sandstones of the south shore are essentially flat-lying, whereas the topography of the north shore indi-

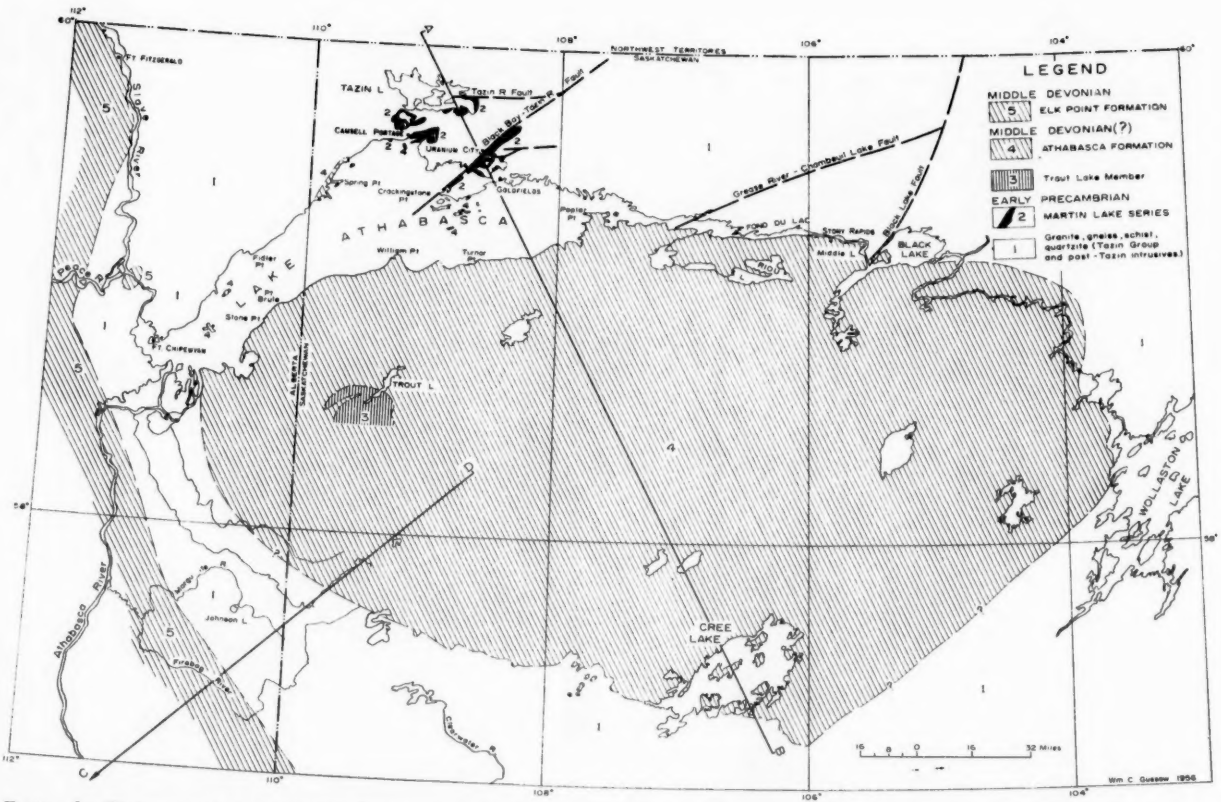

FIGURE 3.—DISTRIBUTION OF ATHABASCA FORMATION AND MARTIN LAKE SERIES, AND OUTCROP AREA OF THE TROUT LAKE DOLOMITE MEMBER

Also indicated are the approximate east edge of the Middle Devonian strata of the Interior Plains; location of cross sections; and some of the post-Martin Lake, pre-Athabasca master faults. Map base traced from Geological Survey of Canada Preliminary Map 55-33 (Blake, 1956). Geology reinterpreted from all available published maps and reports and from unpublished information.

Also indicated are the approximate east edge of the Middle Devonian strata of the Interior Plains; location of cross sections; and some of the post-Martin Lake, pre-Athabasca master faults. Map base traced from Geological Survey of Canada Preliminary Map 55-33 (Blake, 1956). Geology reinterpreted from all available published maps and reports and from unpublished information.

cates the highly folded and contorted nature of the Precambrian rocks there (Fig. 2). This sharply contrasting topography indicates a major angular discordance between the flat-lying rocks of the Athabasca formation and the highly folded, contorted, thrust-faulted, and metamorphosed rocks of the Churchill georogen.[2] Alcock's larger-scale maps (1936) further emphasize this striking difference. The absence of major thrust faults from the highly contorted Precambrian area—an area which seems to have undergone mountain building—induced the author in 1936 to re-study these maps, with the result that a well-defined northeast fault, the Black Bay-Tazin River master fault (northwest side up) along the southeast shore of Black Bay and extending northeast beyond the Tazin Lake Sheet (Map 363A) and across the northwest corner of the Fond-du-Lac Sheet (Map 364A) became apparent. In addition, the east-west Tazin River fault, the Mickey Lake (Tom) fault, and the St. Mary's Channel (Gunnar) fault across the Crackingstone Peninsula were recognized. In the eastern part of the north-shore region, the Grease River-Chambeuil Lake and the Black Lake master faults were postulated (Fig. 3).

These observations indicate that all the formations of the north shore, including the youngest so-called Athabasca series of the Martin Lake and Tazin Lake areas are of pre-fault age.

No structural trends are apparent in the flat-lying formations of the south shore. Along the narrow east arm of Lake Athabasca, Pine Channel, Fond du Lac, and Fond-du-Lac River, the deformed rocks of the north shore terminate abruptly against the flay-lying strata of the south shore (Fig. 2). This angular discordance represents a profound unconformity and indicates that the Athabasca formation of the south shore is post-faulting and post-deformation and very much younger than the contorted Precambrian formations of the north shore. The Tectonic Map of Canada (Derry, 1950)[3] and the new Geologic Map of Canada (1955) show the same unconformable relationships along the southern contact of the Athabasca sandstone area.

Investigations Since 1917

Alcock (1936) carried out a detailed reconnaissance of the north shore and initiated a geological mapping program which has continued ever since. He named and subdivided the Precambrian formations and established a pattern for the work that followed. The Athabasca formation was correlated with the Martin Lake series, although evidence to the contrary had been published at the time. Both were placed in the Proterozoic and assigned to the Keweenawan.

Sproule, mapping the southern margin of the Athabasca formation in the Cree Lake area (Fig. 3), described it as "probably of Palaeozoic age" (1938b), and in 1941 he described it as "early Palaeozoic age" on preliminary maps, but on his final maps it is designated as Late Precambrian, Proterozoic (?)[4], and the marginal notes state it may be Paleozoic. Tyrrell's (1897) diabase dike is again shown on the final maps as cutting the Athabasca sandstone on Diabase Peninsula, on the west side of Cree Lake (but with a north-south strike), although this was not shown on Sproule's preliminary map. The later Geological Survey maps of Saskatchewan (1947) and Alberta (1951) retained the Precambrian designation for the Athabasca formation and assigned it to the Proterozoic. The Geological Map of Canada (1955) assigned it to the Late Proterozoic.

Furnival (1940; 1941a; 1941b), mapping in the extreme northeast corner of the Athabasca sandstone area followed Alcock (1936) in correlation and dating. However, he did not mention any basalt flows or dikes in the Athabasca formation.

During the past 8 years, a new series of 1-mile maps has been published by the Geological Survey of Canada. Christie (1949; 1953) mapped both the Athabasca formation and the Martin Lake series as Precambrian, although abundant structural evidence casts serious doubt on the validity of this assumption.

J. B. Mawdsley (1949; 1956) searched for fossils in the sandstone in the vicinity of Pine Channel (Fig. 2) without success. He observed that "... it rests with profound unconformity

[2] Rice (1949, p. 283) defines an orogen as "... a regional unit involved in mountain-making." A georogen is considered herein to be a tectonic unit of continental proportions.

[3] The Tectonic Map of Canada shows a series of northeast-trending faults in the Athabasca formation south of Black Lake. There is no known evidence for these, and nothing in the topography suggests their presence. Furthermore, it is stated on the map that the sandstones in this area are "... intruded by basic sills." There is no justification for this statement, and this appears to be an erroneous belief that has become firmly established.

[4] Sproule (personal communication, 1958) advised the writer that this was an editorial change made without his concurrence.

on a surface of ancient, probably Archaean rocks" (1949, p. 22).

Age determinations (Collins and Freeman, 1951) on uranium minerals from veins which cut the Martin Lake series indicated that these rocks are older than 1680 million years[5], and as a consequence the rocks of the type area of the Athabasca formation were dated as late Early Precambrian.

Nevertheless Fraser (1954) placed the Athabasca in the Proterozoic. He differentiated as to lithology but not as to age, although rocks of two definite ages can be easily separated on his maps.

Hale, in his Black Bay Map (1954a), also placed the "Athabasca Series" in the Proterozoic but dated it as pre-diabase. The rocks mapped as "Athabasca Series" are undoubtedly equivalents of the Martin Lake series and accordingly are Early Precambrian. No true Athabasca formation is present in the Black Bay map area. Hale (1954b; 1955) differentiated between an Upper and Lower part in the "Athabasca Series"; these are separated by an angular unconformity. Although he noted the fresh appearance of the Upper Part, he placed both in the Late Precambrian (Proterozoic). Now, however, he indicates that the age of the diabase relative to the Upper Part is uncertain (1954b). From his maps and descriptions, it is obvious that both the Martin Lake series and the Athabasca formation are represented.

J. C. Mawdsley (1954, B.Sc. thesis, Univ. Alberta) made a mineralogic study of the Athabasca sandstone and observed that the Martin Lake series has been correlated with the Athabasca formation

> "... in spite of the lack of any lithologic basis for such a correlation. The two types of rock were quite obviously deposited under very different environments."

Mawdsley found a remarkably small percentage of heavy minerals in the Athabasca sandstone and identified minor amounts of tourmaline, zircon, and rutile, and traces of magnetite and garnet. On the basis of optically oriented authigenic tourmaline, he concluded that the Athabasca sandstone must be marine.

In 1952, Blake undertook a reconnaissance of the whole area. He made the startling discovery of, and described, the Trout Lake dolomite member, 40 miles south of Lake Athabasca (Fig. 3). In addition, he recorded valuable data and collected many specimens. Ill health prevented publication of his preliminary report until late in 1956; it represents an interpretation of his field notes. Blake came closest to a clear understanding of the age of this interesting formation, and given an opportunity to thoroughly review the literature in the light of his field discoveries, he probably would have solved the many difficult field problems. With the help of Blake's field notes and photographs of outcrops, the loan of thin sections, and the present author's own field experience, the author is taking the liberty of reinterpreting the evidence which Blake collected.

Blake described "folding" at four widely separated localities. The dips east of Turnor Point, and south of Riou Lake, and along Fond-du-Lac River east of Black Lake are probably cross-bedding and foreset beds. Alcock (1936, Pl. VII B) shows a similar occurrence south of Fond-du-Lac River. The locality described by Blake on Fir Island, however, suggests that these quartzites belong to the basement rocks and are Tazin series? Blake states that "... in no other part of the sandstone area have dips of more than a few degrees been observed ..." (1956, p. 8). He also states that "... no faults have been noted in the main area of the Athabasca formation" (1956, p. 8).

Hale (1954b) mapped a series of dips in the Athabasca (?) formation on Charlot Peninsula and along the shore south of the mouth of Charlot River. In all probability, these represent depositional dips or are foreset beds. At all places the Athabasca formation appears to be flat-lying or with low depositional dips.

Blake observed that

> "... the rocks north and south of the lake [Athabasca] differ lithologically in many respects and have apparently formed under different conditions. Rocks south of the lake are composed almost entirely of well-rounded quartz grains. With few exceptions, conglomerate beds and feldspar grains are virtually absent and the red color so prevalent north of the lake is lacking. These facts indicate that the sediments have been transported a great distance and deposited on a broad, nearly level surface, and suggest that the correlation is unwarranted" (1956, p. 9).

In spite of this, he attributed the difference to a transition from the arkosic type north of the lake to the feldspar-free sandstones south of the lake.

[5] More recent work by Eckelmann and Kulp (1956) concludes that the time of initial uranium deposition was about 1900 ± 20 m.y. ago. The validity of absolute age based on pitchblende, however, is apparently still open to question.

Alcock recently made the same observation (personal communication, 1956) and concluded that there is no reason for correlating the two rock groups.

During 1952, 1953, 1954, and 1955, Tremblay (1955; 1957a; 1957b) mapped the Martin Lake type area and vicinity. On four of his five preliminary map sheets (scale, 1 inch to 800 feet), the Martin Lake series is referred to as the "Athabasca Series" and is called Proterozoic.

A swarm of gabbro dikes and sills which cut the pre-Martin Lake complex northwest of the Black Bay-Tazin River master fault is shown as post-Martin Lake (post-Athabasca by Tremblay's terminology) in age because at two places in the southwest corner of the map area, gabbro cuts rocks of the Martin Lake series or is intruded between them and the underlying Tazin rocks. Tremblay admits that the "late" gabbros also resemble a series of sheets, sills, and dikes intrusive into the lower part of the Martin Lake series, below the series of interbedded extrusive lavas and arkosic sediments. There is thus no evidence that any of the igneous rocks are post-Martin Lake in age. They undoubtedly welled up through fractures in the pre-Martin Lake basement rocks during early Martin Lake time and were intruded into the lower Martin Lake sediments and, later, poured out as extrusive lavas interbedded with arkosic sediments. They are all here considered early Martin Lake in age. Tremblay's basic information was used in compiling Figure 4 but has been reinterpreted with the help of aerial photographs.

S. J. T. Kirkland (1953, unpub. manuscript, Queen's Univ.) concluded that

> "Apart from the clastic nature of the rocks in the two areas (north of Lake Athabasca and south of Lake Athabasca), there is little ground for correlation The so-called Athabasca (Martin Lake) rocks seen by the writer (Kirkland) at the Eldorado Ace mine, near Beaverlodge Lake, bear little resemblance to those in the Middle Lake area . . . They are of a decidedly different nature . . . and the correlation of such rocks with the type Athabasca series is questionable."

In the summer of 1956, Fahrig (1958)[6] mapped the eastern boundary of the Athabasca area and designated it as Proterozoic. The same year, C. K. Bell carried on detailed geological mapping in the Crackingstone Peninsula; the results of Bell's investigations have not been published and are not available to the author.

[6] Published after completion of this manuscript.

The basal member of the Athabasca formation, because it resembles the arkosic sandstones and conglomerates of the Martin Lake series, has led geologists (Alcock, 1920; 1936) working on the north shore to correlate these two on the basis of lithology. This correlation has become so conventional that even though Hale (1954b) discovered a profound angular unconformity within his "Athabasca Series", he placed both parts in the Precambrian. Christie (1949; 1953), mapping in the Beaverlodge Lake area, confidently correlated the Martin Lake arkose and conglomerate with the basal sandstone and conglomerate of the Athabasca formation on the islands south of Crackingstone Peninsula.

Martin Lake Series and Athabasca Formation Redefined

Martin Lake Series

The type area of the Martin Lake series is defined as the vicinity of Martin Lake in the Beaverlodge Lake area, Saskatchewan, and extending northeast and southwest along the Black Bay-Tazin River master fault for about 18 miles (Fig. 4). Structurally, the main part of the area is synclinal, pitching northeast, with dips on both limbs averaging 65°. The total preserved thickness of this series is estimated as 8000 feet and consists of siliceous arkosic sandstones and conglomerates, interbedded with basaltic lava flows which make up approximately 1000 feet of the section. The original thickness is unknown because of erosion. The whole series is offset by numerous faults[7] and is cut by veins containing pitchblende.

Three other areas in which the Martin Lake series crops out are (Fig. 5): (1) a synclinal area at the east end of Tazin Lake, northwest of the type area; (2) the Thluicho-Gulo lakes basin, north of Camsell Portage; (3) the Charlot River basin, between Ellis Bay and Wellington Lake. A remnant occurs along the southeast shore of Black Bay against the Black Bay-Tazin River master fault at Langley Bay, and another remnant occurs on Slate Island and Peninsula. These formations are undoubtedly late Early

[7] A major fault known as the St. Louis fault cuts the main syncline. It is easily traced on the detailed maps of the area (Christie, 1949; 1953; Tremblay, 1957a; 1957b) and on aerial photographs. The fault trends east-west and passes through the narrow cleft used by the portage and road at the northern end of Beaverlodge Lake. Movement on this fault is north side up, relative to the south side, offsetting the synclinal axis and the formational contacts.

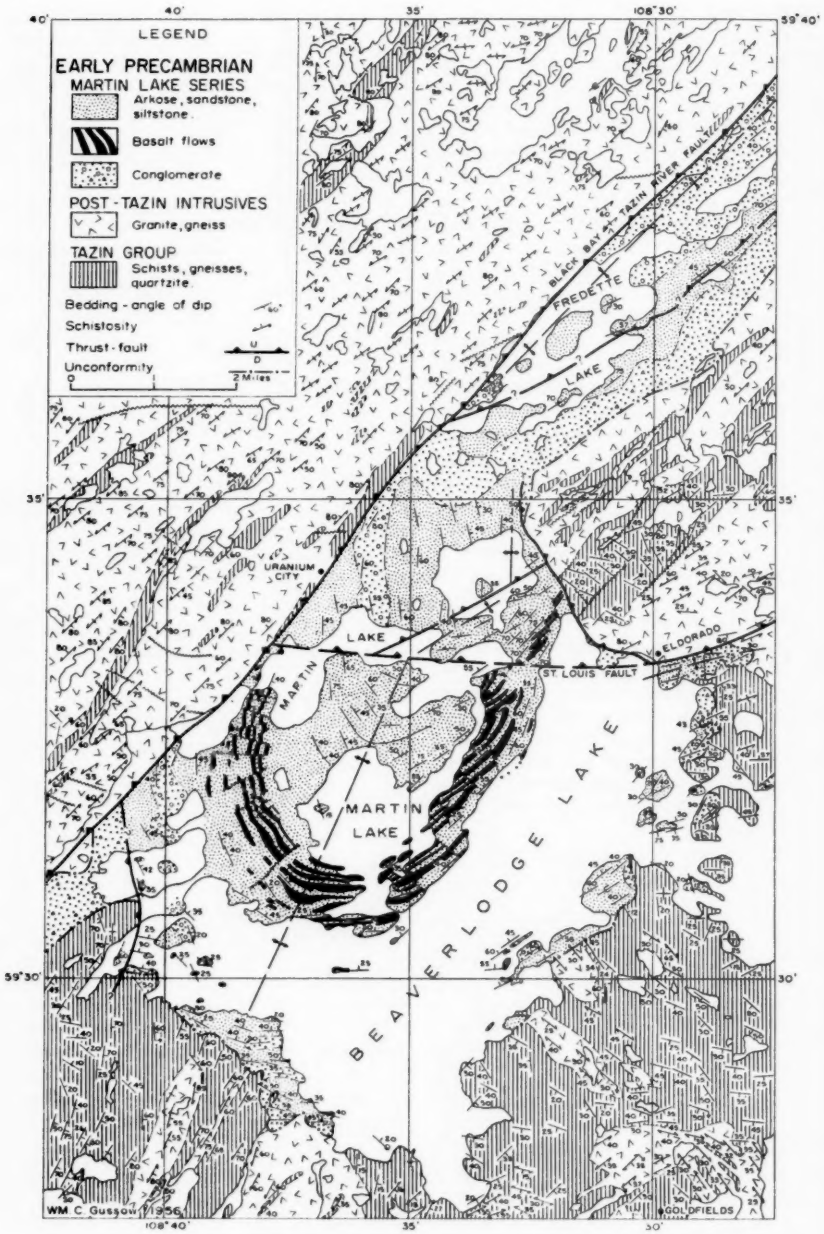

FIGURE 4.—GEOLOGY OF MARTIN LAKE SERIES TYPE AREA

Map base traced from Geological Survey of Canada Map 1015A (Christie, 1953). Geology compiled from Christie and modified from later work by Tremblay (1955, 1957) and reinterpreted by Gussow. Master thrust faults and major fold axes have been added. Undoubtedly, the structure is even more complex.

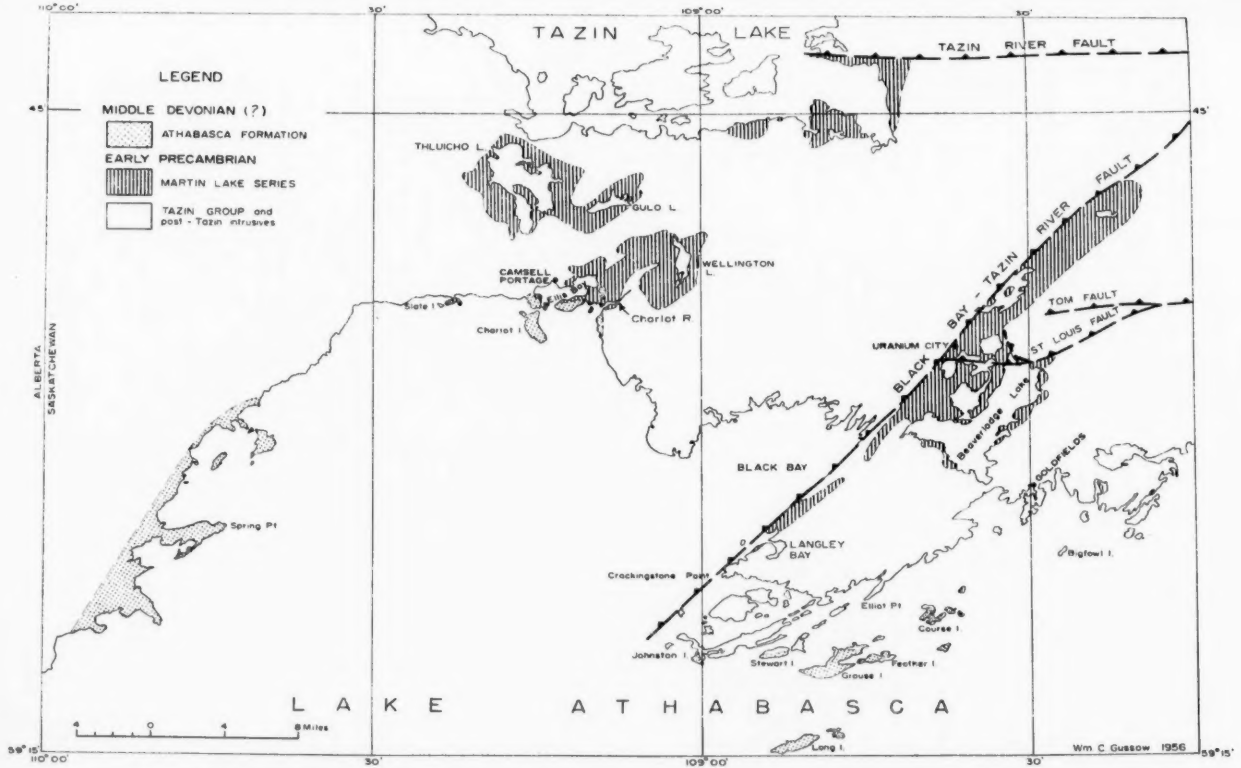

FIGURE 5.—NORTH SHORE DISTRIBUTION OF ATHABASCA FORMATION AND MARTIN LAKE SERIES

Map base traced from Geological Survey of Canada Map 363A (Alcock, 1936). Geology compiled from all available published maps and reports but reinterpreted.

Precambrian as shown by age dating in the type area (Collins and Freeman, 1951; Eckelmann and Kulp, 1956), and can probably be correlated with the sandstone-volcanic series at Dubawnt Lake, Baker Lake, and Great Slave Lake (Fig. 1).

Most of the rocks are of continental freshwater origin and consist predominantly of arkoses to feldspathic sandstones, buff to red, with angular to rounded grains, coarse angular conglomerates, and associated volcanic flows and dikes. The finer-grained beds are cross-bedded, ripple-marked and exhibit sun cracks.

The Martin Lake series lies unconformably on the deeply eroded Tazin group and the associated post-Tazin granitic rocks, which underlie most of the north-shore area. The Martin Lake series has been folded and faulted and deeply incised prior to deposition of the Athabasca formation. The folded Martin Lake series and older rocks are cut by many small, black, dark-green, or brown basic dykes. These are probably early Martin Lake and pre-volcanic in age.

Athabasca Formation

The flat-lying Athabasca formation (Fig. 3) underlies an area of about 28,000 square miles[8]; it extends 260 miles from the Athabasca River[9] east along the south shore of Lake Athabasca, Fond du Lac, Fond-du-Lac River, and Black Lake, to the vicinity of Wollaston Lake, and south for 135 miles to Cree Lake. The southeastern boundary has not been defined and may lie somewhat farther west. The total thickness of the Athabasca formation is unknown; a vertical section 400 feet thick is exposed in the escarpment south of Lake Athabasca. The southern contact at Cree Lake lies nearly 900 feet above the northern contact on Lake Athabasca. The flatness of the regional dips[10] may indicate a total onlapping stratigraphic section of nearly 1000 feet. The Athabasca formation crops out on several islands (Long, Johnston, Stewart, Grouse, Feather, Course, Bigfowl, and numerous unnamed smaller islands) near the north shore of Lake Athabasca (Fig. 5), and some isolated patches or outliers occur on the north shore—notably, a large area north and south of Spring Point, on Slate Island, Charlot Island and Peninsula, as well as in several places described by Alcock as "sandstone dikes"[11]—showing that this formation underlies most of Lake Athabasca and that it once extended even farther north.

The Athabasca formation is almost entirely sandstone, commonly siliceous. A dolomite member, recently discovered at Trout Lake, about 40 miles south of William Point, is described separately. Typically, grains are rounded to subangular. The rounded quartz grains have optically oriented authigenic overgrowths of quartz, many with sutured boundaries. The sandstone is fine- to medium-grained, although grit and pebble bands occur; these mark bedding planes that are otherwise difficult to observe. The weathered surface of the rock is white, but locally it is buff. The rock is massive-bedded to thin-bedded, and cross-bedding is common. In the lower part of the section, the sandstone is iron-stained and ripple marks are common. Locally, red shale layers up to 10 inches thick occur near the base of the formation. In describing the Athabasca formation along the southern margin, Sproule (1941) mentioned numerous, irregular light-colored carbonate pellets up to 1 inch in diameter. A hand specimen from a boulder of Athabasca sandstone in the Mudjatik area contains numerous white, soft, kaolin chips.

It has been suggested that the Athabasca sandstones may be aeolian, which would explain the absence of fossils. However, the authigenic tourmaline overgrowths, the very regular bedding over considerable distances, both horizontally and vertically, the even cross-bedding, the clay chips and irregular carbonate pellets, and the Trout Lake dolomite member seem to show that the sandstone and the dolomite member are of marine origin.

TROUT LAKE DOLOMITE: The author believes that the Trout Lake dolomite member is part of the Athabasca formation.

Blake (1956, p. 5) noted high ridges of dolomite which crop out in the vicinity of Trout Lake, 40 miles south of William Point (Fig. 3)

[8] The total area of New Brunswick.

[9] An unmapped exposure was observed by the author near the mouth of the Athabasca River on the main navigation channel.

[10] Dowling (*in* Tyrrell, 1897) believed that the sandstone beds dip slightly to the west; more recent workers note very gentle south dips. Possibly there is a regional southwest tilt similar to that recognized in the Plains; if so, then older beds should be exposed in the east, with progressively younger beds exposed westward along the present erosion surface.

[11] Sandstone preserved in cracks and fissures in older rocks. One of these, in the vicinity of Elliot Bay, has been traced more than 7000 feet (C. K. Bell, personal communication, 1957).

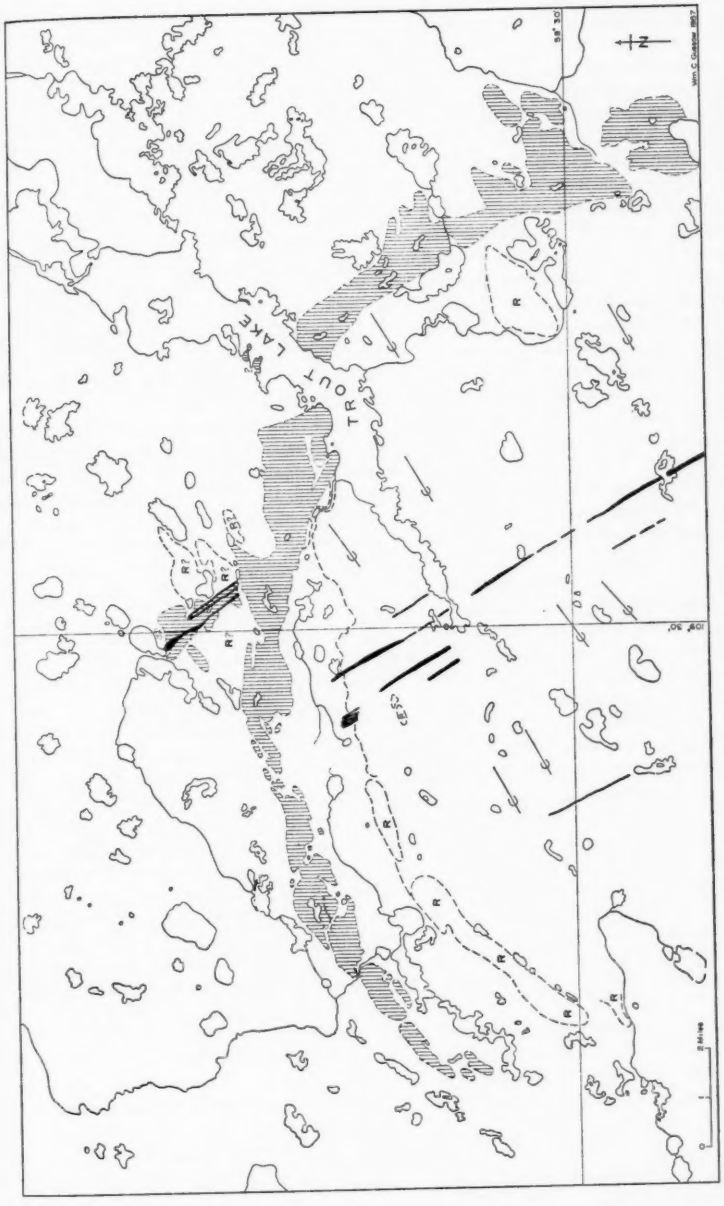

FIGURE 6.—PHOTOGEOLOGIC MAP OF TROUT LAKE AREA, SASKATCHEWAN

Showing the crescent-shaped area (shaded) of highly contorted dolomites(?) which stand in relief as a series of high ridges. The area within the crescent is apparently underlain by flat-lying rocks. Glaciation is southwest. The parallel black lines are sand ridges formed by cracks in the continental ice sheet. R—rock exposures. Compiled from aerial photography by the Royal Canadian Air Force (Roll No. A 14434, Print Nos. 1–9, 101–113).

and are clearly visible in aerial photographs. They extend at least 20 miles in an arcuate direction, east and west from Trout Lake (Fig. 6). They are now known to crop out in a complete circle and are 300–400 feet high (K. D. Hannigan, personal communication).

Blake described the carbonates as exceedingly fine-grained and highly contorted. They may be, he noted, cream, buff, pink, or reddish; the laminae are extremely fine to very coarse. The dolomite is fine-grained or aphanitic. In places it is folded into major anticlines and synclines with dips up to 80°. In addition, the rocks have been deformed locally on a small scale. There are many zones of intense brecciation, intricate contortion, and rupture.

Blake noted thin sections of the carbonate showing delicately laminated beds which are moderately brecciated. Rounded "floating" sand grains of less than 1 millimeter in diameter were found in two sections. The dolomite is unmetamorphosed.

Blake's description, together with an examination of the thin sections, indicated to this author an evaporitic carbonate facies which has undergone soft-rock or penecontemporaneous deformation, or "autoclastic brecciation", due to subaqueous slumping after partial lithification. There is no evidence of metamorphism. The rock is unknown in the Precambrian of the north shore. Similar rock types which are common to the Middle Devonian Elk Point formation of the Interior Plains and to the Ghost River formation of the Front Ranges of the Canadian Rockies will be discussed in following sections.

Extremely fine microlaminae, micro-oolites, microstylolites, and primary orientation of minute, acicular crystals normal to the laminae were observed.

Blake (1956, p. 6) stated "... it is possible that the Trout Lake (carbonate) is a part of the Athabasca series...." The present writer concurs. It appears to be the youngest member of the Athabasca formation.

Shrock (1948, Fig. 236, p. 276) illustrated that subaqueous flowage and deformation can cause sliding on slopes of less than 6°; this may explain the contortion of the sediments. The descriptions of Blake's traverses (unpublished field notes, August 10, 1952) seem to fit such an explanation, and the contortion is interpreted as penecontemporaneous deformation of partly consolidated calcareous oozes, causing folding and brecciation shortly after deposition of the sediments.

Finally, the east-west strike of the Trout Lake outcrop area is sharply discordant with the prevailing northeast grain of the basement. This suggests it is not Precambrian.

Sub-Athabasca Unconformity

The basal contact of the Athabasca formation is exposed at several places along the northern edge. The basal conglomerate lies on the basement complex with a profound angular discordance. This unconformity has been described at the following places: (1) on the islands south of Crackingstone Peninsula; (2) at several points between Stony Rapids and Middle Lake; (3) near the southeast shore of Black Lake (J. S. Ker...en, personal communication); (4) along Pine Channel; (5) east of Poplar Point; (6) north of the mouth of Charlot River; and (7) on Slate Island (Figs. 2, 3, 5).

Tyrrell (1897) assigned the underlying steeply dipping sedimentary rocks (Martin Lake series?) on Slate Island (Fig. 5) to the Huronian and placed the flat-lying strata (Athabasca formation) in the Cambrian.

Alcock (1936) described the unconformity on several of the islands south of Crackingstone Peninsula and mentioned the "sandstone dikes."

Blake (1956, p. 8) described the contact as "...an angular unconformity of great hiatus." East of Poplar Point, a flat-lying sandstone rests on steeply dipping, ferruginous quartzite of the Tazin series. A few inches of quartzite and vein quartz conglomerate lies at the base of the sandstone. Between Stony and Middle lakes, the unconformity is exposed intermittently for 5 miles at the base of a 25- to 50-foot sandstone escarpment. There, too, a thin layer of quartz conglomerate appears at the base of the sandstone. The sandstone in this area is highly hematitized and cross-bedded and contains many grit and pebble bands. The Tazin-type rocks 8 feet below the unconformity were so weathered in pre-Athabasca time that their original character cannot be ascertained. The weathering products are almost entirely quartz and kaolin, with some iron oxide—"typical lateritic residual soils from long-continued weathering or decomposition of the underlying rocks" (S. J. T. Kirkland, 1953, unpub. manuscript, Queen's Univ.).

Hale (1955) described the unconformity at the west end of Slate Island and observed the fresh appearance of the upper part of the series, adding,

"Only negative evidence, the apparent absence of fossils, supports the assignment of this part of the series to the Precambrian."

Hale probably observed the flat-lying Athabasca formation (his Upper Part) lying unconformably on the Martin Lake series (his Lower Part) on Slate Island and north of the mouth of Charlot River.

Along the southern margin of the Athabasca formation, numerous inliers of crystalline basement rocks and outliers of Athabasca formation have been mapped. No actual contacts have been observed, but Sproule (1941a; 1941b; 1941c) described the basement rocks as rotted and disintegrated near the contact by long weathering. They contrast sharply with the freshly glaciated outcrops.

Diabase Dikes

No diabase dikes are known to cut the Athabasca formation. A note on the Tectonic Map of Canada (Derry, 1950) states that the sandstone area is intruded by basic sills, but this statement is correct only for the lower Martin Lake series of the north shore and has been applied erroneously to the whole area.

At one locality on the west shore of Cree Lake, near the southern margin of the sandstone area, Tyrrell (1897) described an outcrop of light-green uralitic diabase striking N.65°E., which he believed cut the Athabasca sandstones. More probably this represents a small embayment in the southern edge or a window of basement rocks. The strike conforms to the regional strike in the basement complex, and the diabase was not actually found in contact with the Athabasca formation. The near-by quartzites could be Tazin group.

Blake (1956, p. 10) mapped a small outcrop of diabase on the south shore of Lake Athabasca, approximately 4 miles east of Turnor Point. Its relationship to the Athabasca formation is not known. If it does cut the Athabasca sandstone, it would be the only known example. It could be a Precambrian inlier.

Correlation of the Athabasca Formation

General Statement

The Martin Lake series is a thick series of late Early Precambrian interbedded continental arkosic sandstones, conglomerates, and basalt flows, which have been folded and metamorphosed and are cut by numerous faults and quartz veins. The Athabasca formation is a relatively thin series of flat-lying, unmetamorphosed, white to pink marine sandstones and minor quartz-pebble conglomerates, with an evaporitic carbonate member. It lies on the Precambrian basement complex with profound unconformity. To date, it has yielded no fossils.

The Martin Lake sedimentary rocks are predominantly arkoses and feldspathic sandstones which exhibit all the characteristics of rapid continental accumulation; the Athabasca sandstones, in marked contrast, are almost entirely pure quartz, the product of long and extensive chemical decomposition of an ancient land surface, followed by erosion and sorting of these residual soils. The end products consist of quartz, kaolin, and minor amounts of iron oxide, with only the most resistant of the accessory minerals.

Regionally, the Athabasca formation and the flat-lying Paleozoic formations of the Interior Plains are structurally conformable, and both lie with profound angular discordance on the crystalline rocks of the Churchill georogen (Fig. 7). Obviously, the Athabasca formation is much younger than even the youngest strata of the basement complex, the Martin Lake series, and is closer in age to the Paleozoic section of the Plains.

Until diagnostic fossils are found, no precise dating is possible. Three possible correlations are: (1) correlation with the basal Cambrian sandstones in the subsurface of the Interior Plains, which are Middle and Upper Cambrian; (2) correlation with the basal Ordovician Winnipeg sandstone; or (3) correlation with the basal Middle Devonian sandstones, which overlie the Precambrian basement immediately west of the Athabasca area, in the northern half of Alberta (Fig. 1).

Basal Cambrian

In the subsurface of the Plains, the lower part of the Middle Cambrian consists of a poorly sorted, basal, white, pink, and red-mottled quartz sandstone with interbedded shales. The sandtones become pebbly and arkosic near the base and are glauconitic. They contain an abundant marine fauna. They grade into Upper Cambrian beds to the east by onlap.

The Athabasca formation lacks the abundant marine fauna and the glauconite and mica which characterize the Middle Cambrian deposits of the region. Furthermore, the Cambrian formations of the Plains thin eastward by

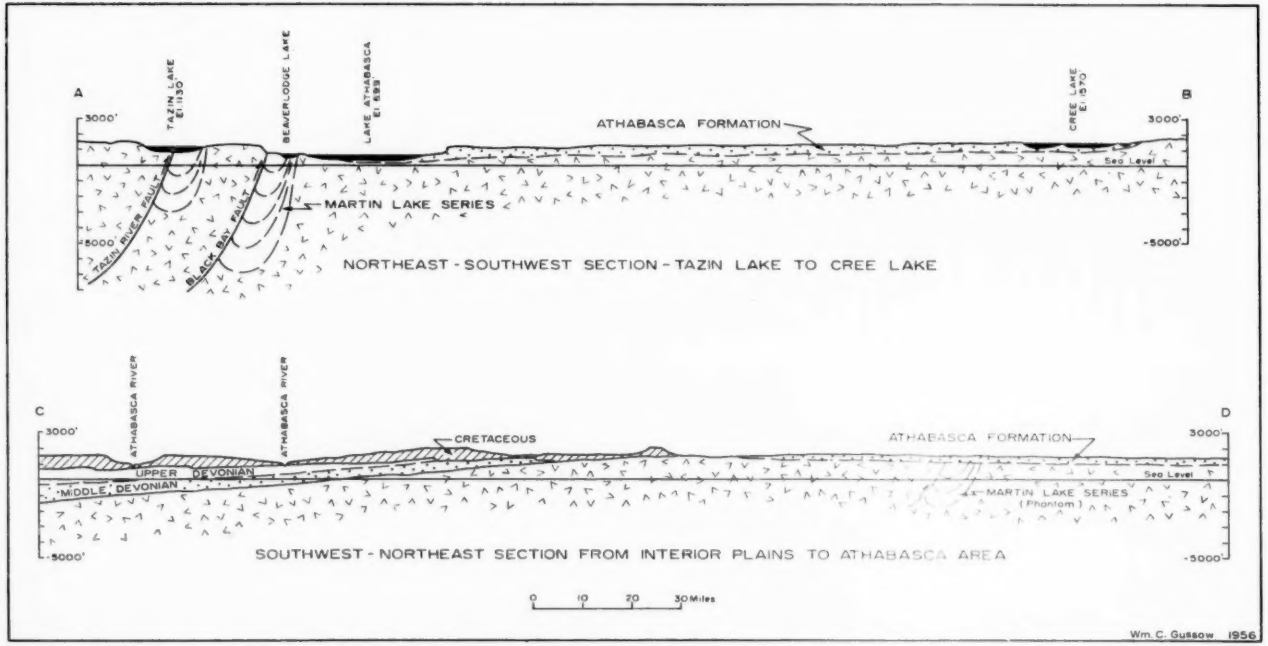

FIGURE 7.—CROSS SECTIONS SHOWING STRUCTURAL RELATIONSHIPS OF ATHABASCA FORMATION, MARTIN LAKE SERIES, AND MIDDLE DEVONIAN OF THE INTERIOR PLAINS; AND THE PRECAMBRIAN BASEMENT COMPLEX

Vertical exaggeration approximately 16×. V-pattern: undifferentiated Tazin schists, gneisses, and quartzites, and post-Tazin granitic intrusives.

onlap and become more shaly. They have a zero depositional edge in the subsurface (with only slight pre-Ordovician erosion) and do not crop out along the margins of the Canadian Shield.

Recent drilling southwest of Lac la Ronge near the north end of Montreal Lake penetrated 650 feet of basal Cambrian sandstone before passing into the Precambrian basement. This is most significant in deciding the age of the Athabasca sandstone.

Basal Ordovician

In Manitoba, basal sandstones crop out along the eastern edge of the truncated Paleozoic section where it borders the Canadian Shield. These, known as the Winnipeg formation, conformably underlie fossiliferous Middle Ordovician rocks (Baillie, 1952). They lie on the Precambrian basement complex with profound unconformity. In the subsurface, these sandstones lie on rocks of Early Ordovician age. North of Lake Winnipeg, the Winnipeg sandstone strikes west into Saskatchewan and disappears beneath Middle Devonian rocks, which here lie unconformably on Ordovician rocks.

In the vicinity of Great Bear Lake, and extending south to Great Slave Lake, sandstones which conformably underlie the Ordovician section and overlie the Precambrian complex with pronounced unconformity are probably age equivalents of the Winnipeg formation, although maps of the Geological Survey date them as Precambrian (Proterozoic). The nearest outcrops of Winnipeg sandstone in both areas are about 200 miles from the Athabasca sandstone area.

Between Lac la Ronge and Great Slave Lake, Ordovician and Cambrian formations are absent because of pre-Devonian erosion, and Middle Devonian rocks lie directly on the granite.

Wallace and McCartney (1928) studied the Winnipeg sandstone microscopically. The sands are well sorted, rounded, and pitted, but unlike the Athabasca sandstone, are cemented by calcite. Minor heavy accessories include, in decreasing order of abundance, zircon, magnetite, tourmaline, staurolite, and rutile. This assemblage and the fossils in the conformably overlying strata indicate a marine environment.

Lithologically, the Winnipeg sandstone is similar to the Athabasca sandstone in hand specimens, and they could be separated only by fossil evidence. The presence of evaporites in the Ordovician, however, is unknown.

Basal Devonian

Between Lac la Ronge and Great Slave Lake, along the truncated east edge of the Paleozoic and the margin of the Precambrian Shield, Middle Devonian strata lie directly on the Precambrian basement. Outcrops have been described at only a few places—at Lac la Ronge, on the Clearwater River, on the Firebag River, along the Slave River south of Fort Fitzgerald, at the junction of the Slave and Peace rivers, and on Great Slave Lake.

McInnes (1910; 1914) and Dowling (*in* Tyrrell, 1897) described the Middle Devonian on the south shore of Lac la Ronge, Saskatchewan. This is approximately 175 miles south and slightly east of Cree Lake, at the northern edge of the truncated Paleozoic. The rocks are fossiliferous magnesian limestone or dolomite, sandstone, and conglomerate, lying directly on the Precambrian. The conglomerate contains limestone, pebbles which must be the remnants of eroded Ordovician about 25 miles to the south. This would date the basal conglomerate as post-Ordovidian.

At Contact Rapids on the Clearwater River, Saskatchewan, at the truncated eastern edge of the Interior Plains, R. deWit (1952, unpub. manuscript, Geological Survey of Canada), described the Paleozoic section immediately above the Precambrian. A thin regolith overlies the granite and is unconformably overlain by flat-lying sandstones of an entirely different character than the underlying "wash." No fossils have been found in the basal sandstone. The maximum thickness of the sandstone is 10.5 feet; beds are 4–12 inches thick. The sandstones grade upward into greenish-gray silts and sandy marls which contain fossil remains similar to the fossils in the overlying dolomite. The silts grade upward into sandy light-gray to buff, cryptocrystalline, dense dolomite and limestone known as the Methy dolomite which contains an abundant Middle Devonian[12] fauna, generally poorly preserved but rich in forms and containing some small brown spores.

Throughout western Canada, the Devonian lies on older rocks with a sharp erosional unconformity. Thus the whole paleozoic section

[12] The first fossil collections from this area were tentatively assigned to the Silurian, but more complete material has established them as Middle Devonian.

on the Clearwater River must belong to the Middle Devonian, as no unconformity is evident within the sedimentary section; the only unconformity is that at the base of the sandstone. The whole conformable section may be assigned to the Middle Devonian and is correlated with the upper part of the Elk Point of the Interior Plains.

The Clearwater section is about 50 miles south of the Athabasca sandstone area. Sproule (1951) correlates this sandstone with the Athabasca sandstone. R. deWit (personal communication) has compared hand specimens of the Athabasca sandstone and the basal Devonian sandstone of the Clearwater River and agrees that they seem identical. However, until fossils are found in the Athabasca formation, an absolute correlation is impossible. Even in the absence of fossils, the presence of an evaporitic member in the Athabasca formation supports such a correlation. The type of environment postulated for the formation o. the authigenic tourmaline described by J. C. Mawdsley (1954, unpub. B.Sc. thesis, Univ Alberta) in the Athabasca formation corresponds with that of the Middle Devonian of the Interior Plains.

The Slave River exposures are small, but the rocks are similar to those on the Clearwater, and the contact with the Precambrian is identical. On Great Slave Lake, the Middle Devonian .s well exposed and abundantly fossiliferous.

TABLE 1.—TENTATIVE REVISED TABLE OF FORMATIONS FOR NORTHERN SASKATCHEWAN

Geologic Time	Formation	Lithology	Remarks
PALEOZOIC Middle Devonian? and/or Upper Cambrian?	Athabasca Formation	Pure white quartz sandstones and occasional quartz-pebble beds, with a dense evaporitic dolomite member	Less than 500 million years
		Profound Unconformity	
PRECAMBRIAN Early Precambrian	Martin Lake series	Interbedded arkose, feldspathic sandstone and conglomerate, and basaltic lava flows Some intrusive sheets, sills and dikes of early Martin Lake age	Greater than 2000 million years
		Major Unconformity	
	Post-Tazin intrusives	Lamprophyre dikes Granite and gneiss	
		Intrusive Contact	
(Archean?)	Tazin group	Metamorphosed sedimentary and volcanic rocks Conglomerate Dolomite and dolomitic quartzite Ferruginous quartzite Quartzite	

Note that the writer does not subscribe to the term "Proterozoic" which is commonly intended to imply "immediate pre-Cambrian age". Obviously, none of the formations of Northern Saskatchewan fits this definition. The term Archean is believed to serve a useful purpose to designate the ancient rocks of the primordial crust. However, it is not certain if the Tazin group is Archean or somewhat younger.

It is subdivided into the Presqu'ile and Pine Point,[13] and is correlated with the Middle Devonian Elk Point section of the Plains. The base is exposed only at Gypsum Point on the North shore, where Silurian? and Ordovician rocks separate the Devonian from the Precambrian. North of Lesser Slave Lake, throughout the northern half of Alberta, the Middle Devonian immediately overlies the Precambrian. Locally developed basal sandstones have a maximum thickness of 60 to 100 feet.

Conclusions

Evidence favors a tentative Middle Devonian? or Upper Cambrian? age for the Athabasca formation. It is also possible that the sandstone is Cambrian and the Trout Lake dolomite is Middle Devonian. The Martin Lake series is late Early Precambrian and much older than the flat-lying Athabasca formation.

The foregoing deductions should be investigated further, and an attempt should be made to find evidence of organic remains such as fossil fish fragments (which have recently been found in the Ghost River formation of the Front Ranges and in the basal Devonian sandstones[14] of the Interior Plains), *Chara*, and plant remains.

The Athabasca formation is either flat-lying or with slight depositional dips; the Martin Lake series is steeply dipping to overturned. Pebbles in the Athabasca are fresh-looking and undeformed, whereas in the Martin Lake series and older formations, they may be gneissic. In the vicinity of the Martin Lake series, the basal conglomerate of the Athabasca formation contains pebbles of the Martin Lake series. The Martin Lake sandstones and conglomerates are commonly associated with volcanic flows and have been faulted and folded and cut by numerous basic dikes; no known dikes or volcanic rocks are associated with the Athabasca formation. The Martin Lake series is of continental origin, the Athabasca is marine.

A tentative revised table of formations for the geology of northern Saskatchewan is given in Table 1.

Economic Geology

The possibility of uranium mineralization in the Athabasca formation should be investigated. The Beaverlodge area testifies to the presence of rich primary uranium mineralization in the basement rocks, and possibly the basal sandstones and conglomerates of the Athbasca formation are the host for Blind River-type mineralization.

Low-grade uranium mineralization has already been discovered in the Athabasca formation on Middle Lake (Blake, 1956; Hriskevich, 1949) and on Stewart Island, and it should be remembered that the absence of ore-grade values at the outcrop does not preclude the possibility of ore-grade mineralization at depth, beyond the zone of surface leaching.

[13] Although E. M. Kindle (1942) places the overlying Slave Point formation in the Upper Devonian, until recently (Law, 1955), it has generally been regarded as Middle Devonian. It was originally assigned to the Middle Devonian by Cameron (1922). No diagnostic fauna has been collected from the type area on Great Slave Lake. However, new fossil collections (W. G. Crook, personal communication, February 1957) from Slave Point equivalent (?) in the subsurface, and identified by P. S. Warren, have established its age as Late Devonian and correlate it with the lower part of the Waterways and the Beaverhill Lake formations.

[14] Fish remains from thin shales interbedded with the basal Middle Devonian granite wash at the Red Earth oilfield, Alberta, have now been identified as *Coccosteus* by Robert H. Dennison (G. E. Meade, personal communication, October, 1958). The same forms have been found in the Ghost River formation where it crops out on End Mountain, in the Front Range of the Rocky Mountains, Alberta.

References Cited

Alcock, F. J., 1915, Geology of the north shore of Lake Athabaska, Alberta and Saskatchewan: Geol. Survey Canada Summary Rept. 1914, p. 60–61

—— 1917, Black Bay and Beaverlodge area, Saskatchewan: Geol. Survey Canada Summary Rept. 1916, p. 133–136

—— 1920, The Athabaska series: Am. Jour. Sci., 4th ser., v. 50, p. 25–32

—— 1936, Geology of the Lake Athabaska Region, Saskatchewan: Geol. Survey Canada Mem. 196, 41 p., maps

Baillie, A. D., 1952, Ordovician geology of the Lake Winnipeg and adjacent areas, Manitoba: Manitoba Dept. Mines and Nat. Res., Mines Br. Pub. 51–6, 64 p., map

Blake, D. A. W., 1956, Geological notes on the region south of Lake Athabasca and Black Lake, Saskatchewan and Alberta: Geol. Survey Canada Paper 55–33, 12 p., map

Cameron, A. E., 1922, Hay and Buffalo rivers, Great Slave Lake and adjacent country: Geol. Survey Canada Summary Rept. 1921, pt. B, p. 1–44, map

Camsell, Charles, 1915, An exploration of the region between Athabasca and Great Slave Lakes, Alberta and Northwest Territories: Geol. Survey Canada Summary Rept. 1914, p. 55–60

Christie, A. M., 1949, Goldfields and Martin Lake map-areas, Saskatchewan: Geol. Survey Canada Paper 49-17, 32 p., maps

Christie, A. M. 1953, Goldfields-Martin Lake map-area, Saskatchewan: Geol. Survey Canada Mem. 269, 126 p., map

Collins, C. B., and Freeman, J. R., 1951, Geological age determinations in the Canadian Shield: Royal Soc. Canada Trans., 3d ser., v. 45, sec. 4, p. 23–30

Derry, D. R., *et al.*, 1950, Tectonic map of Canada: Geol. Soc. America

Eckelmann, W. R., and Kulp, J. L., 1956, Uranium-lead method of age determination, Part 1: Lake Athabasca problem: Geol. Soc. America Bull., v. 67, p. 35–54

Fahrig, W. F., 1958, Wollaston Lake, Saskatchewan: Geol. Survey Canada Map 27-1957 (marginal notes)

Fraser, J. A., 1954, Crackingstone, Saskatchewan: Geol. Survey Canada Paper 54-8 (map with marginal notes)

Furnival, G. M., 1940, Stony Rapids and Porcupine River areas, Saskatchewan: Geol. Survey Canada Paper 40-10, 10 p., maps

—— 1941a, Porcupine River, Saskatchewan: Geol. Survey Canada Map 658A (marginal notes)

—— 1941b, Stony Rapids, Saskatchewan: Geol. Survey Canada Map 659A (marginal notes)

Geological Survey of Canada, Geological Maps: Alberta (1002A, 1951); Saskatchewan (895A, 1947); Canada (820A, 1945; 1045A, 1955)

Gill, J. E., 1957, The Proterozoic in Canada: Royal Soc. Canada, Special Pub. No. 2, 191 p.

Gussow, W. C., 1957, Correlation and age of the Athabasca formation: Alberta Soc. Petroleum Geologists Jour., v. 5, p. 2–5

Hale, W. E., 1954a, Black Bay map-area, Saskatchewan: Geol. Survey Canada Paper 53-15, 18 p., map

—— 1954b, Gulo Lake, Saskatchewan: Geol. Survey Canada Paper 54-6 (map with marginal notes)

—— 1955, Forcie Lake map-area, Saskatchewan: Geol. Survey Canada Paper 55-4 (map with marginal notes)

Hriskevich, M. E., 1949, Radioactive occurrences in Black Lake area, Saskatchewan: Saskatchewan Dept. Nat. Res., Precambrian Geology ser., Rept. No. 2

Kindle, E. M., 1942, Correlation of the Devonian sedimentary formations of North America: Geol. Soc. America Bull. v. 53, p. 1729–1794

Law, J., 1955, Geology of northwestern Alberta and adjacent areas: Am. Assoc. Petroleum Geologists Bull., v. 39, p. 1927–1978

Mawdsley, J. B., 1949, Pine Channel area, Lake Athabasca district, Saskatchewan: Geol. Survey Canada Paper 49-27, 46 p., map

—— 1956, Unfolding of the geology of northern Saskatchewan: Canadian Min. Metall. Bull., v. 49, no. 527, p. 199–203

McConnell, R. G., 1893, Report on a portion of the district of Athabasca comprising the country between Peace River and Athabasca River north of Lesser Slave Lake: Geol. Survey Canada Ann. Rept. 1890–91, v. 5, pt. 1D, 67 p., maps

McInnes, W., 1910, Lac LaRonge, Saskatchewan: Geol. Survey Canada Summary Rept. 1909, p. 151–157

—— 1914, The basins of Nelson and Churchill rivers (with map 58A, 1915): Geol. Survey Canada Mem. 30 (1913), 146 p.

Rice, C. M., 1949, Dictionary of geological terms: Ann Arbor, Mich., Edwards Brothers, 464 p.

Shrock, R. R., 1948, Sequence in layered rocks: New York, McGraw Hill Book Co. Inc., 507 p.

Sproule, J. C., 1938a, Mudjatik area, Saskatchewan: Geol. Survey Canada Paper 38-8, 13 p., maps

—— 1938b, Cree Lake Area, Saskatchewan: Geol. Survey Canada Paper 38-9, 13 p., maps

——1941a, Weitzel Lake, Saskatchewan: Geol. Survey Canada Map 576A (with marginal notes)

——1941b, Brustad River, Saskatchewan: Geol. Survey Canada Map 577A (with marginal notes)

—— 1941c, Upper Clearwater River, Saskatchewan: Geol. Survey Canada Map 578A (with marginal notes)

—— 1951, The McMurray formation in its relation to oil occurrence: Athabasca Oil Sands Conf. Proc., Edmonton, Alberta, p. 6–25

Tremblay, L. P., 1955, Uranium City, Saskatchewan: Geol. Survey Canada Paper 54-15 (Sheets 1 and 2), (maps with marginal notes)

—— 1957a, Uranium City, Saskatchewan: Geol. Survey Canada Paper 55-28 (Sheets 3 and 4) (maps with marginal notes)

—— 1957b, Uranium City, Saskatchewan (Sheet 5): Geol. Survey Canada Map 18-1956 (with marginal notes)

Tyrrell, J. B., assisted by D. B. Dowling, 1897, Report on the country between Athabasca Lake and Churchill River with notes on two routes travelled between Churchill and Saskatchewan Rivers: Geol. Survey Canada Ann. Rept. 1895, v. 8, pt. D, (1896), 120 p., map

Wallace, R. C., and McCartney, G. C., 1928, Heavy minerals in sand horizons in Manitoba and eastern Saskatchewan: Royal Soc. Canada Trans., 3d ser., v. 22, pt. 2, sec. 4, p. 199–414

709—8 Avenue West, Calgary, Alberta, Canada

Manuscript Received by the Secretary of the Society, June 4, 1957

BULLETIN OF THE GEOLOGICAL SOCIETY OF AMERICA
VOL. 70, PP. 19–52, 20 FIGS., 2 PLS. JANUARY 1959

ANALYTICAL AND EXPERIMENTAL STUDY OF SIMPLE GEOLOGIC STRUCTURES

BY ALLAN R. SANFORD

ABSTRACT

An analytical method is derived which gives the elastic response of a homogeneous rock layer to two-dimensional distributions of vertical displacement applied along its lower boundary. Displacement field, stress distribution, and distortional strain-energy density diagrams are presented for three types of displacement applied at the lower boundary of 5-km thick layers possessing average sedimentary rock properties. These three types of displacement are: (1) sinusoidal vertical displacement and no horizontal displacement; (2) an approximate step in vertical displacement and no horizontal displacement; and (3) sinusoidal vertical and horizontal displacement (horizontal displacement 90° out of phase with the vertical). Displacement fields and stress distributions for each type of applied displacement are nearly independent of the elastic characteristics of the layers. The magnitudes of displacement necessary to initiate fracture at some point in the layer are small (3.7–8.2 m) for the three types of applied displacement. For applied displacement (1) and (3), the initial fracture is a vertical tensile crack at the crest of the fold. For applied displacement (2), the initial fracture is either a vertical crack at the upper surface or a shear fracture at the lower surface.

Displacement fields and fracture patterns for scale-model experiments of two problems similar to the analytical examples are presented. For a sinusoidal vertical displacement, the fracture pattern is a complex zone of normal faults which taper inward toward the axis of the fold and die out at depth. For a step in vertical displacement, the fracture pattern is (1) a series of reverse faults which start vertically at the base of the layer, curve, and intersect the upper surface at low angles, and (2) a series of normal faults dipping toward the convex side of the reverse faults. Of particular interest are the reverse faults which show that vertical movement at depth can generate low-angle faulting at the surface.

Displacement fields found in the elastic analyses are good first-order approximations of displacement fields in the scale-model experiments. Points of initial fracture observed in the model experiments agree closely with those computed in the elastic analyses. The line of fracture for the curved reverse faults in the model experiments can be predicted on the basis of the Mohr fracture criterion and the stress distribution from an elastic analysis.

CONTENTS

TEXT

	Page
Introduction	20
Analytical study	20
Method	20
Derivation of analytical method	21
Application of analytical method to examples	24
Numerical examples	26
Introduction	26
Category I examples	27
Category II example	29
Scope of numerical examples in Categories I and II	29
Category III example	31
Prediction of fractures	33
Experimental study	33
Problems investigated	33
Theory	33
Description of experiments	37
Properties of modeling materials	37
Model apparatus	40
Experimental procedure	41
Results of experiments	41
General statement	41
Type I displacement fields	42
Type I fractures with Material 2	42
Type I deformation with Materials 1, 3, and 4	42
Type II displacement fields	42
Type II fractures with Material 2	43
Type II fractures with Materials 1 and 4	47
Type II deformation with Material 3	47
Summary of experimental results	47
Geologic interpretation of experimental results	47
Size relationship between model and geologic structure	47
Fractures	48
Comparison of experimental and analytical results	49

TEXT—Continued

	Page
Type I experiments and Category I numerical examples	49
Displacement fields	49
Fractures	49
Type II experiments and Category II numerical example	49
Displacement fields	49
Fractures	49
References cited	50

ILLUSTRATIONS

Figure	Page
1. Co-ordinates and stress sign convention for the elastic problems	22
2. Diagram of the Mohr fracture criterion	26
3. Classification of numerical examples	27
4. Example Ia diagrams: *A*—Displacement field; *B*—Stress distribution; *C*—Distortional strain-energy density	30
5. Example Ib diagrams: *A*—Displacement field; *B*—Stress distribution; *C*—Distortional strain-energy density	32
6. Example IIa diagrams: *A*—Displacement field; *B*—Stress distribution; *C*—Distortional strain-energy density	34
7. Category I: Effect of layer dimensions and Poisson's ratio on displacements at layer boundaries	36
8. Category II: Effect of layer dimensions on displacements at layer boundaries	37
9. Example IIa: Fracture point location as a function of layer fracture characteristics	37
10. Example IIIa diagrams: *A*—Displacement field; *B*—Stress distribution; *C*—Distortional strain-energy density	38
11. Category III: Effect of layer dimensions on displacements at layer boundaries	39
12. Distribution of grain sizes in modeling materials	40
13. Results of controlled-strain shear tests	41
14. Displacement fields—Type I experiments	42
15. Fracturing and folding—Type I experiments	43
16. Displacement fields—Type II experiments	44
17. Fractures—Type II experiments	45
18. Fracturing and folding—Type II experiments	46
19. Curvature of reverse faults in Type II experiments	47
20. Comparison of theoretical and experimental fractures	50
Plate	Facing page
1. Oblique photographs of experiments	46
2. Multiple-exposure photographs of experiments	47

TABLE

Table	Page
1. Summary of the numerical examples	28

Introduction

Much of the structural deformation in sedimentary basins results from differential vertical movements of underlying basement rock. This paper describes an analytical and experimental investigation of deformation resulting from simple distributions of vertical displacement along the bases of homogeneous rock layers. A special form of the general theory of elasticity was used in the analytical work, and scale models with homogeneous layers of dry sands and clay were used in the experimental work.

Purposes of the investigation were to determine:

(1) The characteristics of the folding and faulting produced by simple two-dimensional distributions of applied vertical displacement along the bases of homogeneous layers.

(2) The degree of similarity between a two-dimensional elastic analysis and a two-dimensional scale-model experiment of the same physical situation.

The physical situations investigated were simple idealized representations of the geologic conditions in sedimentary basins. However, investigation of these simple situations is a necessary first step toward an understanding of the more complex problems occurring in nature.

The writer is indebted to Prof. C. H. Dix, under whose guidance this investigation was carried out at the California Institute of Technology, and to Prof. C. R. Allen, also of the California Institute of Technology, who read the manuscript and made many useful suggestions. Finally the author expresses his appreciation for two years of financial aid received through a Standard Oil Company of California fellowship.

Analytical Study

Method

In the analytical method employed in this study, simple distributions of vertical displacement are specified along the base of a homogeneous elastic layer. The method is similar to one used by Hafner (1951) to describe the response of a homogeneous elastic layer to applied stresses. The two methods give similar results when applied to simple geologic situations such as folding of a layer. However, for certain structures, one method may be superior.

Block faulting of sedimentary layers above a rigid basement can be represented best by specifying displacements. In simple examples of this type of structure, adjacent blocks of basement rock are moved uniformly up or down with respect to each other. The overlying layer is undeformed by the movement except in the region where the two blocks meet. The magnitude and distribution of stress along the base of the layer cannot be determined in the zone of deformation. The best analytical representation can be made by using the only available information—the displacements.

An analytical method based on displacements along the base of an elastic layer has an additional advantage. Displacement can be easily measured in scale-model experiments. Therefore a comparison between model experiments and elastic analyses is possible when displacements similar to those used in the experiments are specified in the elastic analyses.

Derivation of Analytical Method

The analytical method is based on the theory of elasticity (Timoshenko and Goodier, 1951; Love, 1944; Muskhelishvili, 1953). Several assumptions made in this theory restrict its application to idealized representations of geologic structures. The displacements and strains must be small. The material undergoing deformation must be perfectly elastic (able to recover its initial form after removal of stresses), linearly elastic (possessing a linear relationship between stress and strain), homogeneous (possessing the same specific properties throughouts its volume), and isotropic (possessing elastic properties which are the same in all directions).

Even with these assumptions, application of the theory of elasticity to three-dimensional geologic problems remains difficult. However, a simplification is possible within the framework of the theory. If the lower boundary of a layer undergoes displacements in the x- and y-directions only, and these displacements are identical for all xy-cross sections along the z-axis from minus to plus infinity, then all xy-cross sections are in the same condition (see Fig. 1). Therefore, a two-dimensional analysis of a single cross section will describe the stresses and displacements along the length of the z-axis. With this procedure, two-dimensional situations similar to cross sections near the center of elongated geologic structures can be analyzed.

The nomenclature used is as follows (notation is the same as that of Timoshenko and Goodier (1951, p. xvii)):

σ_x , σ_y , σ_z	Normal components of stress parallel to the x-, y-, and z-axes
τ_{xy}	Shearing-stress component
σ_1 , σ_2 , σ_3	Maximum, intermediate, and minimum principal stresses
u, v	Components of displacement in the x- and y-directions
$\epsilon_x = \dfrac{\partial u}{\partial x}$, $\epsilon_y = \dfrac{\partial v}{\partial y}$	Unit elongations in the x- and y-directions (strains)
$\gamma_{xy} = \dfrac{\partial u}{\partial y} + \dfrac{\partial v}{\partial x}$	Shearing strain
G	Modulus of rigidity
ν	Poisson's ratio
λ	Lamé's constant
$K_1 = \dfrac{\lambda + 2G}{G} = \dfrac{2(1-\nu)}{1-2\nu}$	Constant used in this paper
$K_3 = 1 - K_1 = -\dfrac{1}{1-2\nu}$	Constant used in this paper
ρ	Density
g	Gravitational acceleration
$\nabla^2 = \dfrac{\partial^2}{\partial x^2} + \dfrac{\partial^2}{\partial y^2}$	Laplacian operator
$\alpha = m\pi/L$	Coefficient
E_d	Distortional strain-energy density
H	Thickness of the elastic layer
L	Distance between points of zero vertical displacement
B_c	Critical displacement—the maximum amount of displacement without fracture
σ	Normal stress across a potential fracture plane
τ	Shearing stress along a potential fracture plane
τ_0	Shear stress necessary to overcome the initial shear strength due to cohesion
ϕ	Angle of internal friction
θ	Angle between line of fracture and principal stress

The sign convention used for normal and shearing stresses is shown in Figure 1. Positive normal stresses are tensile, negative normal stresses are compressive. Positive shearing stresses have the directions shown in Figure 1, negative shearing stresses have directions opposite from those shown. The displacements u and v are positive if in the direction of increasing x and y, respectively.

The solution of any two-dimensional elastic

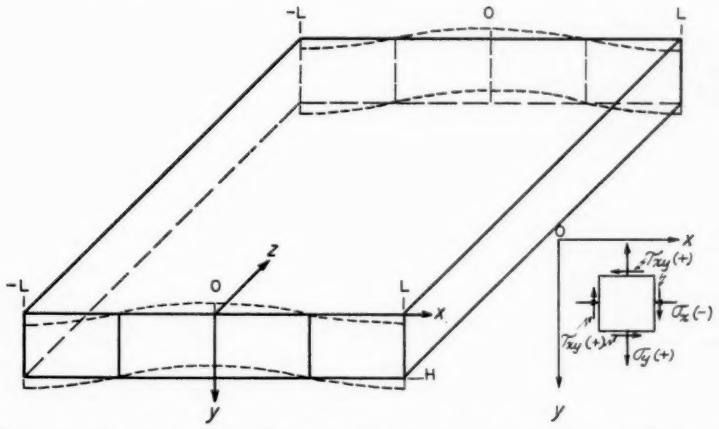

FIGURE 1.—CO-ORDINATES AND STRESS SIGN CONVENTION FOR THE ELASTIC PROBLEMS
For two-dimensional problems, displacements are identical for all xy-cross sections along the z-axis from minus to plus infinity. Positive normal stresses are tensile; negative normal stresses are compressive. Positive shearing stresses have the directions shown; negative shearing stresses are opposite to those shown.

problem must satisfy the following equations (Timoshenko and Goodier, 1951, p. 11–27):

$$\frac{\partial \sigma_x}{\partial x} + \frac{\partial \tau_{xy}}{\partial y} = 0, \tag{1}$$

$$\frac{\partial \sigma_y}{\partial y} + \frac{\partial \tau_{xy}}{\partial x} = 0, \tag{2}$$

$$\nabla^2(\sigma_x + \sigma_y) = 0. \tag{3}$$

(These equations and those which follow omit the terms pertaining to the weight of the layer. The effect of the weight of the layer is incorporated into the solutions in the next section of the text.) Equations (1) and (2) are the differential equations of equilibrium which insure a state of static equilibrium. Equation (3) is the compatibility equation (expressed in terms of stress) which insures a proper relationship between the three components of strain, so that two-dimensional deformation can occur without discontinuities in displacement (Muskhelishvili, 1953, p. 95–97). In addition to satisfying equations (1) through (3), the solution must satisfy specified stress and/or displacement boundary conditions. If the solution of the problem gives stresses and displacements which fulfill all these conditions, then it can be shown that the solution is unique (Timoshenko and Goodier, 1951, p. 236; Muskhelishvili, 1953, p. 66–71).

The stresses in equations (1) through (3) are related to the strains in the following manner:

$$\sigma_x = \lambda\left(\frac{\partial u}{\partial x} + \frac{\partial v}{\partial y}\right) + 2G\frac{\partial u}{\partial x}, \tag{4}$$

$$\sigma_y = \lambda\left(\frac{\partial u}{\partial x} + \frac{\partial v}{\partial y}\right) + 2G\frac{\partial v}{\partial y}, \tag{5}$$

$$\tau_{xy} = G\left(\frac{\partial u}{\partial y} + \frac{\partial v}{\partial x}\right). \tag{6}$$

Rewriting equations (1) through (3) in terms of strains gives:

$$(\lambda + G)\frac{\partial}{\partial x}\left(\frac{\partial u}{\partial x} + \frac{\partial v}{\partial y}\right) + G\nabla^2(u) = 0, \tag{7}$$

$$(\lambda + G)\frac{\partial}{\partial y}\left(\frac{\partial u}{\partial x} + \frac{\partial v}{\partial y}\right) + G\nabla^2(v) = 0, \tag{8}$$

$$\nabla^2\left[2(\lambda + G)\left(\frac{\partial u}{\partial x} + \frac{\partial v}{\partial y}\right)\right] = 0. \tag{9}$$

The displacements can be expressed as algebraic sums of partial derivatives of a scalar potential $\Phi(x, y)$ and a vector potential $\Psi(x, y)$, in the following way (Phillips, 1933, p. 186):

$$u = \frac{\partial \Phi}{\partial x} + \frac{\partial \Psi}{\partial y}, \tag{10}$$

$$v = \frac{\partial \Phi}{\partial y} - \frac{\partial \Psi}{\partial x}. \tag{11}$$

Substituting derivatives of equations (10) and (11) into equations (7) and (8) gives the

equations of equilibrium in terms of the two potentials:

$$(\lambda + 2G)\frac{\partial}{\partial x}(\nabla^2\Phi) + G\frac{\partial}{\partial y}(\nabla^2\Psi) = 0, \quad (12)$$

$$(\lambda + 2G)\frac{\partial}{\partial y}(\nabla^2\Phi) - G\frac{\partial}{\partial x}(\nabla^2\Psi) = 0. \quad (13)$$

Differentiating equation (12) with respect to x and equation (13) with respect to y and adding the two equations gives:

$$\nabla^2(\nabla^2\Phi) = 0. \quad (14)$$

Similarly, differentiating equation (12) with respect to y and equation (13) with respect to x and subtracting one equation from the other gives:

$$\nabla^2(\nabla^2\Psi) = 0. \quad (15)$$

Equations (14) and (15) require that Φ and Ψ be either harmonic ($\nabla^2\Phi = 0$) or biharmonic functions ($\nabla^4\Phi = 0$). Substitution of partial derivatives of equations (10) and (11) into the equations for σ_x and σ_y (equations 4 and 5) and summing the results gives:

$$\sigma_x + \sigma_y = 2(\lambda + G)\nabla^2\Phi. \quad (16)$$

The sum of σ_x and σ_y is zero when Φ is a harmonic function. This condition cannot be satisfied by deformed layers (for example, at a free surface where $\sigma_y = 0$ everywhere and σ_x has finite values). Therefore Φ must be a biharmonic function.

The solutions for Φ and Ψ must satisfy the biharmonic differential equations and prescribed boundary conditions. Of interest here is the deformation of an elastic layer of thickness H which has the following stresses and displacements specified on its boundaries:

At $y = 0$, $\sigma_y = 0$, and $\tau_{xy} = 0$ (stresses zero);

At $y = H$, $v = -B\cos\alpha x$, and $u = BP\sin\alpha x$,

where $0 \leq P < 1$.

The lower surface of the layer undergoes vertical and horizontal displacements proportional to the cos αx and sin αx, respectively. Assume that the vertical and horizontal displacements within the layer are also proportional to the cos αx and sin αx. Equations (10) and (11), which express displacements in terms of the potential functions, indicate that the above distribution of displacements may be possible with potential functions of the form:

$$\Phi = \cos\alpha x\, F(y), \quad (17)$$

$$\Psi = \sin\alpha x\, f(y). \quad (18)$$

At this point, there is no guarantee that equations (17) and (18) will lead to a solution of the problem. Equations (17) and (18) are the correct expressions for the potential functions only if the stresses and displacements derived from them satisfy equations (1) through (3) and the prescribed boundary conditions.

$F(y)$ and $f(y)$ can be determined by substituting equations (17) and (18) into equations (14) and (15) and solving the resulting fourth-order differential equations. This leads to general expressions for Φ and Ψ.

$$\Phi = \cos\alpha x[A_1e^{\alpha y} + A_2ye^{\alpha y} + A_3e^{-\alpha y} + A_4ye^{-\alpha y}], \quad (19)$$

$$\Psi = \sin\alpha x[A_5e^{\alpha y} + A_6ye^{\alpha y} + A_7e^{-\alpha y} + A_8ye^{-\alpha y}], \quad (20)$$

where A_1 through A_8 are arbitrary constants.

Equations (19) and (20) contain eight arbitrary constants, whereas only four boundary conditions are specified in the problem. Four extra arbitrary constants appear in the equations for the potential functions as a result of (1) expressing the displacements as partial derivatives of potential functions (equations 10 and 11), and (2) differentiating the equations of equilibrium to obtain the two biharmonic equations. Some of the constants in the general expressions for Φ and Ψ are related. Substituting equations (19) and (20) into equations (12) and (13) gives:

$$A_6 = \left(\frac{\lambda + 2G}{G}\right)A_2 = \frac{2(1-\nu)}{1-2\nu}A_2 = K_1A_2, \quad (21)$$

$$A_8 = -\left(\frac{\lambda + 2G}{G}\right)A_4 = -\frac{2(1-\nu)}{1-2\nu}A_4 = -K_1A_4. \quad (22)$$

These relationships eliminate two of the extra constants.

The remaining two extra constants were eliminated by trial and error until equations for Φ and Ψ were found which satisfied the four boundary conditions and the equations of equilibrium and compatibility. The equations for Φ and Ψ satisfying the requirements for a solution of stress and strain in the elastic layer are:

$$\Phi = \cos\alpha x[A_1(e^{\alpha y} + e^{-\alpha y}) + A_2ye^{\alpha y} + A_4ye^{-\alpha y}], \quad (23)$$

$$\Psi = \sin\alpha x[A_5(e^{\alpha y} + e^{-\alpha y}) + K_1A_2ye^{\alpha y} - K_1A_4ye^{-\alpha y}]. \quad (24)$$

The constants in the above equations are equal to:

$$A_1 = 0,$$

$$A_2 = \frac{B\alpha C_2}{N} = \frac{B\alpha}{N} \cdot \{K_3[(1 - P)e^{\alpha H} - (1 + P)(1 + 2\alpha H)e^{-\alpha H}] - 2(K_1 - P)e^{-\alpha H}\}, \quad (25)$$

$$A_4 = \frac{B\alpha C_4}{N} = \frac{B\alpha}{N} \cdot \{K_3[(1 + P)e^{-\alpha H} + (1 - P)(2\alpha H - 1)e^{\alpha H}] - 2(K_1 + P)e^{\alpha H}\}, \quad (26)$$

$$A_5 = \frac{BC_5}{N} = -\frac{BK_3}{N} \cdot [(K_1 + \alpha H P K_3)(e^{\alpha H} + e^{-\alpha H}) + (P - \alpha H K_3)(e^{\alpha H} - e^{-\alpha H})], \quad (27)$$

where

$$N = \alpha N_1 = \alpha[K_3(2 - e^{2\alpha H} - e^{-2\alpha H}) - K_1 K_3(2 + e^{2\alpha H} + e^{-2\alpha H}) + 4\alpha^2 H^2 K_3^2 + 4K_1], \quad (28)$$

and

$$K_3 = (1 - K_1) = -\frac{1}{1 - 2\nu}. \quad (29)$$

The general equations for v, u, σ_y, σ_x, and τ_{xy} are:

$$v = \frac{B \cos \alpha x}{N_1}[C_2 e^{\alpha y}(\alpha y K_3 + 1) - C_4 e^{-\alpha y}(\alpha y K_3 - 1) - C_5(e^{\alpha y} + e^{-\alpha y})], \quad (30)$$

$$u = \frac{B \sin \alpha x}{N_1}[-C_2 e^{\alpha y}(\alpha y K_3 - K_1) - C_4 e^{-\alpha y}(\alpha y K_3 + K_1) + C_5(e^{\alpha y} - e^{-\alpha y})], \quad (31)$$

$$\sigma_y = \frac{2GB\alpha \cos \alpha x}{N_1} \cdot [C_2 K_3 \alpha y e^{\alpha y} + C_4 K_3 \alpha y e^{-\alpha y} - C_5(e^{\alpha y} - e^{-\alpha y})], \quad (32)$$

$$\sigma_x = -\sigma_y + \frac{2GB\alpha \cos \alpha x}{N_1} \cdot [-2K_3(C_2 e^{\alpha y} - C_4 e^{-\alpha y})], \quad (33)$$

$$\tau_{xy} = \frac{2GB\alpha \sin \alpha x}{N_1}[C_5(e^{\alpha y} + e^{-\alpha y}) - C_2 K_3 e^{\alpha y}(\alpha y + 1) + C_4 K_3 e^{-\alpha y}(\alpha y - 1)]. \quad (34)$$

Also of interest in elastic analysis are the equations for the principal stresses. The principal stresses at a point within a stressed layer are the stress values normal to three perpendicular planes across which the shearing stresses vanish. In a two-dimensional analysis, the intermediate principal stress (σ_2) parallels the z-axis. The equations for the principal stresses in terms of σ_x, σ_y, and τ_{xy} are:

$$\sigma_1 = \frac{\sigma_x + \sigma_y}{2} + \sqrt{\left(\frac{\sigma_x - \sigma_y}{2}\right)^2 + \tau_{xy}^2}, \quad (35)$$

$$\sigma_3 = \frac{\sigma_x + \sigma_y}{2} - \sqrt{\left(\frac{\sigma_x - \sigma_y}{2}\right)^2 + \tau_{xy}^2}. \quad (36)$$

The response of an elastic layer to general distributions of displacement along its lower boundary can be determined by superposing equations of the type which have been shown herein (Timoshenko and Goodier, 1951, p. 235). Combination of equations is accomplished by means of a Fourier series, which can be used to approximate a variety of geologically reasonable displacements at the base of a sedimentary layer.

Superposition can also be used to incorporate into the equations an initial state of stress due to the weight of the layer. In this work, a state of hydrostatic stress:

$$\sigma_x = -\rho g y, \quad \sigma_y = -\rho g y, \quad \text{and} \quad \tau_{xy} = 0,$$

which satisfies the equilibrium and compatibility requirements, has been superposed with stresses arising from the deformation of the layer. This superposition of equations gives the correct stress values for layers which are assumed to be in hydrostatic equilibrium prior to deformation.

Application of Analytical Method to Examples

The internal stress distribution of a deformed elastic layer can be portrayed by a set of orthogonal curves called stress trajectories. These stress trajectories are tangent to the directions of the principal stresses at all points within the layer. The equation for the direction of one of the principal stresses (σ_1 or σ_2) in the two-dimensional case is:

$$\tan 2\beta = \frac{2\tau_{xy}}{\sigma_x - \sigma_y}, \quad (37)$$

where β is the angle between the positive x-axis and the principal stress measured in the direction of the positive y-axis. In the numerical examples discussed in following sections, a graphical construction of the stress trajectories

was made on the basis of β values computed for a grid of points within the layer.

The only factors which influence the orientations of the stress trajectories are the shape of the layer (ratio of H to L) and Poisson's ratio. Rigidity (G), maximum applied vertical displacement (B), and hydrostatic stress cancel out of equation (37). The shape of the layer (H/L) and Poisson's ratio appear in the stress equations through the constants K_1, K_3, C_2, C_4, and C_5.

The distribution of displacement in a deformed layer can be portrayed by a field of displacement vectors. The orientation and length of each vector indicate the direction and magnitude of the net displacement at the point from which the vector originates.

The only factors which influence the orientations and relative magnitudes of the displacement vectors are the shape of the layer and Poisson's ratio. Rigidity (G) does not appear in the displacement equations. The shape of the layer (H/L) and Poisson's ratio enter into the displacement expressions through constants K_1, K_3, C_2, C_4, and C_5.

Stress distributions and displacement fields of different examples can be compared if each numerical example sustains an amount of applied displacement which is just necessary to initiate fracture at some point within the layer. In the numerical examples which follow, displacements necessary to initiate fracture were computed on the basis of a special case of the Mohr fracture criterion. The equation for this fracture criterion is:

$$\tau = \tau_0 - \sigma \tan \phi, \tag{38}$$

where τ and σ are the shearing and normal stresses across a potential fracture plane, τ_0 is the shear stress necessary to overcome the initial shear strength due to cohesion, and ϕ is the angle of internal friction. The shear strength is dependent on the type of stress (tensile or compressive) and the amount of confining (hydrostatic) stress. The criterion is diagrammed in Figure 2.

This special form of the Mohr criterion was selected because it satisfactorily describes the shear strength of many sedimentary rocks under the confining pressures encountered at depth in sedimentary basins (1000–2000 kg/cm²) (Jaeger, 1956, p. 82). For zero or low confining pressures, the criterion may not explain tensile fracture of rock subjected to tensile stress. Inasmuch as present experimental data are inadequate for establishing a fracture criterion for rocks under tension, the assumption was made that the Mohr criterion does describe fracture under tensile stresses.

Critical displacements in the numerical examples were determined as follows:

(1) Principal stresses were found for a grid of points by substituting computed values of σ_x, σ_y, and τ_{xy} into equations (35) and (36). However, in computing these stresses, B (which appears in the equations for σ_x, σ_y, and τ_{xy}) was not given a value. By carefully examining these computed principal stresses, all but a few points in the layer could be eliminated as probable points of fracture.

(2) A displacement (B) necessary to initiate fracture at each of the probable points of fracture was found by substituting the values of the principal stresses (expressed as fractions of B plus a hydrostatic stress term) into a rearranged form of equation (38):

$$\left|\frac{\sigma_1 - \sigma_3}{2}\right| = \tau_0 \cos \phi - \left(\frac{\sigma_1 + \sigma_3}{2}\right) \sin \phi, \tag{39}$$

and solving for B.

(3) The point giving the smallest value of B was selected as the point of fracture, and the computed B was taken as the critical displacement B_c.

The Mohr criterion explains satisfactorily the shear strength of brittle materials which are generally elastic up to the point of fracture. However, some materials, after an initial period of elastic deformation, yield by plastic flow rather than by fracture. In the elastic region of the deformation, the analysis of stress and displacement is the same regardless of the type of failure which occurs. The initiation of plastic flow, however, is probably controlled by a different condition than fracture in brittle substances. Flow is believed to occur when the strain energy of distortion per unit volume reaches a value characteristic of the material (Jaeger, 1956, p. 93). The formula for this criterion in the two-dimensional plane strain case is (Timoshenko and Goodier, 1951, p. 149):

$$E_d = \frac{1}{12G}\{[\sigma_x - \sigma_y]^2 + [\sigma_y - \nu(\sigma_x + \sigma_y)]^2 + [\nu(\sigma_x + \sigma_y) - \sigma_x]^2 + 6\tau_{xy}^2\}. \tag{40}$$

This criterion, credited to R. von Mises, differs from the Mohr criterion in that initiation of plastic flow is independent of confining stress

and occurs regardless of whether the stresses are tensile or compressive.

In the numerical examples, values of distortional strain-energy density were calculated using the values of stress dictated by the Mohr fracture criterion. The values obtained in this manner are not related to any characteristic values for rock materials. However, the distributions of distortional strain-energy density do show the regions susceptible to flow in materials which favor this mode of failure.

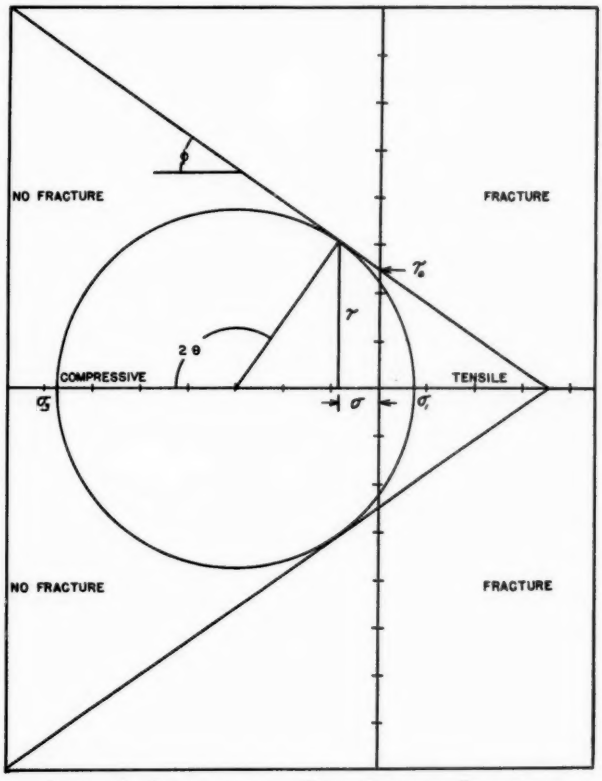

FIGURE 2.—DIAGRAM OF THE MOHR FRACTURE CRITERION

τ and σ are the shearing and normal stresses across a potential fracture plane, τ_0 is the shear strength due to cohesion, ϕ is the angle of internal friction, and θ is the angle between the stress trajectory and the line of fracture.

Numerical Examples

Introduction.—Table 1 summarizes the numerical calculations. The examples are categorized according to the nature of the displacement specified along the lower boundary of the elastic layer (see Fig. 3). In Category I, the lower boundary of an elastic layer undergoes sinusoidal vertical displacement and no horizontal displacement. Equations (25) through (34) (with $P = 0$) were used for the numerical examples in the first category. In Category II, the lower boundary of an elastic layer undergoes an approximate step in vertical displacement and no horizontal displacement. Eight solutions of the type given by equations (25) through (34) (with $P = 0$) were superposed by means of a Fourier series to obtain the numerical example in this category. In Category III, the lower boundary of an elastic layer undergoes sinusoidal vertical and horizontal (90° out of phase with the vertical) displace-

ments. Equations for the numerical example in this category are given in a later section.

The boundary conditions at the upper surface of the elastic layer are $\sigma_y = 0$ and $\tau_{xy} = 0$. The cohesive strength, 250 kg/cm², was calculated from crushing-strength data on sedimentary rocks (Birch *et al.*, 1942, p. 116; Marin, 1952, p. 381; Mills *et al.*, 1955, p. 310)

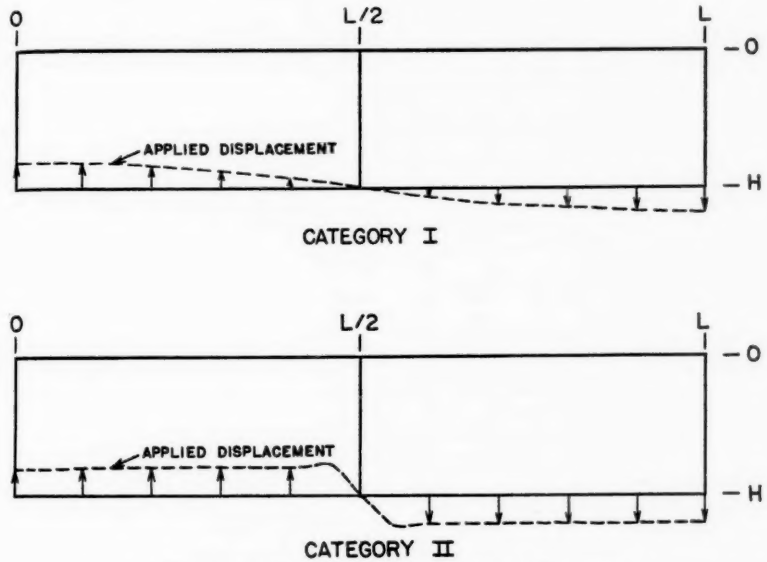

FIGURE 3.—CLASSIFICATION OF NUMERICAL EXAMPLES

Applied vertical displacement in Category I is sinusoidal; applied vertical displacement in Category II is an approximate step.

These conditions specify a free upper surface which corresponds to the surface of the earth. In Categories I and II, the boundary conditions on the lower surface are (1) no horizontal displacement and (2) a specified distribution of vertical displacement. The latter conditions approximate the situation along the lower surface of an elastic sedimentary layer which is deformed by vertical movement of rigid bedrock beneath it. The contact between rigid bedrock and elastic sedimentary rock is "welded" so that horizontal movement along the contact is prevented.

Average values of the properties of sedimentary rocks are used in each example. The density, 2.5 gms/cm³, and Poisson's ratio, 0.25, are based on the values listed in Birch *et al.* (1942, p. 8–37, 76). The rigidity value adopted, 2.0×10^{11} dynes/cm², is Gutenberg's estimate of rigidity for Tertiary sandstone at a depth of 2 km (Gutenberg, 1951, p. 367). The angle of internal friction, 35°, is based on experimental evidence cited by Hubbert (1951). and the adopted angle of internal friction of 35°.

Results of the numerical calculations are diagrammed in Figures 4–6 and 10. These figures are drawn for a short portion of a layer between the limits $x = 0$ and $x = L$. However, the symmetry of the problem permits visualization of results for longer layers if the drawings are rotated 180° about vertical axes in the plane of the figure.

The displacements shown in these figures are only those resulting from the application of vertical displacements on the lower boundary of the layer. The stress values, on the other hand, include the initial hydrostatic stresses as well as the stresses arising from the deformation of the layer.

Category I examples.—Displacement fields for Category I examples are shown in Figures 4*A* and 5*A*. Theoretically, two factors influence the relative magnitudes and orientations of the displacement vectors in these figures—the dimensions of the layer and Poisson's ratio.

TABLE 1.—SUMMARY OF THE NUMERICAL EXAMPLES

		Category I		Category II	Category III
Boundary Conditions	At $y = 0$	$\sigma_y = 0; \tau_{xy} = 0$		$\sigma_y = 0; \tau_{xy} = 0$	$\sigma_y = 0; \tau_{xy} = 0$
	At $y = H$	$v = -B \cos \frac{\pi x}{L}$; $u = 0$		$v = \frac{4B}{\pi} \sum_{n=1}^{8} \frac{(-1)^{n+1}}{(2n-1)} \cdot \cos(2n-1) \frac{\pi x}{L}$; $u = 0$	$\sigma_y = -A \sin \frac{\pi x}{L}$; $\tau_{xy} = 0$
Examples		Ia	Ib	IIa	IIIa
1. Dimensions of layer					
H—km		5	5	5	5
L—km		25	15.7	25	15.7
2. Elastic properties					
ν—Poisson's ratio		0.25	0.25	0.25	0.25
G—10^{-11} dynes/cm²		2.0	2.0	2.0	2.0
3. Fracture properties					
ϕ—degrees		35	35	35	35
τ_0—kg/cm²		250	250	250	250
4. Fracture point location					
x		0	0	$0.375L$	$L/2$
y		0	0	0	0
5. Magnitude and location of maximum stresses					
σ_x—kg/cm²		−1261	−1275	−1578	−1508
x		0	0	$0.45L$	$L/2$
y		H	H	H	H
σ_y—kg/cm²		−1282	−1324	−2229	−1292
x		0	0	$0.45L$	$L/2$
y		H	H	H	H
τ_{xy}—kg/cm²		74	103	489	63
x		$L/2$	$L/2$	$L/2$	0
y		H	H	H	$H/2$
6. Magnitude and location of maximum displacements at the upper boundary					
v—meters		7.8	3.9	3.7	5.7
x		0	0	0	$L/2$
u—meters		3.8	2.4	3.0	2.5
x		$L/2$	$L/2$	$L/2$	0
7. Magnitude and location of maximum displacements at the lower boundary					
v—meters		8.2	4.5	3.7	5.8
x		0	0	.....	$L/2$
u—meters		0	0	0	2.4
x		—	—	—	0

Figure 7 shows the relative changes in the maximum displacements at the boundaries with changes in these factors. The shape of the layer has a strong influence on the displacement field, whereas Poisson's ratio has little effect.

The stress distributions for Category I examples are shown in Figures 4*B* and 5*B*. The orientations of the stress trajectories in these figures are determined by the shape of the layer (H/L) and Poisson's ratio. Comparison of

Figures 4*B* and 5*B* shows the influence of shape on the direction of the stress trajectories. Stress distributions calculated for two other examples (layer dimensions same as Fig. 4*B*) with Poisson's ratios of 0.167 and 0.333 were nearly identical in appearance. Between these two values, orientation of stress trajectories is nearly independent of variations in Poisson's ratio.

Of interest in the stress diagrams (Figs. 4*B* and 5*B*) is the area of horizontal tensile stress centered over the crest of the deformed layer and extending to a depth of approximately 1 km. Inasmuch as rocks are very weak under tensile stress, point *F* on Figures 4*B* and 5*B*, where the tensile stresses are greatest, is the point of initial fracture. For brittle rock, the type of fracture under the stress conditions at *F* is a vertical crack (Jaeger, 1956, p. 74). The maximum applied displacement or critical displacement before fracture occurs at *F* in Figures 4*B* and 5*B* is 8.2 and 4.5 m, respectively.

Two regions are equally susceptible to yielding by plastic flow according to the distortional strain-energy density distributions in Figures 4*C* and 5*C*. One region is centered over the crest of the deformed layer, the other is centered in the trough of the deformed layer. The high distortional strain-energy at the crest of the fold reaches a maximum value at the point of fracture determined by the Mohr criterion. Fracture does not occur in the other region of high distortional strain-energy, inasmuch as the compressive stresses in this region are insufficient to initiate fracture according to the Mohr criterion.

Category II example.—Figure 6.1 shows the displacement field for the Category II example. The influence of layer shape on the maximum displacements at the boundaries is given in Figure 8.

Figure 6*B* shows the stress distribution for the Category II example. Two features are notable. First, most of the vertical stress along the bottom of the layer is concentrated toward the ends of the adjoining uplifted and downdropped blocks. Second, the stresses in the central regions of the uplifted and downdropped blocks are nearly zero if initial hydrostatic stresses are disregarded. Both these features indicate that deformation of the layer is restricted to the region where the two blocks meet. In addition, the lack of stress in the central regions of the layer indicates that a uniform displacement superposed on any of the examples will not change the stress distribution. Therefore the results shown in Figures 4*B*, 5*B*, and 6*B* are also solutions for examples in which all vertical displacements applied along the lower boundary are in one direction.

In Figure 6*B*, a region of nearly horizontal tensile stress lies just to the left of $x = L/2$, $y = 0$ and extends to a maximum depth of 1 km. The point of initial fracture (F_1) is at $x = 0.375L$, $y = 0$, where these tensile stresses are greatest. The type of fracture under the stress conditions at F_1 is a vertical tensile crack. The amount of applied vertical displacement required to initiate fracture at F_1 is 3.7 m.

The same applied displacement will cause fracture at F_2 ($x = 0.53L$, $y = H$) as well as F_1 if the fracture properties (τ_0 and ϕ) of the layer are changed. Figure 9 shows the conditions under which fracture will occur simultaneously at F_1 and F_2. The stresses at F_2 are compressive in both the *x*- and *y*-directions. The type of failure for brittle rock under these stress conditions is a shear fracture.

Two separate regions of high distortional strain-energy density occur along the upper boundary of the layer (Fig. 6*C*). The maximum value in each of these regions is equal to the maximum values found in the Category I examples. The highest distortional strain-energy concentration occurs at the bottom of the layer directly above the point at which the rate of change of applied displacement is greatest.

Scope of numerical examples in Categories I and II.—Theoretically, two factors influence the orientations of the displacement vectors and the stress trajectories—the dimensions of the layer and Poisson's ratio. The calculations which have been described indicate that layer shape has a strong influence on these orientations, whereas Poisson's ratio has little effect. As a result, the numerical solutions given here are applicable to any homogeneous elastic layer providing (1) its shape is the same as the shape of the layer in the example, and (2) an appropriate scaling factor is used to determine the magnitudes of stress in the stress diagram. The scaling factor is based on the rigidity of the layer and the maximum applied displacement. The maximum applied displacement must be less than the amount of displacement necessary to initiate fracture.

Elastic properties of the layer do not have to be known for a comparison of elastic analyses and scale-model experiments. Displacements and fractures (see "Prediction of fractures"), the only items easily observed in model experiments, are independent of the elastic constants in the elastic analyses. Therefore,

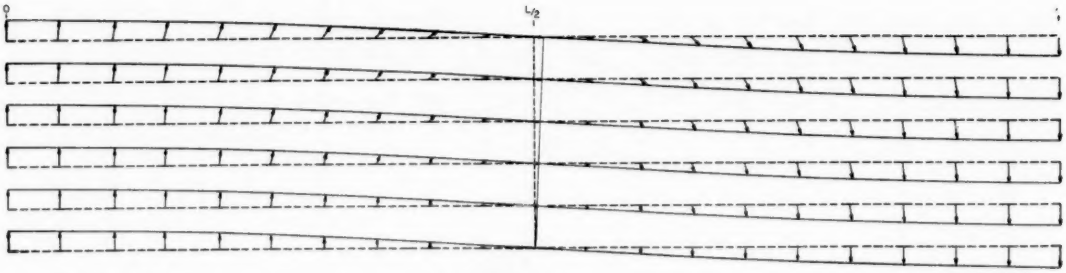
0
L/2
0 1 2 KM
HORIZONTAL-VERTICAL DISTANCES
BEFORE DEFORMATION
AFTER DEFORMATION
0 10 20 30 M
HORIZONTAL-VERTICAL DISPLACEMENT

A

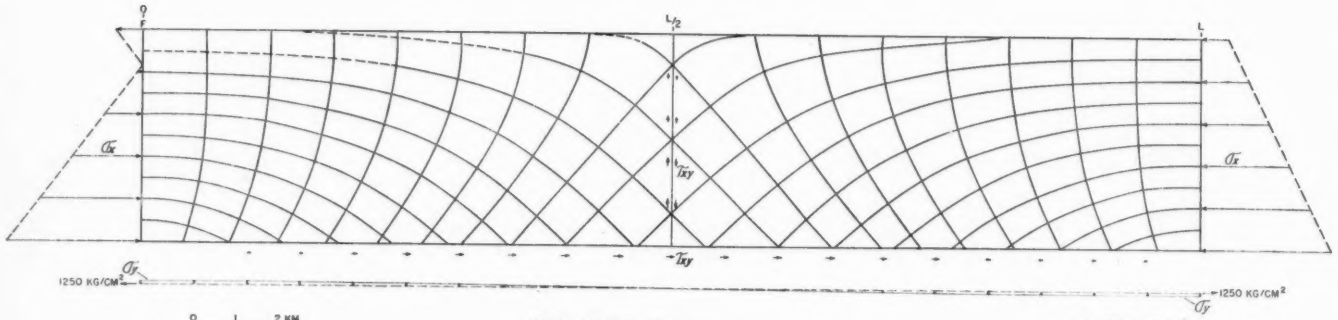
0
L/2
L
σx
τxy
σy
1250 KG/CM²
1250 KG/CM²
0 1 2 KM
HORIZONTAL-VERTICAL DISTANCES
TENSILE PRINCIPAL STRESS
COMPRESSIVE PRINCIPAL STRESS
0 200 400 600 KG/CM²
STRESSES

B

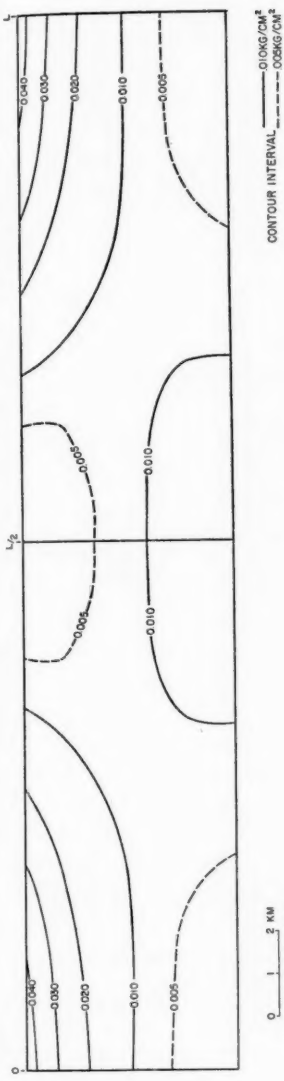

FIGURE 4.—EXAMPLE Ia DIAGRAMS: *A*—DISPLACEMENT FIELD; *B*—STRESS DISTRIBUTION; *C*—DISTORTIONAL STRAIN-ENERGY DENSITY
In example Ia, the lower boundary of an elastic layer 5 km thick and 25 km long undergoes half a wave length of sinusoidal vertical displacement.

geometrical similarity of layer shapes is the only requirement for a comparison between a two-dimensional elastic analysis and a two-dimensional scale model.

Category III example.—A "welded" contact, which is specified along the lower boundary in Categories I and II examples, is one extreme of many possible contact conditions. The opposite extreme is a "frictionless" contact. The frictionless lower-boundary case was analytically investigated to determine the effect of contact conditions on deformation resulting from a sinusoidal distribution of vertical displacement.

A frictionless condition at the lower boundary means that the shearing stress is zero along that boundary. The magnitude of applied horizontal displacement which gives zero shearing stress along the lower boundary is difficult to compute. The easiest approach is to specify stresses on the lower boundary as Hafner (1951) did in his work.

The solution of problems in which all boundary conditions are expressed in terms of stress reduces to the solution of a single biharmonic equation which will lead to stresses satisfying equilibrium (equations 1 and 2), compatibility (equation 3), and the prescribed boundary conditions. Of interest here is the deformation of an elastic layer of thickness H under the following boundary conditions:

$$\text{At } y = 0, \quad \sigma_y = 0, \quad \tau_{xy} = 0 \qquad \text{(stresses zero)};$$

$$\text{At } y = H, \quad \sigma_y = -A \sin \alpha x, \quad \tau_{xy} = 0.$$

The biharmonic equation and the boundary conditions are satisfied by:

$$\Phi = \sin \alpha x [D_1 \cosh \alpha y + D_2 \sinh \alpha y + D_3 y \cosh \alpha y + D_4 y \sinh \alpha y]. \quad (41)$$

The constants in equation (41) are equal to:

$$D_1 = 0,$$

$$D_2 = -\frac{D_3}{\alpha} = \frac{D_4 k_1}{\alpha} = \frac{D_4}{\alpha}\left[\frac{\sinh \alpha H + \alpha H \cosh \alpha H}{\alpha H \sinh \alpha H}\right], \quad (42)$$

$$D_3 = -D_4 k_1 = -D_4\left[\frac{\sinh \alpha H + \alpha H \cosh \alpha H}{\alpha H \sinh \alpha H}\right], \quad (43)$$

$$D_4 = \frac{A}{\alpha k_2} = \frac{A}{\alpha[(\alpha H + k_1) \sinh \alpha H - k_1 \alpha H \cosh \alpha H]}. \quad (44)$$

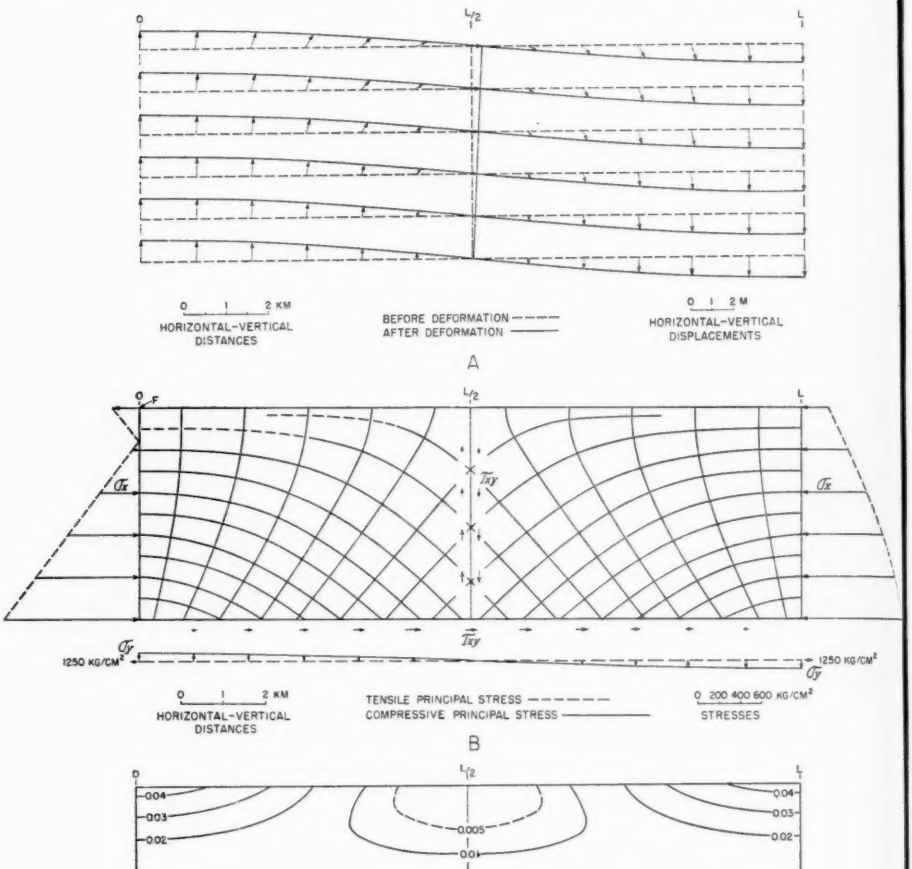

FIGURE 5.—EXAMPLE Ib DIAGRAMS: *A*—DISPLACEMENT FIELD; *B*—STRESS DISTRIBUTION; *C*—DISTORTIONAL STRAIN-ENERGY DENSITY

In example Ib, the lower boundary of an elastic layer 5 km thick and 15.7 km long undergoes half a wave length of sinusoidal vertical displacement.

The general equations for σ_y, σ_x, τ_{xy}, v, and u are:

$$\sigma_y = -\frac{A \sin \alpha x}{k_2} \cdot [(\alpha y + k_1) \sinh \alpha y - \alpha y k_1 \cosh \alpha y], \quad (45)$$

$$\sigma_x = \frac{A \sin \alpha x}{k_2} \cdot [(\alpha y - k_1) \sinh \alpha y + (2 - \alpha y k_1) \cosh \alpha y], \quad (46)$$

$$\tau_{xy} = -\frac{A \cos \alpha x}{k_2} \cdot [(1 - \alpha y k_1) \sinh \alpha y + \alpha y \cosh \alpha y], \quad (47)$$

$$v = \frac{A \sin \alpha x}{2\alpha G k_2} [(1 - 2\nu) \sinh \alpha y + \alpha y k_1 \sinh \alpha y - 2k_1(1 - \nu) \cosh \alpha y - \alpha y \cosh \alpha y] + \text{constant}, \quad (48)$$

$$u = -\frac{A \cos \alpha x}{2\alpha G k_2} [-k_1(1 - 2\nu) \sinh \alpha y + \alpha y \sinh \alpha y + 2(1 - \nu) \cosh \alpha y - \alpha y k_1 \cosh \alpha y] + \text{constant}. \quad (49)$$

The elastic constants appear in the displacement equations, but not in the stress equations.

Table 1 summarizes the results obtained from numerical example IIIa. In example IIIa, a sinusoidal vertical stress is applied to the lower boundary of an elastic layer. The elastic constants and fracture properties for the layer are the same as in the previous examples. The results of the calculations are diagrammed in Figure 10. In addition, calculations were made to determine the influence of layer shape on the relative magnitudes of maximum displacement at the boundaries (Fig. 11). Fracture point and critical displacement were determined by the Mohr fracture criterion (equations 38 and 39).

A comparison of examples IIIa and Ib shows the maximum influence of the conditions at the lower boundary on the deformation resulting from a sinusoidal distribution of applied vertical displacement. The layers in these examples have identical dimensions, elastic constants, and fracture characteristics. Both undergo the same distributions of vertical displacement along the lower boundary. The only difference is the contact between the layer and underlying material. Example IIIa has a frictionless contact, and example Ib has a welded contact.

The following are not greatly affected by the nature of the contact:

(1) The point of initial fracture as determined by the Mohr criterion (compare position of *F* on Figs. 5*B* and 10*B*).
(2) The distribution of vertical and horizontal displacements at the upper boundary as a function of the dimensions of the layer (compare Figs. 7*A* and 11).

The features which change when the lower boundary is frictionless are:

(1) The amount of applied vertical displacement before fracture is slightly greater.
(2) Two additional areas are susceptible to yielding by plastic flow (compare Figs. 5*C* and 10*C*).
(3) Horizontal displacements nearly equal to those on the upper boundary occur along the lower boundary (compare Figs. 5*A* and 10*A*).

If displacement does occur along the lower contact of a layer, it will always be less than the amount found in example IIIa. An absolutely frictionless contact between rock layers is not a reasonable boundary condition in geologic problems. For this reason, most features of the deformation in a homogeneous layer will tend to be closer to those occurring in the "welded" contact case.

Prediction of Fractures

According to the Mohr criterion, fracture occurs along lines which intersect the principal stresses at constant angles. The angle between the line of fracture and the stress trajectories is equal to (see Fig. 2):

$$\theta = 45° \pm \frac{\phi}{2}. \quad (50)$$

The extent to which the stress distributions in the analytical work can be used in predicting fractures with the Mohr criterion is difficult to determine. Any fracturing within the layer changes the stress distribution determined in the elastic analysis. If this change is confined to regions near the fracture, then formation and propagation of fractures are controlled by the original stress distribution. On the other hand, if the change extends a large distance from the fractures, formation and propagation of fractures are controlled by a stress distribution which changes continuously as the fractures are formed. One method of determining whether or not stress distributions from an elastic analysis can be used to predict fractures is to perform experiments.

Experimental Study

Problems Investigated

Two problems similar to the analytical examples were investigated in the scale-model experiments. The first dealt with the deformation of a homogeneous layer resulting from the application of a broad curve in vertical displacement along its lower boundary. The second problem dealt with the deformation of a homogeneous layer resulting from the application of a step in vertical displacement along its lower boundary.

Theory

Only the scale-model theory needed for this discussion is summarized here. A more detailed

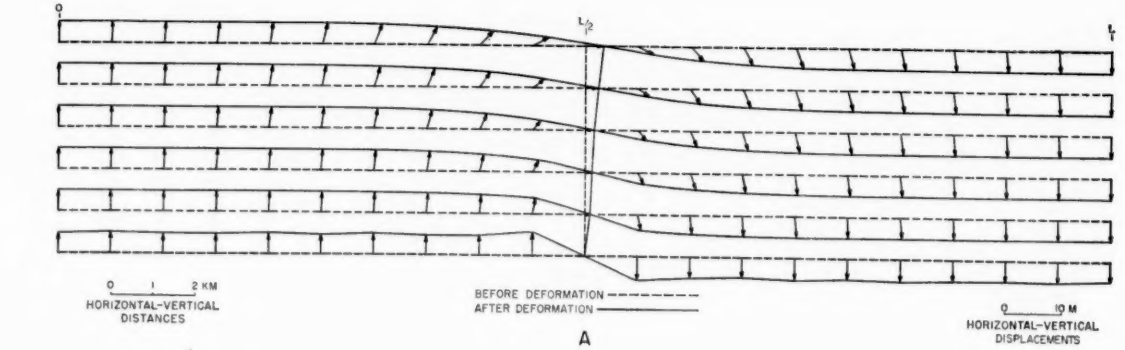
0
L/2
L
0 1 2 KM
HORIZONTAL-VERTICAL DISTANCES
BEFORE DEFORMATION
AFTER DEFORMATION
0 10 M
HORIZONTAL-VERTICAL DISPLACEMENTS

A

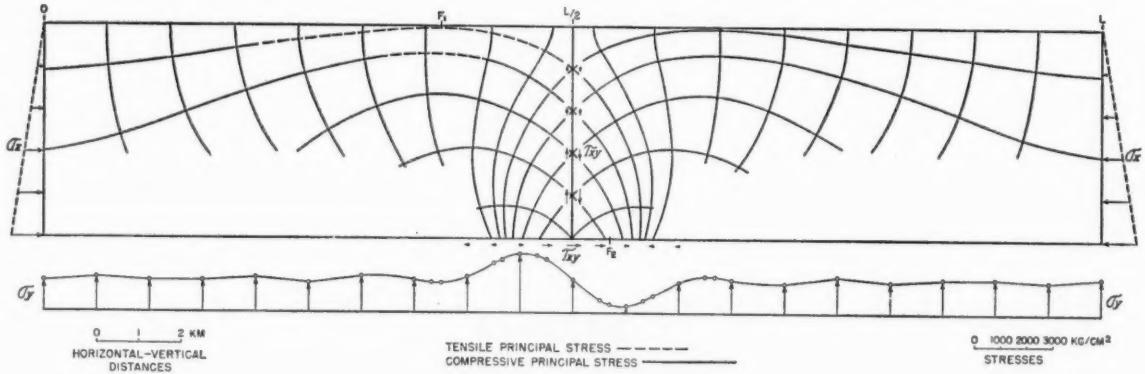
0
F1
L/2
L
σx
σy
τxy
0 1 2 KM
HORIZONTAL-VERTICAL DISTANCES
TENSILE PRINCIPAL STRESS
COMPRESSIVE PRINCIPAL STRESS
0 1000 2000 3000 KG/CM2
STRESSES

B

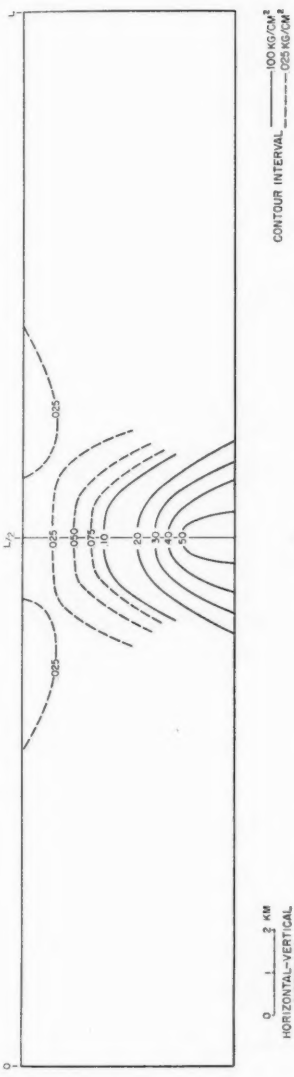

FIGURE 6.—EXAMPLE IIa DIAGRAMS: *A*—DISPLACEMENT FIELD; *B*—STRESS DISTRIBUTION; *C*—DISTORTIONAL STRAIN-ENERGY DENSITY
In example IIa, the lower boundary of an elastic layer undergoes an approximate step in vertical displacement.

account of scale-model theory and its application to geologic problems is given by Hubbert (1937).

A geologic structure and a scale-model representation of the same structure must have certain similarities. The model must be similar in shape to the geologic structure; that is, lengths, areas, and volumes must be proportional:

$$L_m = \lambda L_n ,$$
$$A_m = \lambda^2 L_n^2 , \tag{51}$$
$$V_m = \lambda^3 L_n^3 .$$

(Subscripts m and n indicate model and nature, respectively.) The mass distributions must be similar; that is, the mass for any element of volume in the model must be proportional to the mass of the corresponding element in the geologic structure:

$$dM_m = \mu dM_n . \tag{52}$$

The time required for any given change of shape or position in the model must be proportional to the time required in the geologic structure:

$$T_m = \tau T_n . \tag{53}$$

The constants of proportionality in these equations, λ, μ, and τ, are the model ratios of length, mass, and time, respectively. From these model ratios, it can be seen that dynamic similarity between the model and the original exists if the ratio of each force acting on an element of mass in the model is proportional to the same force acting on the corresponding element of mass in the geologic structure:

$$\frac{dM_m L_m T_m^{-2}}{dM_n L_n T_n^{-2}} = \mu\lambda\tau^{-2} = \phi. \tag{54}$$

In the formation of geologic structures and also in the modeling of these structures, accelerations are generally so small that forces due to inertia are negligible. If inertia forces are negligible, dynamic similarity is completely satisfied (for independent values of the model ratios λ, μ, and τ) as long as all forces conform to the model ratio of the gravity forces (Hubbert, 1937, p. 1489). The geologic structure and the model are subjected to the same gravitational field, therefore, the model ratio of gravity force is:

$$\frac{F_m}{F_n} = \frac{dM_m g}{dM_n g} = \mu. \tag{55}$$

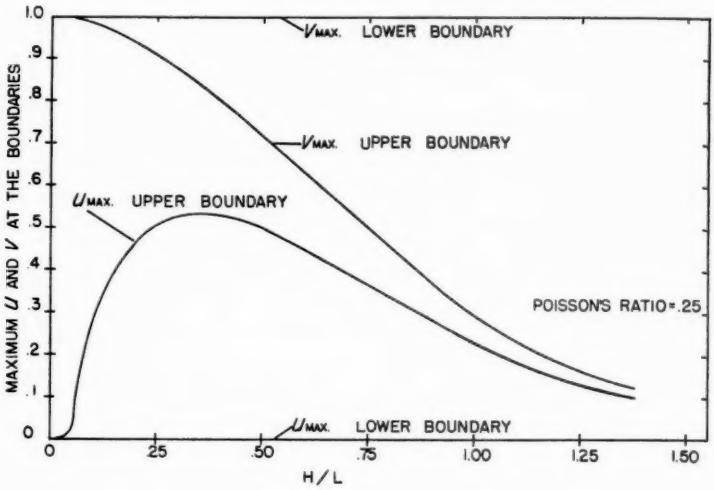

A

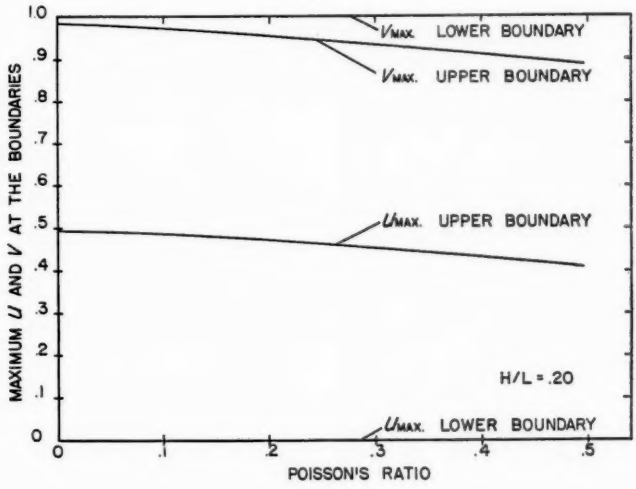

B

FIGURE 7.—CATEGORY I: EFFECT OF LAYER DIMENSIONS AND POISSON'S RATIO ON DISPLACEMENTS AT LAYER BOUNDARIES

A shows relative change in maximum displacements at layer boundaries with change in layer dimensions; *B* shows relative change due to change in value of Poisson's ratio.

From equation (55) the ratio of strength between the model and the original structure is derived:

$$\sigma = \mu\lambda^{-2}. \tag{56}$$

The model ratio of mass can be expressed as:

$$\mu = \delta\lambda^3, \tag{57}$$

where δ equals model ratio of density. Substituting equation (57) into equation (56) gives for the model ratio of strength:

$$\sigma = \delta\lambda. \tag{58}$$

Replacing λ with the ratio of lengths gives:

$$L_m = \frac{\delta L_m}{\sigma}. \tag{59}$$

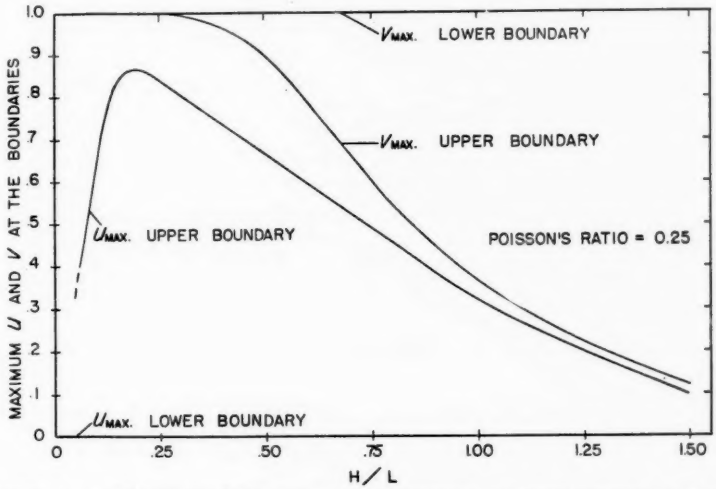

FIGURE 8.—CATEGORY II: EFFECT OF LAYER DIMENSIONS ON DISPLACEMENTS AT LAYER BOUNDARIES

Figure shows relative change in maximum displacements at layer boundaries with change in layer dimensions.

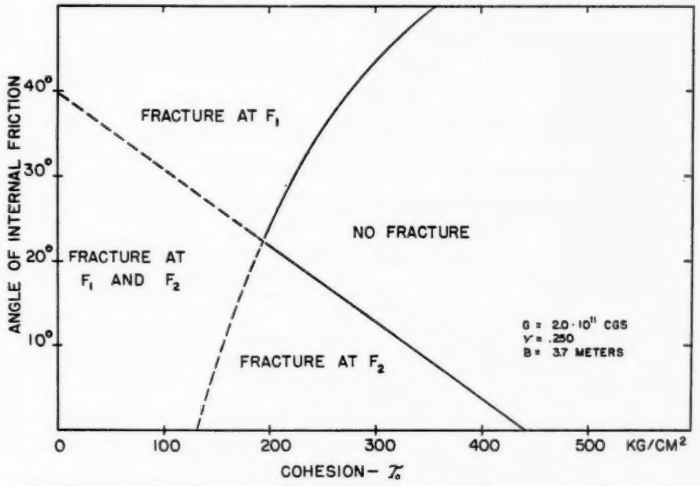

FIGURE 9.—EXAMPLE IIa: FRACTURE POINT LOCATION AS A FUNCTION OF LAYER FRACTURE CHARACTERISTICS

Location of fracture point in example IIa (F_1 or F_2 on Fig. 6*B*) is a function of fracture characteristics of the material of the layer.

Equation (59) can be used to establish the size of the geologic structure being modeled if the model ratios of strength and density are known.

Description of Experiments

Properties of modeling materials.—The composition of the materials used in the experiments was:

Material 1 Beach sand.
Material 2 Beach sand 85 per cent, clay 15 per cent (OM-4 Kentucky-Tenn. Clay Co.).
Material 3 Coarse St. Peter sand (Ottawa Silica Sands, flint shot).
Material 4 Fine St. Peter sand (Ottawa Silica Sands, #102).

Density values for the two degrees of compaction used in the experiments were:

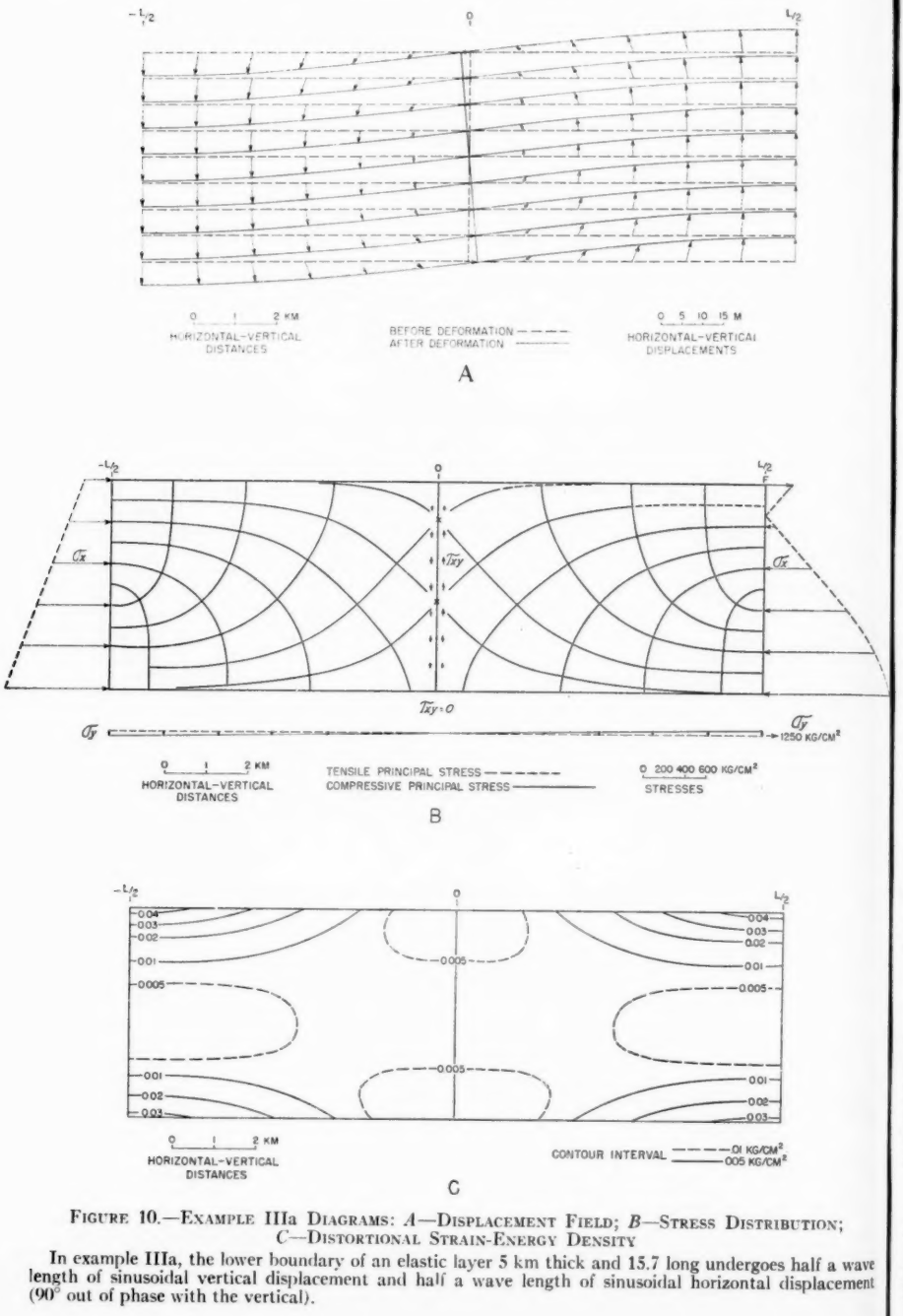

FIGURE 10.—EXAMPLE IIIa DIAGRAMS: *A*—DISPLACEMENT FIELD; *B*—STRESS DISTRIBUTION; *C*—DISTORTIONAL STRAIN-ENERGY DENSITY

In example IIIa, the lower boundary of an elastic layer 5 km thick and 15.7 long undergoes half a wave length of sinusoidal vertical displacement and half a wave length of sinusoidal horizontal displacement (90° out of phase with the vertical).

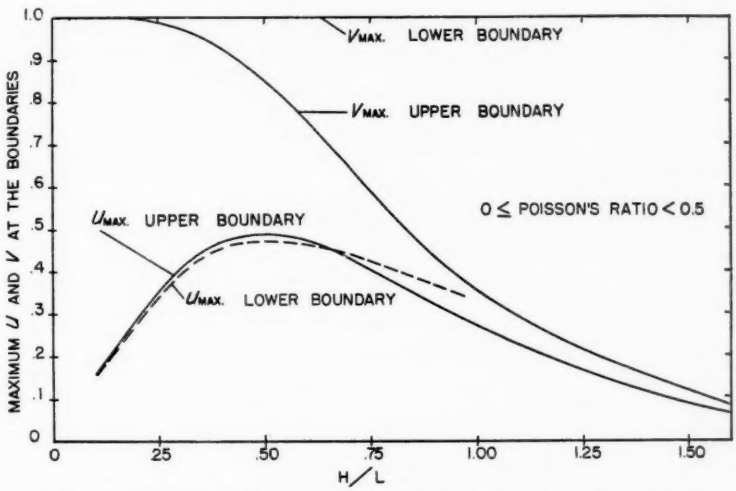

FIGURE 11.—CATEGORY III: EFFECT OF LAYER DIMENSIONS ON DISPLACEMENTS AT LAYER BOUNDARIES

Figure shows relative change in maximum displacements at layer boundaries with change in layer dimensions.

	Uncompacted	*Compacted*
Material 1	1.3 gms/cm³	1.6 gms/cm³
Material 2	1.3	1.7
Material 3	1.5	1.7
Material 4	1.4	1.7

The first value is an average density for the material when it is poured into a container. The second value is an average density for the material when moderately tamped (at approximately 10,000 dynes/cm²).

No water was added to any of the materials used. However, a small percentage of moisture was absorbed from the air. Water-content measurements showed that (1) 2.4 per cent of the total weight of the clay in Material 2 was water, and (2) 0.9 per cent of the total weight of Material 2 was water.

The distribution of grain sizes in the materials is shown in Figure 12.

Numerical values were assigned for the degree of roundness and sphericity of the sand grains by comparing the grain shapes with published charts (Krumbein and Sloss, 1951, p. 81). Grains which approach a perfect sphere have the highest values of roundness and sphericity (maximum value equals 1.0).

	Roundness		*Sphericity*	
	Range	*Average*	*Range*	*Average*
Materials 1 and 2	0.1–0.9	0.45	0.3–0.9	0.65
Material 3	0.8–1.0	0.90	0.8–1.0	0.90
Material 4	0.1–0.9	0.65	0.3–0.9	0.70

Measurements of the strength of the modeling materials were made in two ways. In the first, the fracture characteristics for the material, τ_0 and ϕ, were determined by placing the material in a rectangular container and removing the support for one vertical edge. The angle of fracture caused by removal of support at one vertical edge is related to the angle of internal friction by:

$$\theta = 45° - \frac{\phi}{2}. \tag{60}$$

If the material possesses cohesive strength, an unsupported vertical edge of a thin layer will stand without fracturing. The maximum thickness or critical height (h_{cr}) without fracture is related to the cohesive strength (Tschebotarioff, 1952, p. 169–172):

$$\tau_0 = \frac{\rho g h_{cr}}{4 \tan \theta}. \tag{61}$$

(Equations (60) and (61) assume the special linear case of the Mohr fracture criterion.) Equation (61) does not consider the horizontal tensile stresses introduced by movement of material prior to fracture. These horizontal tensile stresses are located near the surface close to the unsupported edge. Inasmuch as the tensile strength of granular materials is low, vertical tensile fractures form at the surface

before shear fracture occurs lower in the layer. Formation of the tensile cracks reduces the critical height. The maximum depth of the material fractures according to the special linear case of the Mohr criterion. Although the data are scattered at low normal stresses, the

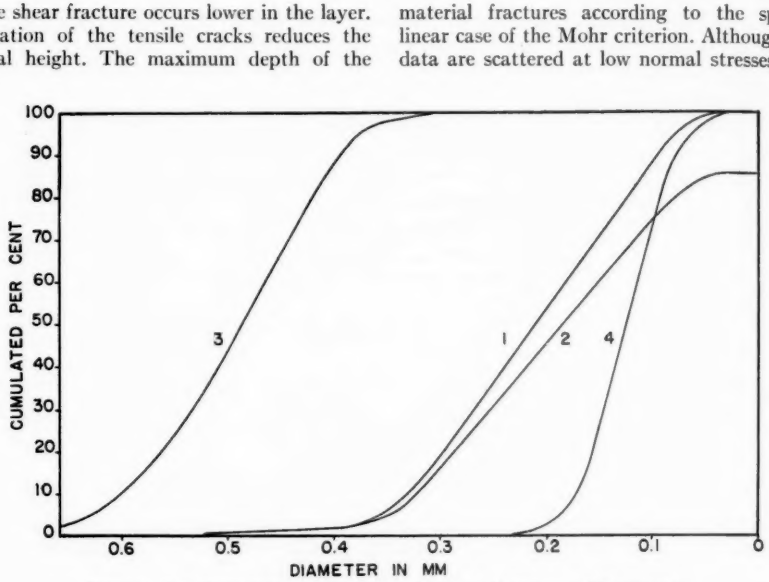

FIGURE 12.—DISTRIBUTION OF GRAIN SIZES IN MODELING MATERIALS

cracks is estimated to be one-half the critical height (Tschebotarioff, 1952, p. 171). Thus, the maximum effect of the tensile cracks can be considered qualitatively by multiplying the observed critical height by $\frac{3}{2}$.

This method was applied to all modeling materials with the following results:

	Uncompacted		*Compacted*	
	τ_0(dynes/cm²)	ϕ	τ_0(dynes/cm²)	ϕ
Material 1	0	34°	0	54°
Material 2	140–210	42°	1100–1700	58°
Material 3	0	22°	0	45°
Material 4	0	27°	0	52°

The strength measurements were taken under conditions similar to those used in the experiments. In the uncompacted tests, material was poured into the box. In the compacted tests, material was placed in the box by layers which were moderately tamped (approximately 10,000 dynes/cm²) after each layer was added.

The second procedure used for measurement of strength was the controlled-strain shear test (Tschebotarioff, 1952, p. 143–145). With these tests, the shear strength of Material 2 was determined under very low confining pressures. Tests were conducted for two degrees of compaction, strong and moderate (Fig. 13). The best curves drawn by eye give the following values of τ_0 and ϕ for Material 2:

	Strong Compaction	*Moderate Compaction*
τ_0	4000 dynes/cm²	1000 dynes/cm²
ϕ	53°	40°

Also plotted on Figure 13 are data for controlled-strain shear tests on moderately compacted dry clay.

Model Apparatus.—The model experiments were performed in a rectangular box (inside dimensions 44.5 by 22.8 by 11.4 cm) with glass sides and wooden ends (Pl. 1). The bottom of the box was fitted with three felt-edged blocks for experiments that required steps in vertical displacement at the base of a layer. Each block could be moved independently in the vertical direction by four screws projecting through the bottom of the box.

The bottom of the box was fitted with a felt-edged rubber pad for experiments that required gradual changes in vertical displacement at the base of a layer. The central and end portions of the rubber pad could be moved independently in the vertical direction by screws projecting through the bottom of the box.

At the two ends of the box were vertical blocks which followed the vertical movement of the end blocks or end portions of the rubber

pad. This feature eliminated the drag which would occur if the ends of the box were fixed.

One feature of the apparatus may influence the experimental results—the drag of the material along the glass face. Theoretically this drag should be zero if the model is to represent accurately the deformation normal to the long axis of a geologic structure. Controlled-strain shear tests were performed to find the coefficient of friction between Material 2 and a glass surface (Fig. 13). The normal stress of Material 2 against the glass face in the box ranged from 0 to 10,000 dynes/cm². The maximum coefficient of friction for this range of normal stress is 0.12. This agrees closely with the coefficient of friction for quartz grains moving over a solid quartz plate (Tschebotarioff, 1952, p. 122–124). Inasmuch as the measured coefficient for Material 2 moving over a glass surface was only one-fifth to one twenty-fifth the coefficient of friction of Material 2 moving over Material 2, drag along the glass face probably did not have a major influence on the experimental results.

Experimental procedure.—Material was placed in the box in successive layers 0.6–1.2 cm thick. These layers were separated by thin marker lines of flour or quartz sand dyed black. The marker lines extended a short distance into the box from the glass face. Two degrees of compaction were used after each layer was added—zero and approximately 10,000 dynes/cm².

Displacements were applied to the base of the layer in small increments. Direct and oblique photographs (Pl. 1) of the model were taken between intervals of displacement. In some instances, several increments of displacement were recorded in a multiple exposure (Pl. 2). This was used to record displacement fields. The total time required for a complete experiment was about 1 hour.

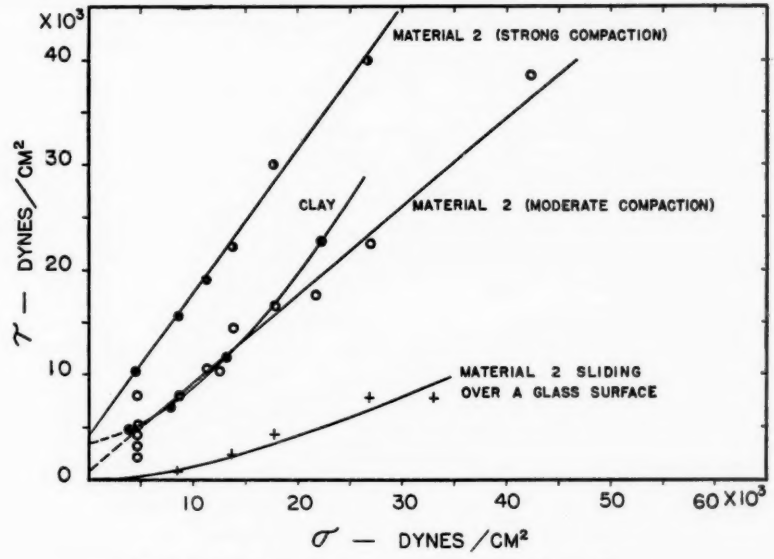

FIGURE 13.—RESULTS OF CONTROLLED-STRAIN SHEAR TESTS

Results of Experiments

General statement.—Two types of experiments were performed in the model studies. In Type I, a broad curve in vertical displacement was applied to the lower boundary of a homogeneous layer. In Type II, a step in vertical displacement was applied to the lower boundary of a homogeneous layer. Layers of each kind of modeling material were used one or more times in both types of experiments. The experiments performed were:

	Experiments With Material				Total
	1	2	3	4	Experiments
Type I	1	2	3	1	7
Type II	2	13	3	1	19

Several figures showing different stages of deformation in the model experiments have been used in the discussion of experimental results. These figures are tracings of photo-

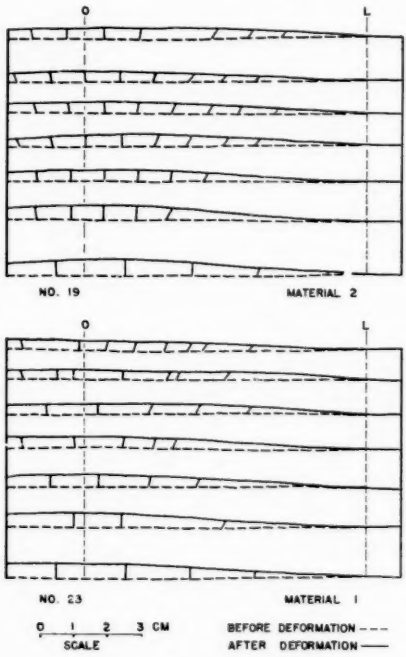

FIGURE 14.—DISPLACEMENT FIELDS—TYPE I EXPERIMENTS

graphs taken during the experiments. The coordinates for the figures are the same as those used in the numerical examples (see Fig. 1).

Type I displacement fields.—Figure 14 gives examples of the observed displacement fields. The important features of the displacement fields were:

(1) No measurable change in the displacement field with a change in the composition of the layer.
(2) An increase in horizontal displacement from the lower to the upper boundary of the layer.
(3) Maximum horizontal displacement at or very near the point of inflection in the fold ($x = L/2$ or $-L/2$).
(4) A decrease in vertical displacement from the lower to the upper boundary of the layer.

Type I fractures with Material 2.—Only models in which layers of Material 2 were used produced fracturing at large displacements (see No. 9 and No. 19 of Fig. 15). The sequence of fracture formation with increase in applied displacement was as follows:

(1) Vertical tensile cracks at the crest of the fold.
(2) A series of normal faults at or near the crest of the fold.
(3) Additional normal faults intersecting the surface at progressevely greater distances from the crest of the fold.

The depth of the tensile cracks was not greater than 1 cm and in most cases was much less. The major normal faults were straight, had maximum displacement at the surface, and dipped toward the axis of the fold. Average dip of the major normal faults was 65°.

The angle of fracture and the depth of the tensile cracks (equivalent to the unsupported height in the strength measurements) can be used to determine the strength of the material in the layer at the time of fracture. The computed angle of internal friction from equation (60) is 40°. The computed cohesive strength from equation (61) is 100—200 dynes/cm^2. These values are nearly identical to the values found in the strength measurements of uncompacted samples of Material 2.

Type I deformation with Materials 1, 3, and 4.—No fracturing was observed in the experiments with layers of Materials 1, 3, and 4 However, a cup-shaped area over the crest of the fold was disturbed by the folding (see No. 23 and No. 21 in Fig. 15). The main features of the disturbed zone were blurring of the marker lines, flattening of the upper boundary, and thinning of the layer. The thinning over the crest of the fold was about 6 per cent of the original thickness for an applied vertical displacement of 1 cm at $x = 0$, $y = H$.

Type II displacement fields.—Figure 16 gives examples of the observed displacement fields. The important features of the displacement fields were:

(1) No measurable change in the displacement field with a change in the composition of the layer.
(2) An increase in horizontal displacement from the lower to the upper boundary of the layer.
(3) Maximum horizontal displacement at or very near $x = L/2$ or $-L/2$ along any horizontal line through the layer.
(4) A progressively less abrupt transition in vertical displacement from the lower to the upper boundary of the layer.

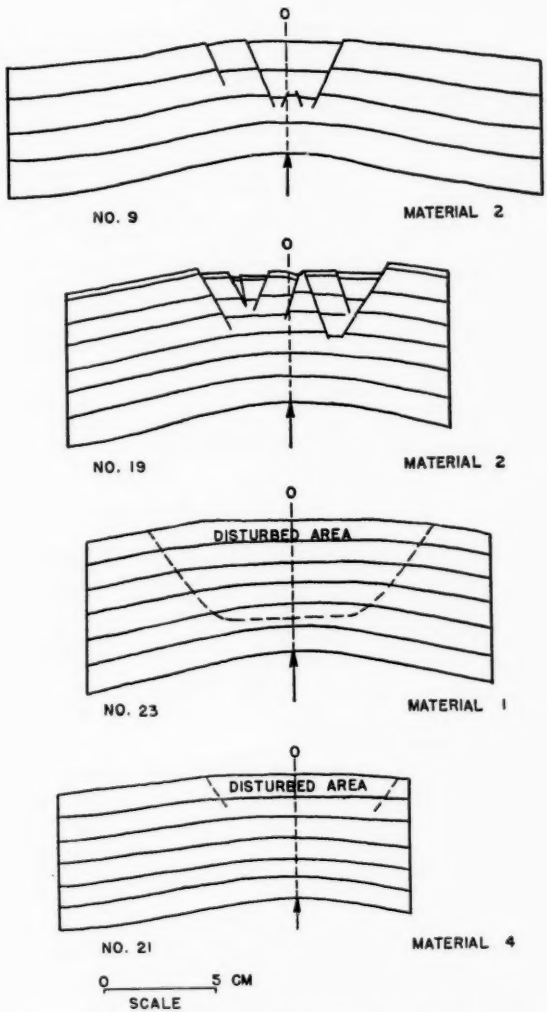

FIGURE 15.—FRACTURING AND FOLDING—TYPE I EXPERIMENTS

Type II fractures with Material 2.—Type II experiments with layers of Material 2 produced distinct fractures at large applied vertical displacements (Fig. 17). The usual sequence of fracture formation with increasing applied vertical displacement was:

(1) Simultaneous or nearly simultaneous formation of tensile cracks at the upper boundary and shear fractures at the lower boundary.
(2) Propagation of one or more shear fractures (reverse faults) to the surface and deepening and widening of the tensile cracks (Fig. 17).
(3) Formation of normal faults in the tensile crack zone (see No. 12 of Fig. 18).
(4) Formation of a major normal fault from the tensile crack zone to the edge of the uplifted block at the lower boundary of layer (see No. 12 of Fig. 18).

In most of the experiments a series of reverse faults rather than a single fault formed at the

edge of the uplifted block. Formation of these fractures followed a definite sequence; progressively younger fractures started at progressively smaller angles to the vertical edge of the uplifted block. The end result was a series of diverging fractures, the oldest starting at about 8° to the vertical, and the youngest starting vertically. Most of the fractures that started at an angle to the vertical propagated only a short distance. Many of these fractures were probably undetected in the experiments. Most of the fractures that started vertically eventually extended all the way to the upper surface. The applied vertical displacement that was required to propagate a shear fracture all the way to the upper surface was equal to about one-twentieth of the total length of the fracture. The same ratio between applied displacement and length of fracture (1 to 20) appeared to hold for all intermediate stages in the development of the fracture as well.

The most interesting feature of the reverse faults (Figs. 17 and 18) was the curvature of the line of fracture away from the uplifted block. Two factors influenced the curvature of the reverse faults, (1) the thickness of the layer, and (2) the number of short reverse faults formed before a particular reverse fault propagated to the surface. The influence of the second factor on curvature was eliminated by omitting the vertical portion of the fractures in the curvature measurements. These measurements were then correlated with an effective thickness (H') for each layer which was equal to the vertical distance over which the fracture actually curved (Fig. 17).

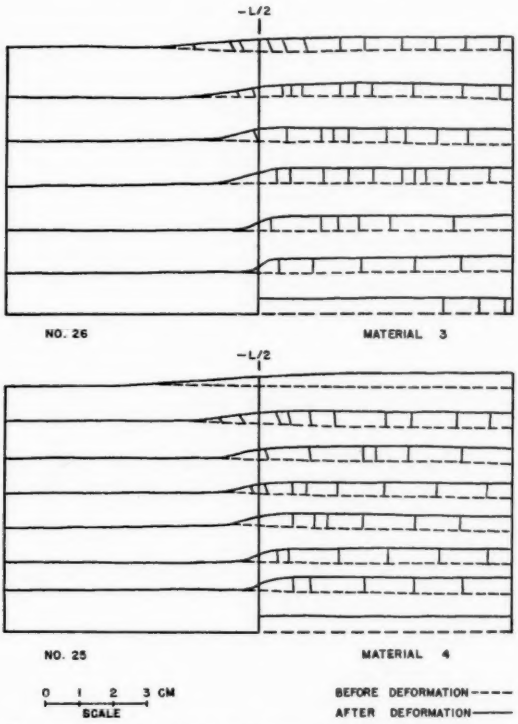

FIGURE 16.—DISPLACEMENT FIELDS—TYPE II EXPERIMENTS

Curvature measurements for three intervals of effective thickness are summarized in Figure 19. Although curvature measurements in adjacent intervals of effective thickness overlap, the mean values in each interval show a small systematic change of curvature with the effective thickness of the layer. With a decrease in the effective thickness, the frac-

tures have (1) progressively greater curvature and (2) progressively lower dip at the upper surface.

were thrust out over the upper surface of the stationary blocks. In one experiment (Fig. 2 of Pl. 2), the horizontal movement of the front

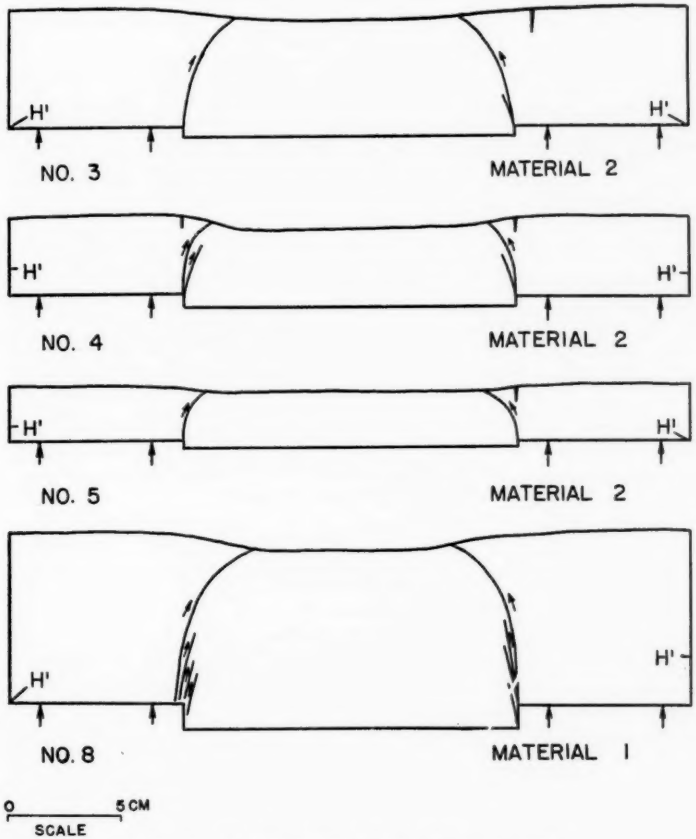

FIGURE 17.—FRACTURES—TYPE II EXPERIMENTS

The curvature of the reverse faults was independent of the relative movement of the blocks. In one experiment, the center section was allowed to drop while the two end sections remained stationary. The reverse faults produced by this mode of displacement were nearly the same as the reverse faults produced by keeping the center section stationary and pushing up the two end sections (Nos. 3, 4, 5, and 8 of Fig. 17).

In all Type II experiments with Material 2, displacements occurred along the reverse faults after they had reached the upper surface. As a result of this movement, thin wedges of material of the wedge was 0.5 cm after a total of 2.0 cm vertical displacement of the lower boundary.

In most of the experiments, vertical tensile cracks appeared at the upper surface at nearly the same time as the reverse faults were formed. The measured positions of the tensile cracks for three intervals of effective thickness are summarized in Figure 19. There is a systematic shift of the crack position with a change in the effective thickness of the layer.

Fracturing in the region of the tensile cracks followed the same pattern as the fracturing at the crest of the folds in the Type I experiments. The tensile cracks became deeper and wider

with increased applied displacement. Eventually the crack reached a critical depth at which the material on each side of the crack was unable to support itself, and normal fractures dipping toward the tension zone were formed. The maximum depth of the tensile cracks before normal faults were formed was 2.5 cm.

The final fracturing in the experiments was the propagation of a steep normal fault (average dip 78°) from the tensile crack zone to the edge of the uplifted block. After formation of the normal fault, displacement occurred along both the normal fault and the reverse faults. However, more displacement occurred along the normal fault than along the reverse faults.

The depth of the tensile cracks and the angle at which the reverse faults intersected the upper surface can be used to estimate the strength of the material in the layer at the time of fracture. The computed cohesive strength from the depths of the tensile cracks is 200–500 dynes/cm². The angle of internal friction from the average angle at which the fractures intersected the free upper surface (29°) is 32°. These values are fairly close to those obtained in the strength measurements on uncompacted samples of Material 2.

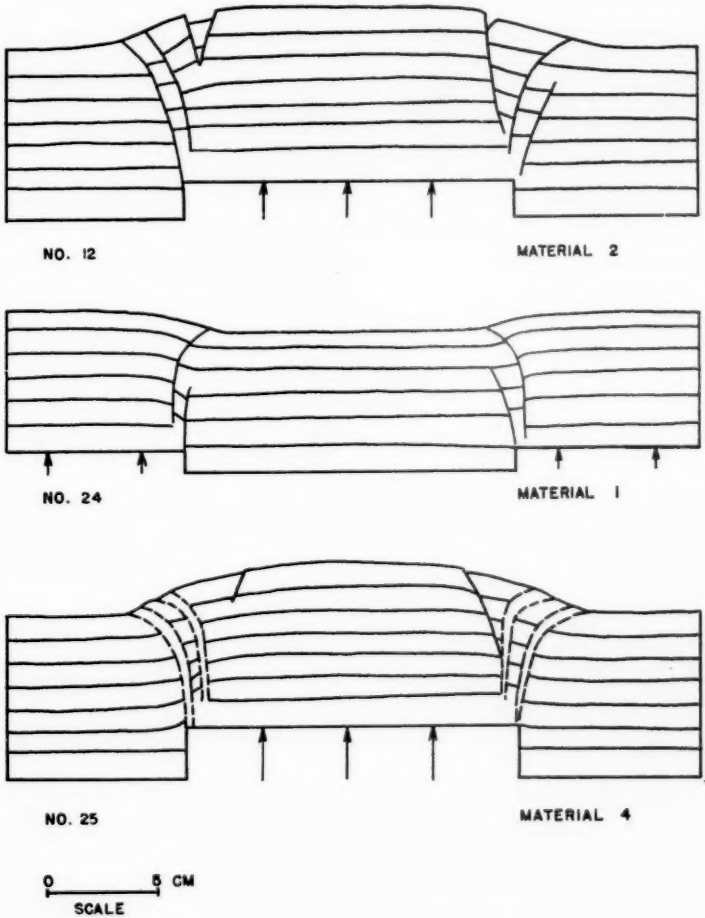

FIGURE 18.—FRACTURING AND FOLDING—TYPE II EXPERIMENTS

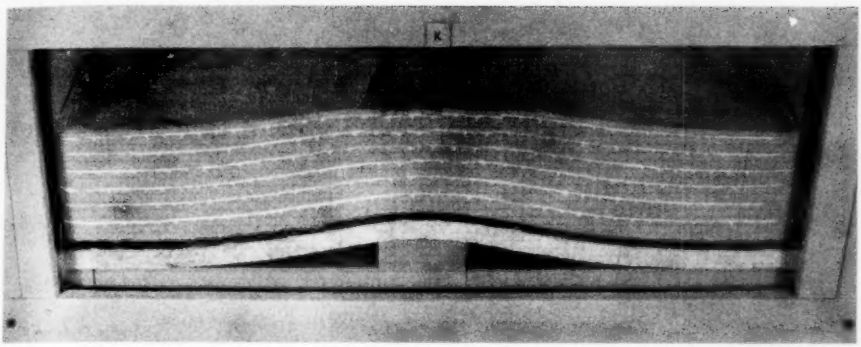

No. 19 Material 2

(GRID LINES ARE 0.5 CM APART)

FIGURE 1. — TYPE I EXPERIMENT

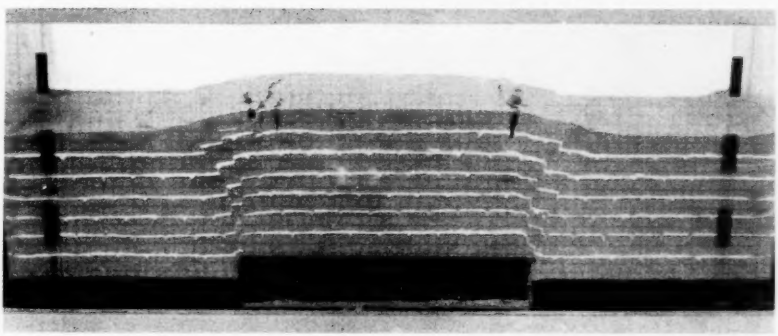

No. 12 Material 2

(GRID LINES ARE 0.5 CM APART)

FIGURE 2. — TYPE II EXPERIMENT

OBLIQUE PHOTOGRAPHS
OF EXPERIMENTS

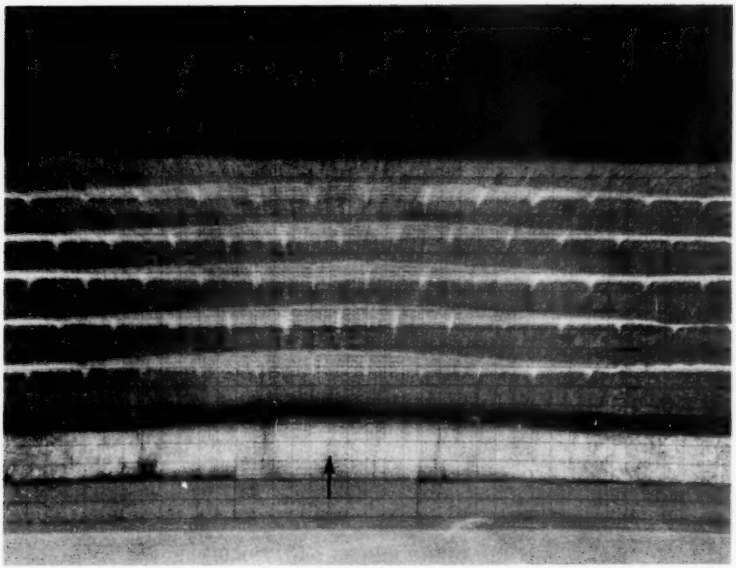

No. 23 Material 1

(GRID LINES ARE 0.5 CM APART)

FIGURE 1. — TYPE I EXPERIMENT — MULTIPLE EXPOSURE

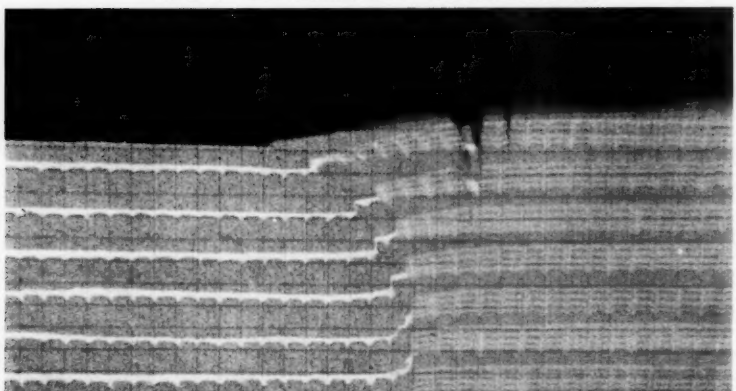

No. 15 Material 2

(GRID LINES ARE 0.5 CM APART)

FIGURE 2. — TYPE II EXPERIMENT — MULTIPLE EXPOSURE

MULTIPLE-EXPOSURE PHOTOGRAPHS
OF EXPERIMENTS

Type II fractures with Materials 1 and 4.—The fracture behavior of layers of Materials 1 and 4 differed in two respects from the fracture behavior of layers of Material 2; (1) tensile cracks were not formed (No. 8 of Fig. 17); and (2) the reverse faults formed were not sharp breaks, but narrow shear zones (No. 25 of Fig. 18). The curvature of the shear zones, however, was nearly identical with the curvature of the sharp reverse faults produced in the experiments with layers of Material 2. Layers of Material 1, which has a greater range in grain sizes and more irregularity in grain shape and roundness than Material 4, had narrower zones of fracture than layers of Material 4.

Type II deformation with Material 3.—Folding rather than fracturing was dominant in experiments in which layers of Material 3 were used. However, there were broad zones in the layers where the movement of the sand particles described trajectories which curved away from the uplifted block. In addition, ridges were formed on the upper surface similar to those associated with the reverse faults in the other experiments.

Summary of experimental results.—The displacement fields, at small applied vertical displacements, appeared to be independent of the size, shape, and sorting of the grains used for the layers. Fracture, however, was influenced by the properties of the modeling materials. The sharpest fractures were formed in layers of material which had cohesive strength (Material 2). The next sharpest fractures were formed in layers of material which lacked cohesive strength but were composed of poorly sorted, irregular sand grains (Material 1). Layers composed of well-sorted, well-rounded, and spherical sand grains (Material 3) did not appear to fracture.

The strength of the material in the layer at the time of fracture was nearly the same as measured strengths of uncompacted samples of the modeling materials. Movement of the layer prior to fracturing apparently decreased the initial compaction of the material and thus reduced its strength.

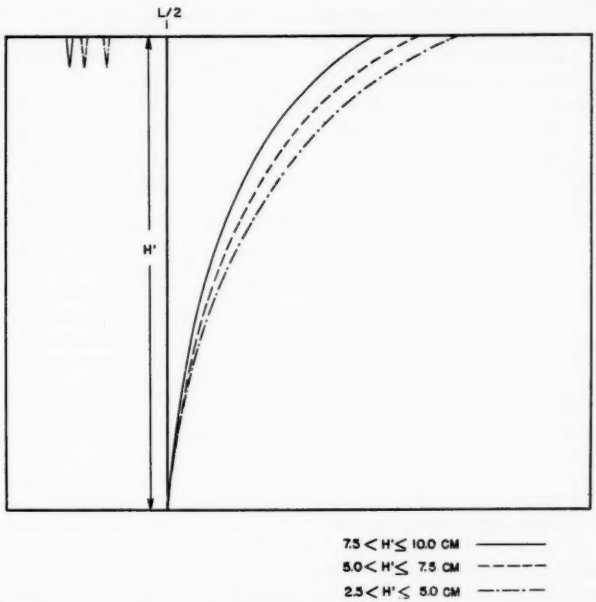

FIGURE 19.—CURVATURE OF REVERSE FAULTS IN TYPE II EXPERIMENTS

Reverse faults in Type II experiments had (1) progressively greater curvature and (2) progressively lower dip at the upper surface with a decrease in the effective thickness of the layer.

Geologic Interpretation of Experimental Results

Size relationship between model and geologic structure.—The size relationship between a

model and the geologic structure that it represents is determined from equation (59). The model ratios of strength and density must be known to use this equation. Unfortunately, there is no means of estimating the strength of extensive layers of sedimentary rock in nature. The strength is probably determined to a large extent by the degree of jointing in the layer. Layers of rock which have undergone extensive jointing have little or no cohesive strength and probably react to applied vertical displacements like layers of Material 1 do in the model experiments. Layers of rock which have not undergone jointing have a cohesive strength and probably react to applied vertical displacements like layers of Material 2 do in the experiments.

A rock layer with no cohesive strength can be modeled with a dry sand (similar to Material 1) which also has no cohesive strength. If the angles of internal friction in the sand and the rock layer are equal, the strengths of the layers are identical. However, the cohesive strength of the rock layer is zero only if one considers an extensive layer. The individual pieces between joints have considerable cohesive strength. The strengths of the sand and rock layers will be identical only when the dimensions of individual blocks are related to the size of the rock layer in somewhat the same manner as the individual grains are related to the size of the sand layer.

Equation (59) cannot be used to establish a size relationship between the model and the geologic structure if the rock and the sand layers have no cohesive strength. However, a crude size relationship can be obtained by comparing the size of sand grains with the size of joint blocks. The mean grain diameter for Material 1 is 0.2 mm. A reasonable diameter for a joint block is 10 m. The size relationship based on the above values is 1 cm of Material 1 equals 0.5 km of jointed rock.

A relationship between the size of the model and the geologic structure can be established with equation (59) if the layer of rock in the geologic structure has a cohesive strength. A rock layer with cohesive strength can be modeled with Material 2 which has a small cohesive strength of 1000 dynes/cm^2 and an angle of internal friction of about 40°. Representative values of cohesive strength and angle of internal friction for sedimentary rock are 250×10^6 dynes/cm^2 and 40°. The size relationship, on the basis of the above values, is 1 cm of Material 2 equals 1.5 km of sedimentary rock.

The τ_0 and ϕ values used to establish this size relationship are based on controlled-strain shear tests of moderately compacted samples of Material 2 and triaxial tests on small samples of sedimentary rock. In the model experiments, the strength of a moderately compacted layer of Material 2 is considerably reduced by deformation of the layer prior to fracturing. A similar reduction in the strength of a layer of sedimentary rock probably occurs in nature. However, the strengths of the two layers may not be reduced in the same proportion. For this reason, the size relationship between the model and the geologic structure may change during the course of an experiment.

Fractures.—The characteristic fracture pattern for Type I experiments is a complex zone of normal faults at the crest of the fold (Fig. 15). The fractured zone tapers inward to the axis of the fold and dies out at depth. The Kettleman Hills anticline (Woodring *et al.*, 1940) has this type of fracture pattern.

The characteristic fracture pattern for Type II experiments is a series of curved reverse faults intersecting the upper surface at low angles, and a series of normal faults in the uplifted block (Fig. 18). The reverse faults start as vertical faults at the lower boundary but become thrusts at the upper boundary. The low-angle or thrust portion of the fracture at the upper surface is due to horizontal compressive stresses. However, the horizontal compression is the result of vertical movement at depth and not of horizontal compression of the entire layer.

The characteristic fracture pattern formed for each of the two types of experiments is perhaps the most significant feature of the model experiments. Each pattern is relatively complex in view of the simplicity of the two distributions of applied displacement. The individual fractures in each pattern are related. Formation of one fracture triggers another in a definite sequence. The type and location of the primary fractures, which initiate the fracture sequence, are controlled by the distribution of applied displacement. The type and location of secondary fractures are determined partly by the distribution of applied displacement and partly by conditions arising from the formation of the primary fractures.

The manner in which the fracture pattern forms in the two types of experiments suggests that other distributions of applied displace-

ment at the base of a layer may also lead to distinctive fracture patterns. If the models are a true representation of fracturing in nature, fracture patterns observed in the models might be compared with fracture patterns observed on the surface of the earth, and in this manner be used to determine the distribution of displacement at depth.

Comparison of Experimental and Analytical Results

Type I Experiments and Category I Numerical Examples

Displacement fields.—The displacement fields in Type I experiments and Category I numerical examples are very similar, although this is not immediately apparent from an examination of the displacement-field diagrams. Displacement fields in the analytical work (Figs. 4*A* and 5*A*) are produced by applied vertical displacements which change periodically in amplitude and direction. Displacement fields in the experimental work (Fig. 14) are produced by applied vertical displacements which change in amplitude but not direction. The only major difference between the two displacement fields is a uniform displacement in one direction. As previously noted, uniform movement of a layer does not change the stress distribution. Therefore, superposition of a uniform upward displacement (equal to one-half the total amplitude of the applied vertical displacement) on the analytical displacement field will bring the two displacement fields into approximate agreement.

Although the general appearance of the displacement fields is similar, they differ considerably in detail. The maximum vertical and horizontal displacements at the boundaries of the model and the corresponding theoretical displacements from Figure 7*A* (for the average H/L ratio of 0.85 in the experiments) are:

		Experimental	*Theoretical*
$v_{max.}$	Lower boundary	1.00 *B*	1.00 *B*
$v_{max.}$	Upper boundary	0.60 *B*	0.40 *B*
$u_{max.}$	Lower boundary	0.30 *B*	0
$u_{max.}$	Upper boundary	0.70 *B*	0.30 *B*

(*B* equals the maximum applied vertical displacement.)

Two factors are responsible for most of the difference between theoretical and experimental values above. First, the boundary conditions in the experiments differed slightly from the boundary conditions in the analytical examples. In the experiments, the applied vertical displacement did not vary exactly as the cosine of the horizontal distance, and horizontal displacement occurred along the lower boundary. Second, the displacements required in the experiments to record the displacement fields photographically were much larger than the critical displacements (B_c) in the analytical work. In nearly all the experiments, there was evidence of failure in the layer while the displacement field was being photographed.

Fractures.—In the experiments with layers of Material 2, the position of the vertical tensile cracks is the same as the position of the initial tensile fractures predicted in the numerical examples.

Type II Experiments and Category II Numerical Example

Displacement fields.—The general appearance of the displacement fields in Type II experiments (Fig. 16) and Category II example (Fig. 6*A*) is very similar if a uniform upward displacement (equal to one-half the total amplitude of the applied displacement) is superposed on the analytical displacement field. However, the displacement fields differ slightly in detail. Listed below are the maximum vertical and horizontal displacements at the boundaries of the model and the corresponding theoretical displacements from Figure 8 (for the average H/L ratio of 0.47 in the experiments):

		Experimental	*Theoretical*
$v_{max.}$	Lower boundary	1.00 *B*	1.00 *B*
$v_{max.}$	Upper boundary	0.95 *B*	0.89 *B*
$u_{max.}$	Lower boundary	0	0
$u_{max.}$	Upper boundary	0.60 *B*	0.67 *B*

(*B* equals the maximum applied vertical displacement.)

The difference between the experimental and theoretical values is small. In this case, the boundary conditions in the experimental work were nearly equivalent to the boundary conditions in the theoretical example. Fracturing in the layer while the displacement fields were being photographed probably accounts for most of the difference in the experimental and theoretical values.

Fractures.—The predicted positions of the reverse faults in the Category II numerical example are based on the stress distribution in

Figure 6*B* and equation (50). The constant angle obtained from equation (50) is the orientation of the reverse faults with respect to the position of maximum compressive principal stresses throughout the layer. Inasmuch as the principal stress trajectories are curved, the reverse faults will also be curved. In Figure 20, three reverse faults based on the stress distribution have been drawn for three different angles of internal friction. Also shown on Figure 20 is a shear fracture based on measurements of reverse faults in model experiments which were geometrically similar to the numerical examples. The agreement between the experimental fracture and the theoretical fracture for a ϕ equal to 28° is very good. A value of 28° is a reasonable average angle of internal friction for the entire layer.

The tensile cracks in the experiments do not occur at the positions predicted in the analytical work (compare the position of tensile cracks on Fig. 19 with the position of F_1 on Fig. 6*B*). Apparently the formation of the reverse faults shifts the position of the large horizontal tensile stresses closer to the position of the reverse faults.

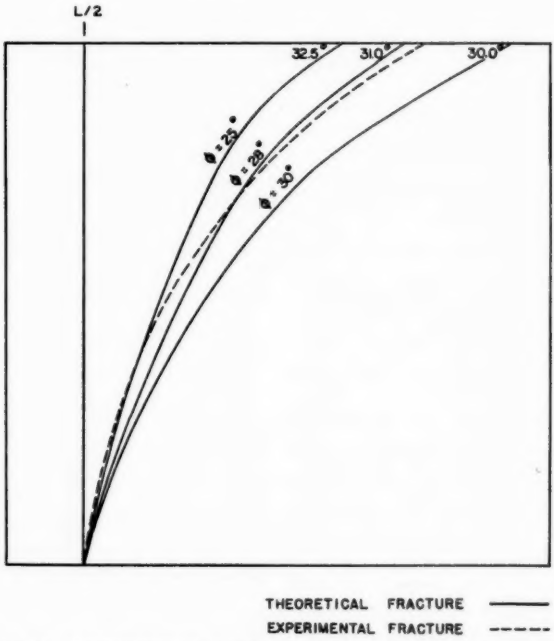

FIGURE 20.—COMPARISON OF THEORETICAL AND EXPERIMENTAL FRACTURES

The shear fracture determined from Example IIa stress distribution (Fig. 6*B*) and Mohr's fracture criterion (with $\phi = 28°$) agrees closely with the shear fracture in the experiments which were geometrically similar to Example IIa.

REFERENCES CITED

Birch, F., *et al.*, 1942, Handbook of physical constants: Geol. Soc. America Special Paper 36, 325 p.

Gutenberg, B., 1951, Internal constitution of the earth: 2d ed., N. Y., Dover Publications, Inc., 438 p.

Hafner, W., 1951, Stress distributions and faulting: Geol. Soc. America Bull., v. 62, p. 373–398

Hubbert, M. K., 1937, Theory of scale models as applied to the study of geologic structures: Geol. Soc. America Bull., v. 48, p. 1459–1520

——, 1951, Mechanical basis for certain familiar geologic structures: Geol. Soc. America Bull., v. 62, p. 355–372

Jaeger, J. C., 1956, Elasticity, fracture, and flow: N. Y., John Wiley and Sons, Inc., 152 p.

Krumbein, W. C., and Sloss, L. L., 1951, Stratigraphy and sedimentation: San Francisco, W. H. Freeman and Co., 497 p.

Love, A. E. H., 1944, A treatise on the mathematical theory of elasticity: 4th ed., N. Y., Dover Publications, Inc., 643 p.

Marin, J., 1952, Engineering materials: N. Y., Prentice-Hall, Inc., 491 p.

Mills, A. P., *et al.*, 1955, Materials of construction: 6th ed., N. Y., John Wiley and Sons, Inc., 650 p.

Muskhelishvili, N. I., 1953, Some basic problems of the mathematical theory of elasticity: 3d ed., Groningen-Holland, P. Noordholf, Ltd., 704 p.

Phillips, H. B., 1933, Vector analysis: N. Y., John Wiley and Sons, Inc., 236 p.

Timoshenko, S., and Goodier, J. N., 1951, Theory of elasticity: 2d ed., N. Y., McGraw-Hill Book Co., Inc., 506 p.

Tschebotarioff, G., 1952, Soil mechanics, foundations, and earth structures: 1st ed., N. Y., McGraw-Hill Book Co., Inc., 655 p.

Woodring, W. P., Stewart, R., and Richards, R. W., 1940, Geology of the Kettleman Hills oil field, California: U. S. Geol. Survey Prof. Paper 195, 170 p.

New Mexico Institute of Mining and Technology, Socorro, New Mexico

Manuscript Received by the Secretary of the Society, March 14, 1958

Contribution No. 903, Division of the Geological Sciences, California Institute of Technology

BULLETIN OF THE GEOLOGICAL SOCIETY OF AMERICA
VOL. 70, PP. 53-90, 16 FIGS., 2 PLS. JANUARY 1959

HYDROTHERMAL ALTERATION IN THE FRONT RANGE MINERAL BELT, COLORADO

By Félix González Bonorino

Abstract

Hydrothermal alteration associated with ore veins in a large part of the Front Range mineral belt was studied in an attempt to correlate it with the mineralogic, petrologic, and structural features of the ore deposits. Six patterns of alteration were found; they range from the simplest type with a single zone of hydromica to the most complex type with five zones that are characterized by phlogopite carbonate (fringe zone), montmorillonite, kaolinite, orthoclase, and hydromica (innermost zone). A regular mixed-layer illite-montmorillonite mineral may substitute for hydromica either in the whole or in the outer part of the innermost zone, thus producing two subpatterns. Phlogopite and siderite represent the alteration of biotite; they extend to and suddenly increase at the hydromica zone. The remaining zones are based on the alteration of plagioclase. Microcline and quartz are stable in all zones.

Generally, the simplest alteration patterns are found in the southwestern part and along the western side of the belt. They are closely related to Laramide stocks, and most of the associated mineralization is of lead and zinc sulfides. The most complex patterns predominate along the eastern side and are concentrated in the middle to northeastern part of the belt; they are associated preferably with tungsten, pyritic gold, and telluride gold deposits.

The origin of the complex patterns is explained in terms of chemical fronts developed as the altering fluids migrated away from the conduit. The altering fluids were probably gaseous and are believed to have been derived by fractional distillation from the main body of hydrothermal liquids. The remaining silica-rich, less volatile fraction filled the veins after wall-rock alteration. The fluids changed in composition through reaction with the wall rock and successively reached the stability fields of the various secondary minerals. The critical changes responsible for the front (and zone) formation are increase of Si/Al ratio, decrease of K concentration, and increase of pH. No evidence of mutual replacement among hydrothermal minerals was found. The amount of matter transferred during alteration was small. The formation of other patterns is explained on the same principles, assuming slightly different compositions of the altering fluids. An attempt is made to correlate the patterns of alteration with the distribution of the intrusive bodies.

CONTENTS

TEXT

	Page
Introduction	54
Scope of problem	54
Present study	55
Acknowledgments	55
Summary of regional geology and ore deposits	55
Pre-Laramide alteration	57
Laramide alteration	58
General statement	58
Zone patterns	58
Mineralogy	58
Description of individual patterns	66
Chemical changes	72
Origin of hydrothermal alteration	74
General statement	74
Alteration and vein formation	74
Hydrothermal differentiation	74
Mechanism of zone development	76
Mechanism of zone development (*Cont'd.*)	Page
Sequential versus simultaneous origin of zones	76
Nature of alteration fronts	77
Development of alteration fronts	77
Problem of front migration	79
Transfer of matter during alteration	80
Nature of the replacement mechanism	80
Origin of other patterns of alteration	81
Silicification	82
Alteration pattern and wall-rock type	82
Alteration pattern and ore type	83
Alteration pattern and Laramide intrusions	83
Summary and conclusions of relation of wall-rock alteration to Laramide intrusions and ores	83
Comparison with alteration in other areas	84
Supergene alteration	85
Alteration as a guide to ore	85

Page
General conclusions 86
Addendum 87
References cited 88

ILLUSTRATIONS

Figure Page
1. Index map of the Front Range mineral belt, Colorado, showing distribution of alteration patterns 56
2. Patterns of hydrothermal alteration in the Front Range mineral belt, Colorado .. 59
3. X-ray diffraction curve of hydromica containing 25 per cent of randomly interlayered montmorillonite 61
4. Relation between gamma refraction index and montmorillonite content in mixed-layer illite-montmorillonite clay minerals 62
5. Differential thermal curves of mixed-layer, illite-montmorillonite clay minerals 62
6. X-ray-diffraction curves of regular mixed-layer, 1:1 illite-montmorillonite clay mineral 64
7. Relation between ool spacing and nature of exchange cation in montmorillonite 65
8. Cross section of alteration zones at Caribou mine, Idaho tunnel 68
9. Idealized cross section of a vein showing alteration pattern VI 70
10. Diagram showing degree and type of alteration of main primary minerals in pattern VI veins 71
Figure Page
11. Alteration of biotite in the kaolinite zone 72
12. Cross section of the alteration zones at Crackerjack tunnel 72
13. Chemical changes in the alteration zones, Chance mine 73
14. Diagram of gains and losses, Chance mine .. 75
15. Stability fields of hydrothermal minerals in the wall-rock environment during alteration 78
16. Map of alteration zones, Footwall vein, Clyde tunnel 86
Plate Facing page
1. Veins showing pattern VI of hydrothermal alteration 66
2. Microscopic features of hydrothermal alteration 67

TABLES

Table Page
1. ool spacings in montmorillonite and nontronite 60
2. Chemical analyses of hydromica and mixed-layer clay mineral 62
3. Tabulation of lattice basal spacings of regular mixed-layer illite-montmorillonite clay minerals 63
4. Chemical analyses of the altered wall-rock zones, Chance mine 74

Introduction

Scope of Problem

Studies on wall-rock alteration associated with ore veins are important from the standpoint of the nature of the hydrothermal processes, as well as of their possible use in the search for ore. Workers in this field disagree with regard to the mechanism of the alteration and its significance in the ore-forming processes. The present emphasis on the laboratory approach to the study of hydrothermal phenomena looks fairly promising, but a program of systematic field investigation seems necessary. Alteration should be studied and compared from district to district beginning with those with the simplest structural setting.

The Front Range mineral belt, having various types of relatively simple vein deposits associated with igneous bodies of diverse composition, offers an excellent opportunity for the correlation between hydrothermal alteration, ore-forming processes, and magmatic differentiation. An excellent background for such a study is provided by the detailed geologic and petrologic work done in this area by several workers, in particular Lovering and his associates (Lovering, 1941; Lovering and Goddard, 1938; 1950; Lovering and Tweto, 1953). Wright (1954) described the alteration related to the uranium-bearing veins of Caribou mine, west of Nederland, Colorado, and Tooker (1955; 1956) and his colleagues of the U. S. Geological Survey studied the geology and hydrothermal alteration in the Central City-Idaho Springs area. The results of the latter work were not available when this was written.

The exploitation of all the possibilities offered by the Front Range mineral belt for the study of hydrothermal alteration would require many years. Only a few of the problems have been studied here. Future work calls for integration of the results here presented with those of others working elsewhere in the same area, for further studies of critical features related to age and magmatic relationships of the veins and intrusives, and for extension of the studies to other districts in the Front Range.

Present Study

Field studies were carried out during parts of two summers (1955–1956). Although an effort was made to cover the entire mineral belt (with the exception of the Central City-Idaho Springs district), the major part of the work was focused on the northwest part of the belt, where alteration is most complex and workings most accessible. Only a few mines were active throughout the entire belt at the time of this study, and these only in part. The majority of the veins examined were in idle or abandoned tunnels where most of the ore had been mined. The difficulties presented by this area for this kind of work were aptly summarized by Tooker (1955).

Samples were studied by optical methods, supplemented by X-ray and thermal analyses. Most of the petrographic analyses were made by immersion techniques and thin-section studies. Using properly spaced X-ray analyses as supporting data a large number of profiles can be studied in a short time. For estimating the relative proportions of clay minerals, thin sections were also used, but if the minerals were too intimately mixed, X-ray studies were necessary. The mineralogical study of clay minerals and other alteration products was handicapped by the scarcity of material, which generally had to be dug painstakingly out of the pseudomorphs. Fortunately, the writer had access for a short time to an ultrasonic disperser at the X-Ray Laboratory of the U. S. Geological Survey in Denver, through the courtesy of A. J. Gude, 3rd. This apparatus proved to be very effective in the quick separation of clays from pseudomorphs, using the minimum amount of crushing and therefore reducing contamination.

Acknowledgments

This study was carried out under a Fellowship of the John Simon Guggenheim Memorial Foundation. A grant from the Penrose Bequest of The Geological Society of America made possible the chemical analyses and thin sections, and the Geochemical Exploration Section and the X-Ray Laboratory of the U. S. Geological Survey in Denver, Colorado, furnished laboratory facilities. To these organizations the author wishes to convey his deepest gratitude. Part of the work was done while the author was a member of the staff of the Department of Geology in the Missouri School of Mines & Metallurgy at Rolla, Missouri.

The writer is greatly indebted to Dr. T. S. Lovering, Head of the Geochemical Exploration Section of the U. S. Geological Survey, for suggesting this study and for giving generous support and advice in different phases of the work. Critical reading of part of the manuscript by Prof. P. M. Bethke, of the Missouri School of Mines & Metallurgy, is gratefully acknowledged. Prof. E. N. Goddard kindly lent a suite of thin sections of rocks of the Jamestown district.

Summary of Regional Geology and Ore Deposits

Lovering and Goddard (1950) gave a detailed account of the geology of the Front Range mineral belt and its ore deposits. The following summary is taken from their monograph.

The belt extends from Jamestown to Breckenridge (Fig. 1). The veins are located in igneous, metamorphic, and mixed rocks of different ages. The oldest rocks are the micaschists and hornblende schists of the Idaho Springs formation (early Precambrian), with an approximate thickness of 20,000 feet. The schistosity strikes generally between north and east and dips very steeply. Migmatization by granitic material is widespread, especially on the eastern end, and various forms of gneiss and arterites are found. Hornblende schists are predominant in the southwest end of the belt.

Irregular, largely interconnected bodies of Precambrian granitic rock cut the Idaho Springs formation and form the host rock of the majority of the veins. They are most abundant in the northeast and central parts of the belt and least abundant in the southwest end where metamorphic rocks predominate. Two main granite types are distinguished in the mineral belt: The Boulder Creek granite, in the northeastern part of the belt, is a coarse-grained, foliated rock with considerable amount of biotite and numerous schist inclusions and schlieren. The other type is represented by the Silver Plume granite, which predominates around and west of Georgetown-Empire. The latter is a medium-grained, slightly porphyroid biotite granite, which lacks the strong foliation of the Boulder Creek granite. Numerous pegmatite dikes cut both the granites and the metamorphic rocks.

Outward dipping, Paleozoic and Mesozoic sedimentary formations flank the Front Range at both ends of the mineral belt and enclose the stock to which the Breckenridge veins are re-

lated. Tertiary rocks are also included in the sedimentary series.

A series of small igneous bodies of Laramide age extends parallel to the mineral belt ("porphyry belt") on the northwestern side. In the mineral belt proper dikes and small irregular bodies are abundant. The rock types range generally from diorite (and andesite) porphyry to quartz monzonite (and latite) porphyry, but gabbroic and syenitic bodies are also found. In general, the age of the Laramide intrusions increases toward the southwest.

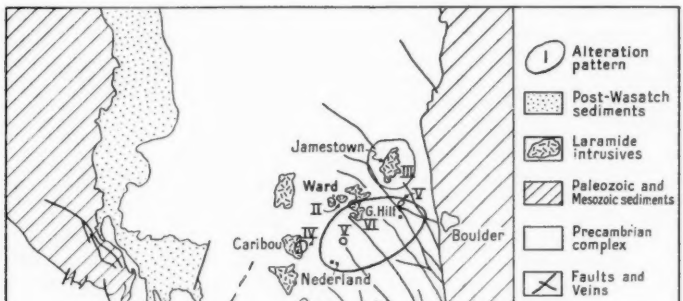

FIGURE 1.—INDEX MAP OF THE FRONT RANGE MINERAL BELT, COLORADO, SHOWING DISTRIBUTION OF ALTERATION PATTERNS
Base map after Lovering and Goddard, 1950.

The mineral deposits in the belt are distributed in several districts, which, northeast to southwest, are: Jamestown, Gold Hill, Ward, Caribou, Nederland, North Gilpin County, Central City, Idaho Springs, Georgetown, Silver Plume, Montezuma, and Breckenridge. They are represented by veins of predominantly northeast to east trend, formed in Laramide times. Many persistent, northwest-trending barren breccia zones ("reefs") cross the belt; the veins are generally richer closer to their intersection with the reefs. The mineral belt is almost coincident with the line of Laramide porphyry stocks, although somewhat to the southeast. The related origin of igneous bodies and veins seems evident. The veins are younger than the porphyry and in places cut the Laramide igneous rocks.

The Jamestown district is characterized by pyritic gold telluride veins, more or less clustered around a composite stock of granodiorite-sodic granite. Fluorspar veins and lenses are closely associated with gold telluride veins. Silver-lead veins are also present. Most of the veins are in Boulder Creek granite.

The Gold Hill district (Fig. 1) has pyritic gold telluride mineralization. Most of the veins are in Boulder Creek granite, some in gneissic schists. The district is separated from the Ward district by an irregular body of Laramide age.

The deposits in the Ward area are varied, with pyritic gold-silver, copper-gold-silver,

lead-silver, and tungsten veins. Only a silver-lead deposit (White Raven) was accessible to the author.

The Nederland tungsten district (Lovering and Tweto, 1953) is characterized by simple quartz-ferberite veins. Most of the veins are in Boulder Creek granite and biotite aplite. No Laramide intrusions are found here except some hornblende monzonite and hornblende diorite dikes.

The Caribou vein system, west of Nederland, is partly in a composite, gabbro-syenite stock with concentration of titaniferous magnetite. The veins contain lead-silver-zinc ore and in places also pitchblende.

The districts in the middle part of the mineral belt (Blackhawk, Central City, Idaho Springs, and Empire), which have not been included in this study, contain a variety of pyritic gold, lead-silver-zinc, gold telluride, and uranium veins.

The Georgetown-Silver Plume district consists of silver-lead-zinc, as well as some pyritic gold veins cutting Idaho Springs schists and gneisses and Silver Plume granite. The near-by Argentine district has similar characteristics.

The Montezuma district is separated from the Argentine district by a body of quartz monzonite porphyry. Lead-silver-zinc veins cut Idaho Springs hornblende-rich schists. The Breckenridge district contains also lead-silver-zinc veins, but they cut extensive bodies of quartz monzonite and quartz latite porphyries which in turn intrude Paleozoic and Mesozoic sediments.

The general sequence of mineralization was as follows (Lovering and Goddard, 1950): (1) pyrite, (2) sphalerite, (3) chalcopyrite, (4) galena and chalcopyrite, (5) silver-bearing sulfoantimonides, sulfarsenides, and bismuthinides, (6) pyrite and subordinate chalcopyrite, (7) free gold, (8) minor amounts of sphalerite, galena, and silver minerals, (9) gold tellurides and sparse pyrite, gold, sphalerite, and galena, and (10) ferberite and sparse sulfides. Most of the ores between Breckenridge and Idaho Springs belong in groups 1–5. The ores to the north belong in groups 6–10. This is at least partly in agreement with the fact that the latest members of the porphyry series are found in the northeastern part of the belt. Southwest of Georgetown, where complex lead-silver-zinc ores predominate, the igneous rocks are diorite, monzonite, quartz monzonite, and sodic quartz monzonite. Northeast of Silver Plume, as the pyritic gold deposits appear, the igneous bodies change to more potassic types (bostonite, syenite). The gold telluride veins between Idaho Springs and Jamestown are coexistent with dikes of biotite latite, biotite monzonite, and latite. The pitchblende veins at Central City represent a local modification of the pyritic gold veins.

Pre-Laramide Alteration

The igneous rocks of the Front Range mineral belt show alteration that is unrelated to the veins of the Laramide cycle. The chief alteration is sericite in plagioclase. Penninite and epidote replace biotite in a few places, and a little carbonate of doubtful origin is present. The amount of alteration varies within a given district, but no attempt was made to map such changes. Sericite is moderately abundant, amounting in places to about a quarter of the plagioclase host. Compared with the hydromica associated with ore veins, sericite shows much better crystallinity; in places, coalescence of subparallel plates has given rise to large individuals. The plates are commonly arranged along the crystallographic planes of plagioclase. Measurements of a few samples gave refractive-index values well above 1.590 for gamma, approaching the index of well-crystallized muscovite.

The nature of sericite alteration of this type is a problem of general significance but is beyond the scope of this paper. Significant features of this alteration are the widespread distribution, the coarse grain, and the simplicity of the mineral assemblage. The first two features point toward a highly pervasive, hot fluid; the third characteristic indicates lack of differentiation. These conditions are best given during the deuteric stage of the consolidation of igneous bodies. At this stage, the residues of the magmatic crystallization, containing little else than water, CO_2, silica, and alkalies, are dispersed in the rock under considerable vapor pressure. In the presence of this fluid, plagioclase is unstable, whereas potassium feldspar is generally insoluble. Therefore, sericite replaces the former but leaves generally untouched the potassium feldspar. This is an example of what the writer believes to be a general principle in alteration: the localization of a secondary mineral is often a question of available space rather than of direct chemical contribution from the host.

The interpretation of the sericite replacement as deuteric presupposes that most of the granitic rocks of the mineral belt are of igneous origin. They are thus explained by Lovering

and Goddard (1950), and the writer sees no evidence to the contrary.

The recognition of this alteration is important for a correct interpretation of the later cycles. Failure to recognize and separate the pre-Laramide alteration would result in a much more confused picture of the later phenomena.

Laramide Alteration

General Statement

In contrast with the older alteration, the Laramide hydrothermal alteration in the mineral belt is closely related to the ore veins. The rock decomposition is more intense as well as more concentrated than in the pre-Laramide sericitization. The intensity and, generally, the mineralogical nature of the alteration vary laterally from the veins. These changes manifest themselves in the color and hardness of the wall rock, but some mineral variations are not detectable by simple observation. All external changes correspond to mineral variations, but the reverse is not true.

The Laramide alteration is not everywhere restricted to the individual veins. In some deposits (*e.g.*, in the Georgetown area) a widespread alteration comprises several veins or perhaps a whole vein system. No attempt was made to determine the spatial relationships in the deposits. The present study deals with the alteration that can be correlated with individual veins, which give a better opportunity to study the critical genetic features.

The zoning, *i.e.*, the systematic lateral distribution of the mineral assemblages—varies from simple (one zone) to complex (up to five zones, excluding the fringe zone), each zone characterized by a given mineral assemblage. Each combination of zones is here called a "pattern".

Zone Patterns

According to the lateral distribution of the alteration minerals, the veins of the Front Range mineral belt studied by the writer can be divided into six patterns of zoning (Fig. 2):

PATTERN I: The simplest pattern is a single zone of bleached "sericitized" wall rock, in places silicified. It is found at the Wellington (Breckenridge) and Silver King (Montezuma) mines (Pb-Ag-Zn) in the southwestern part of the belt, and at the Oregon-Quaker City mine, Nederland (tungsten).

PATTERN II: A single zone characterized by a mixture of kaolinite, hydromica, and montmorillonite in variable proportions. Georgetown and Ward districts (Pb-Ag-Zn; Au-pyrite).

PATTERN III: A single zone with predominant hydromica and potassium feldspar. Jamestown district (Au-Te-pyrite).

PATTERN IV: Two separate zones, characterized respectively by kaolinite (inner) and montmorillonite. Caribou mine, Nederland (Pb-Ag-Zn).

PATTERN V: Three zones, characterized respectively by hydromica (inner), kaolinite, and montmorillonite. Found sporadically within the area of pattern VI.

PATTERN VI: The most complex pattern consists of four main zones: hydromica (inner), orthoclase, kaolinite, and montmorillonite. It is typical of Nederland tungsten-Gold Hill pyritic gold districts. Two subpatterns are recognized in a few places, as the regular mixed-layer clay mineral described above substitutes, either partly or totally, for the hydromica in the inner zone.

The above classification is based on the alternation of plagioclase. Further subdivisions of zones and/or patterns may be made by considering also the alteration of mafic constituents. For instance, a fringe zone, characterized by the partial alteration of biotite and (in places) hornblende is distinguished in most veins. A zone of complete alteration of biotite is superimposed on the hydromica zone in nearly all veins of the most complex patterns.

Mineralogy

The prominent primary constituents of the rocks of the mineral belt are plagioclase, quartz, potassium feldspar in most places, and biotite. Hornblende and muscovite average less than 1 or 2 per cent each in the mines examined, whereas pyroxene was found at only one locality (Caribou mine).

Plagioclase is unstable in all but the fringe zone. The degree of alteration is low in the montmorillonite zone of patterns V and VI but reaches 100 per cent between there and the vein. Quartz is essentially stable in all zones; microscopic textures suggesting peripheral replacement by clay aggregates are seen in the kaolinite zones at a few mines, but modal and chemical analyses do not support the idea of quartz replacement to any measurable extent. Potassium feldspar is stable in all zones. Biotite

is generally unstable, but the degree of alteration varies considerably. Its replacement is complete only in the innermost zone, where it

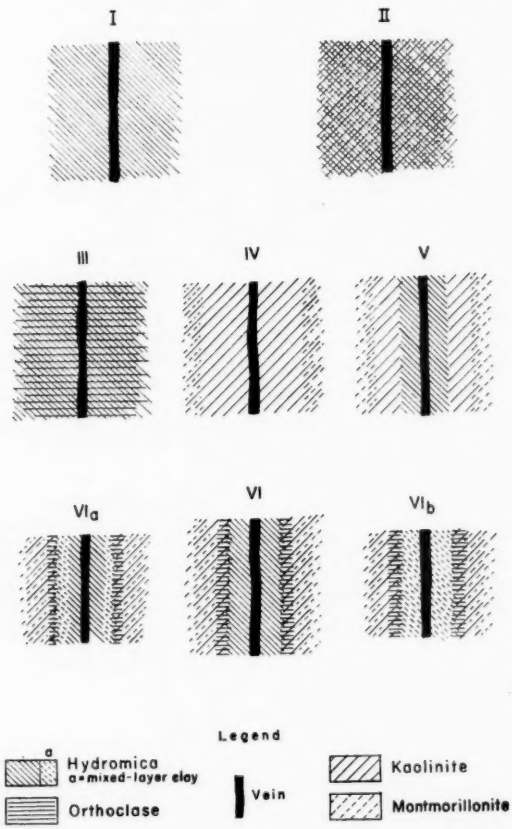

FIGURE 2.—PATTERNS OF HYDROTHERMAL ALTERATION IN THE FRONT RANGE MINERAL BELT, COLORADO

has the character of a cationic substitution within the mica framework (phlogopitization). Hornblende and pyroxene are also unstable in all zones; however, in the fringe zone the alteration of the amphibole may be incomplete. Muscovite, as well as apatite, is stable everywhere.

The main alteration minerals, representing more than 99 per cent of most of the hydrothermal products, are described below.

KAOLINITE: Kaolinite is the only representative of its group that the writer found in association with the veins of the mineral belt. Two generations are present. First-generation kaolinite is more abundant than second and is strictly related to the alteration zoning; it appears in white, soft aggregates replacing plagioclase and, to a lesser extent, biotite, hornblende, and microcline. Most individuals are tiny booklets, but a few show hexagonal outlines under the highest power. Vermicular development is uncommon. Most of the kaolinite is mixed with montmorillonite stringers that separate the booklets.

Second-generation kaolinite is found in veinlets in which quartz lines the walls and kaolinite fills the middle part. Opal may be found intimately mixed with the clay. This kaolinite is in general coarser-grained than the first generation and free from montmorillonite.

Kaolinite that replaces biotite and horn-

blende differs in habit from the type that replaces plagioclase: it forms white, fibrous aggregates. Montmorillonite (or nontronite) may be mixed in the aggregates. In some aggregates of this type (Chance mine) these fibers are seen to be subhedral plates 10–20 times longer than wide, elongated in the direction of one of the edges of the pseudohexagonal basal pinacoids. Thin montmorillonite films separate the kaolinite laths.

TABLE 1.—(ool) SPACINGS IN MONTMORILLONITES AND NONTRONITE

	1 Poorman		2 White Raven		3 Caribou		4 Cold Spring	
	d(Å)	I	d(Å)	I	d(Å)	I	d(Å)	I
001	16.9	10	17.1	10	16.7	10	16.4	10
002	8.42	1	8.6	1	8.3	1	8.4	3
003	5.62	1	5.72	1	5.64	1	5.56	1
004	4.23	1	4.26	1	4.23	1	?	
005	3.38	1	3.44	1	3.34	1	?	
006	2.87	0.5	2.86	1	2.84	0.5	2.69	1

(1–3) Montmorillonite; (4) Nontronite; all samples glycolated.

One sample of kaolinite gave the following indices of refraction: $\alpha = 1.561$, $\gamma = 1.567$.

No dickite, halloysite, or any other member of the group was found in spite of extensive microscopic and X-ray investigations.

MONTMORILLONITE: Montmorillonite is nearly everywhere mixed with kaolinite to form pseudomorphs chiefly after plagioclase. Where montmorillonite predominates, the aggregates are light gray; if kaolinite is predominant they are white. Veinlets of pure montmorillonite are found in largely unaltered plagioclase in the marginal zone of alteration of some veins (Pl. 2, fig. 6). They form a network of stringers and threads enclosing the kaolinite individuals.

The gamma index of refraction measured in several samples has a value around 1.530, although values as low as 1.513 were found in samples from the Prospect tunnel. Montmorillonite about 95 per cent pure, with a little kaolinite, was recovered by ultrasonic dispersion of samples from Poorman, White Raven, and Caribou mines. X-ray-diffraction spacings of these clays are shown in Table 1. The dry and glycolated $d_{(001)}$ spacings of the H-, Na-, NH_4-, and Ca-saturated montmorillonite from Poorman and White Raven mines are shown on Figure 7. The diffraction patterns suggest that montmorillonite varies little throughout the mineral belt.

NONTRONITE: Nontronite is found, together with kaolinite and siderite, replacing hornblende. It is pale greenish brown, and the indices of refraction are: $\alpha = 1.545$; $\gamma = 1.580$, variable. Although comb texture is found in some aggregates, nontronite generally forms films or screens separating kaolinite aggregates along planes parallel to the original cleavage of the hornblende. Table 1 shows the X-ray basal reflections of an impure sample obtained from a pseudomorph after hornblende. Very small amounts of this clay mineral were available for study.

HYDROMICA: The term hydromica is used here, following Brown and McEwan (1951), to include illites as well as interstratified mixtures of illite and other clay minerals in which the former predominates.

Hydromica is the most abundant alteration mineral in the Front Range mineral belt. It appears in aggregates of tiny, ill-defined, leafy booklets and in more elongated individuals arranged approximately parallel to the twinning planes of the plagioclase they usually replace (Pl. 2, fig. 1). Most hydromica can be distinguished from the earlier sericite, which shows better defined plates. There are, however, many indistinguishable border cases. Hydromica forms grayish or creamy-white, locally iron-stained aggregates, pseudomorphic after plagioclase. Creamy or yellowish tinges indicate phosphate.

The argillaceous (as opposed to micaceous) nature of the mineral forming the bulk of the secondary minerals of the inner alteration zone in most of the veins is substantiated by optical, X-ray, thermal, and chemical analyses. The results prove that the mineral is a hydromica, not a sericite. Sericite of an earlier period of alteration is present in many aggregates.

Optically, the hydromica shows relatively low refraction indices; the majority have $\alpha = 1.545 \pm 3$, $\gamma = 1.580 \pm 3$. The range of variation for gamma is 1.585 to 1.570, and the alpha varies accordingly. Associated sericite has a gamma index of about 1.590. The above measurements were made on untreated flakes.

X-ray-diffraction patterns (Fig. 3) indicate some degree of disorder in the stacking of layers. Moreover, the (001) reflections show a relatively low spacing, generally between 9.9 Å and 9.8 Å, and in one case 9.7 Å was recorded (Fig. 3). This low spacing is attributed

to the random interstratification of montmorillonite within the illite, in a proportion of 10 to 15 per cent in the common case, and as much as 25 per cent in the case of the lowest spacing, 9.7 Å. These proportions are obtained by means

The curve of Figure 4 may be used to ascertain the approximate proportions of illite and montmorillonite in the mixed-layer clays of the mineral belt. It could presumably be used also in other areas, but the nature of components

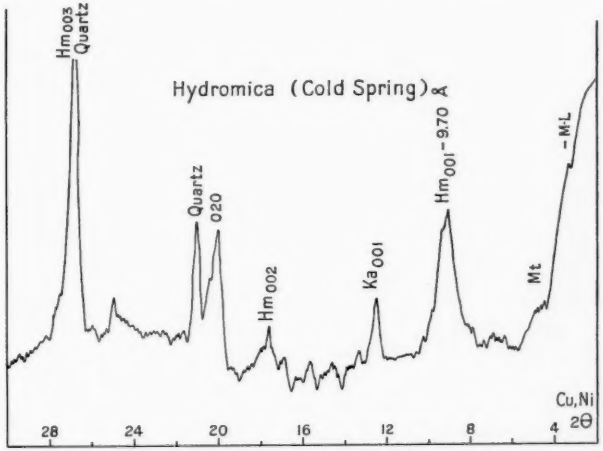

FIGURE 3.—X-RAY-DIFFRACTION CURVE OF HYDROMICA CONTAINING 25 PER CENT OF RANDOMLY INTERLAYERED MONTMORILLONITE

of the curves calculated by Brown and McEwan (1951); *see* Weaver, 1956). The slight but significant displacement of the (001) reflection is due to the influence of the (002) reflection of montmorillonite, and it is best observed after glycolation. As the amount of randomly interlayered montmorillonite increases, the (001) illite peak is displaced, and the (001) montmorillonite peak answers (Fig. 3).

The comparatively low indices of refraction of the hydromica of the Front Range mineral belt are also attributed to the presence of interlayered montmorillonite. Figure 4 shows the γ indices of three samples plotted against the percentage of montmorillonite as determined by means of Brown and McEwan's curves. Sample 1 represents the common hydromica in the area. Sample 2 is the hydromica with the highest content of interlayered montmorillonite (Cold Spring mine). Sample 3 corresponds to a regularly interlayered, 1:1 illite-montmorillonite clay mineral described below. A straight line traced through these three points intersects the ordinates of pure illite and montmorillonite at values of 1.590 and 1.513, respectively. Such indices of refraction fit well with the standard values for these minerals.

must be established first. The presence of interlayered montmorillonite in illite may be recognized or suspected by a decrease in the indices without perceptible change in birefringence. Interlayered kaolinite would diminish the birefringence with relatively little effect on refractivity, except where present in large amounts. Chlorite would be indicated by reduced birefringence and by coloration. Pyrophyllite would be impossible to detect.

The displacement of the (001) peak of illite by montmorillonite interlayering is enhanced by glycolation; this is due not to the expansion but to the intensification of the second-order peak of montmorillonite, which is very weak in the air-dried state.

Differential thermal analysis of an $Ill_{87}Mt_{13}$ clay mineral (Fig. 5) shows the mid-temperature endothermic peaks of the two components to be about 600°C. and 700°C., respectively. The X-ray pattern of the same clay indicates almost pure mixed-layer hydromica. The thermal curve is practically identical to that of the clay from Sarospatak, Hungary, which is also a mixed-layer hydromica (Grim and Rowland, 1942). The name "bravaisite" has been suggested for this type of clay mineral.

The chemical analysis of a typical hydromica

(Ingram mine) is shown in Table 2,*a*. The sample was purified by sedimentation but still contains minor amounts of quartz (5 per cent),

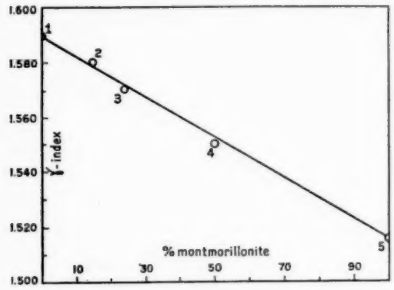

FIGURE 4.—RELATION BETWEEN GAMMA REFRACTION INDEX AND MONTMORILLONITE CONTENT IN MIXED-LAYER ILLITE-MONTMORILLONITE CLAY MINERALS

1, "theoretical" illite; 2, hydromica, Hummer vein; 3, hydromica, Cold Spring mine; 4, 1:1 illite-montmorillonite clay, Chance mine; 5, "theoretical" montmorillonite.

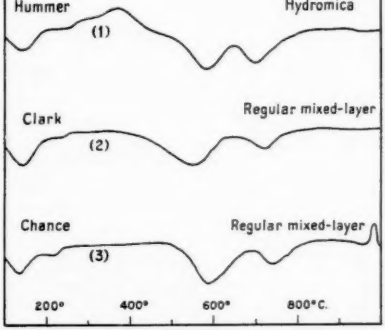

FIGURE 5.—DIFFERENTIAL THERMAL CURVES OF MIXED-LAYER, ILLITE-MONTMORILLONITE CLAY MINERALS

1, hydromica with 13 per cent montmorillonite; 2 and 3, 1:1 illite-montmorillonite. The presence of about 10 per cent kaolinite enhances the 600°C. peak in the last two samples.

pyrite (3.2 per cent), phosphates (2 per cent), and gypsum (.8 per cent). With the exception of quartz, these impurities can be reckoned out of the analysis. The percentage of quartz was found by X-ray methods, using the following procedure: The relative intensities of the 4.45 Å (clay) and 4.25 Å (quartz) peaks were determined for samples containing increasing amounts of added quartz. A curve was thus obtained which by extrapolation gave a quartz content of 5 (±1) per cent for the original sample. The structural formula shown below,

TABLE 2.—CHEMICAL ANALYSES OF HYDROMICA AND MIXED-LAYER CLAY MINERAL

Analyst: Doris Thaemlitz, Rock Analysis Laboratory, University of Minnesota

	(a) Ingram FR112	(b) Chance FR156
SiO_2	53.74	53.13
Al_2O_3	23.78	27.02
TiO_2	.76	.03
Fe_2O_3*	3.87	1.01
MnO	.02	.00
MgO	2.02	1.30
CaO	.55	.11
Na_2O	.15	.06
K_2O	6.96	4.96
BaO	.02	.02
H_2O+	3.94	6.83
H_2O-	1.23	3.66
SO_3	.89	n.d.
S	1.70	.08
P_2O_5	.34	.08
	99.97	98.29

* Total Fe as Fe_2O_3

(a) Hydromica, including about 10 per cent of randomly interstratified montmorillonite

(b) Regular mixed-layer 1:1 illite-montmorillonite mineral

calculated from the corrected analysis, shows that the charges are distributed between the tetrahedral and octahedral layers:

$$K_{1.32}Na_{.04}(Si_{7.26}Ti_{.07}Al_{.67})(Al_{3.27}Fe_{.16}Mg_{.46})O_{20}(OH)_4$$

This formula does not reflect the real structure because, according to X-ray data, this mineral contains about 10 per cent interlayed montmorillonite.

REGULAR MIXED-LAYER CLAY MINERALS: The existence of clay minerals formed by regularly interstratified unit layers of two different species has been recognized only recently. Alternating vermiculite and pyrophyllite (rectorite) wat described by Bradley (1950). Vermiculite or montmorillonite interstratified with chlorite (corrensite) has been found by Stephen and McEwan (*in* Bradley and Weaver, 1956), Honeyborne (*in* Bradley and Weaver, 1956),

Lippmann (1954), Sudo *et al.* (1954), Early *et al.* (1956), and Bradley and Weaver (1956). Illite-montmorillonite has been found by Heystek (1954). In all instances the ratio of the two constituents is 1:1.

Table 3.—Tabulation of Lattice Basal Spacings of Regular Mixed-Layer Illite-Montmorillonite Clay Minerals

See Figure 6 for relative intensities.

(In Å Units)

Order	Chance		Crackerjack		Clark		Lily		Prospect	
	Air-dried	Glycolated	Air-dried	Glycolated	Air-dried	Glycolated	Air-dried	Glycolated	Air-dried	Glycolated
001	23.10	26.8	23.5	26.3	24.5	26.8	22.3	26.0	24.5	26.0
002	11.55	13.4	11.9	13.1	11.5	13.2	11.5	13.2	12.0	13.3
003	7.87	8.94	7.5	8.93	—	9.0?	—	8.4	—	—
004	5.46	6.73	5.95	6.6	—	6.6		—	—	—
005	4.70	5.37	4.97	5.30	4.97	5.2		5.3	4.95	5.2
006	3.93	4.49	—	4.44		4.40				
007	3.36	3.88	3.30	3.75		3.78				
008	—	3.38	3.13	3.33		3.30				
009	2.62	3.01		2.98		2.99				

Examples of the illite-montmorillonite mixed-layer mineral were found in the course of the present study in the Chance (Tungsten), Clark, Crackerjack, Prospect, and Lily mines. The mixed-layer clay occupies a definite position within the alteration halo of the veins and plays essentially the same role as hydromica (see below). Where reasonably pure, it forms gray-white aggregates pseudomorphic after plagioclase. Under the microscope the aggregates resemble those of hydromica although they are somewhat finer-grained. These aggregates are much more easily dispersed than those of hydromica. In some aggregates the ill-defined, tiny (5–10 microns) booklets of mixed-layer clay show interstratification of a low-index substance. X-ray analysis failed to reveal the nature of these intercalations. The refraction indices are fairly consistent:

$\alpha = 1.520 \pm 2, \quad \gamma = 1.552 \pm 2, \quad B = 0.032.$

The angle $2V(-)$, as measured on oriented aggregates, is somewhat smaller than that of muscovite. Possibly randomness in the *a*, *b* orientation of the plates has reduced the apparent optic angle. The indices of refraction are the arithmetic mean of the two interlayered clays, as shown in Figure 4.

The interlayered nature of the clay is revealed by its X-ray-diffraction pattern. Figure 6 shows the diffraction curves of three mixed-layer clays from different localities, in air-dried and glycolated conditions. The mounts are oriented aggregates, so that only the basal reflections are recorded. The corresponding spacings are shown in Table 2. The significant feature of all patterns is the presence of a 001 periodicity between 23 Å and 24 Å in the air-dried state and between 26 Å and 28 Å in the glycolated state. This large spacing is due to the alternation of illite and montmorillonite layers in a 1:1 ratio. The glycolation increases the basal spacing by about 3 Å. Furthermore, glycolation reinforces the basal reflection (especially the weak higher orders) and makes the series more rational. In the Chance and Crackerjack clays the 003 (8.94 Å) reflection appears after glycolation. This is explained by its partial reinforcement by the 001 reflection of illite (10 Å) and the 002 reflection of montmorillonite (8.2 Å–8.4 Å). The presence of free hydromica as impurity, as in the samples from Clark and Lily tunnels, masks this reflection.

The differences in the 001 spacings depend largely upon the exchangeable cations. The result of leaching in Chance clay with different cations can be seen in Figure 7, where the 001 spacings of the air-dried and glycolated H-, Na-, NH_4-, and Ca-saturated clays are plotted together with those of two montmorillonite clays. To facilitate the comparison the spacing corresponding to the illite layer (10 Å) has been subtracted from the 001 spacing of the mixed-

layer clay. The coincidence in the plotting is further proof of the presence of montmorillonite layers in the structure.

temperature, exothermic peak shown by the Chance sample is probably reinforced by kaolinite.

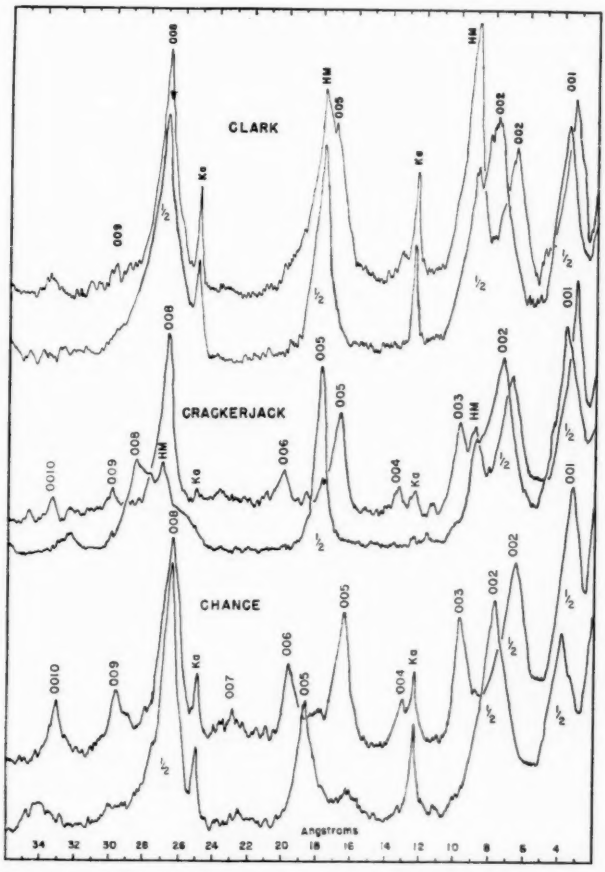

FIGURE 6.—X-RAY-DIFFRACTION CURVES OF REGULAR MIXED-LAYER, 1:1 ILLITE-MONTMORILLONITE CLAY MINERALS

Some peaks have been reduced in a ratio indicated in each case. Glycolated (top) and air-dried (bottom) samples used in each pair.

The thermal behavior of the mixed-layer clay is demonstrated by the D.T.A. curves of Figure 5. They show a low-temperature endothermic peak with a shoulder (indicating that Ca as the predominant exchangeable cation) and two middle endothermic peaks near 600°C. and 700°C. The last two peaks correspond, respectively, to the illite and montmorillonite layers. The 600°C. peak appears to be reinforced by the kaolinite (Chance) and hydromica (Clark) present as impurities. The high-

Table 2, *b* presents a chemical analysis of the mixed-layer clay from the Chance mine. The sample, which contains about 2 per cent kaolinite, has been HCl-leached. The structural formula, after correcting for kaolinite and a small amount of pyrite and woodhouseite, is as follows:

$$K_{.59}(Al_{1.70}Si_{7.30})(Fe^{3+}_{.11}Mg_{.20}Al_{3.62})O_{20}(OH)_4$$

If the formula is split into a 1:1 illite and montmorillonite layering it becomes:

Illite: $K_{1.78}(Al_{1.40}Si_{6.60})(Mg_{.38}Al_{3.62})O_{20}(OH)_4$

$$\text{Montmorillonite: } Si_{8.00}(Fe^{3+}_{.22}\ Mg_{.22}\ \overset{M_{.22}}{\overbrace{\quad\quad}}\ Al_{3.62})O_{20}(OH_4)$$

The above formulas probably do not represent the actual distribution of atoms in the layers, which is possibly as follows:

	$Si_{4-x} + Al_x$
	O_6
	K_{1-2}
	O_6
	$Si_{4-x} + Al_x$
	$O_4 + (OH)_2$
	$Al_{4-y} + (Mg, Fe^{3+}, Fe^{2+})_y \quad (y = 0\text{–}4)$
	$O_4 + (OH)_2$
	Si_4
±25 Å	O_6
	Exchangeable cations + water
	O_6
	Si_4
	$O_4 + (OH)_2$
	$Al_{4-y} + (Mg, Fe^{3+}, Fe^{2+})_y$
	$O_4 + (OH)_2$
	$Si_{4-x} + Al_x$
	O_6
	K_{1-2}

PHLOGOPITE: The magnesian mica phlogopite results from the alteration of biotite. It appears as monocrystalline pseudomorphs generally including abundant siderite or ankerite (Pl. 2, fig. 2). Unaltered remnants of biotite parallel to the cleavage planes are common. The pseudomorphs are light green, darker where the iron-rich carbonate is abundant, and yellowish where jarosite is also present. Under the microscope phlogopite appears pale green to colorless and shows numerous inclusions of rutile needles, tiny euhedral tablets of epidote, and iron oxides. The rutile needles lie in hexagonal pattern on the cleavage planes. The gamma index ranges from 1.560 to 1.585, with the majority between 1.565 and 1.570. The birefringence is about 0.035, and the optic negative angle is about 10°. Some single plates show changes in 2V values from one area to another, from 0° to 45°, indicating different degrees of phlogopitization. X-ray analyses show a 060 reflection at 1.54 Å, thus confirming the trioctahedral character of this mica. The above data indicate a very low Fe:Mg ratio.

BIOTITE: Secondary biotite is found only in the Jamestown area. It appears in fine-grained clusters of relatively well-formed, sharp individuals with good pleochroism. In one case a bluish tint (indicating Cr?) was detected on Z. Pale biotite with weak pleochroism is also found.

Secondary biotite is not related to the vein alteration but belongs to an earlier Laramide, greisenlike replacement (see below).

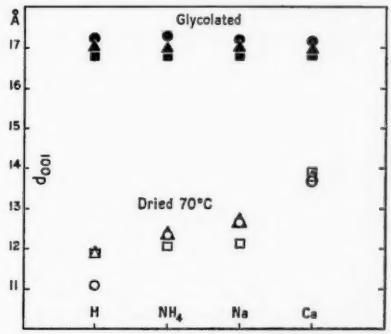

FIGURE 7.—RELATION BETWEEN ool SPACING AND NATURE OF THE EXCHANGE CATION IN MONTMORILLONITE

Triangles, Poorman mine; circles, White Raven mine; squares, Chance mine. The Chance sample is a 1:1 illite-montmorillonite; plotted value is d_{001} minus 10 Å.

POTASSIUM FELDSPAR: Orthoclase is found as replacement of plagioclase, generally associated with kaolinite and hydromica (Pl. 2, figs. 3 and 4). Whether or not feldspar is the predominant secondary mineral in the pseudomorphs after plagioclase, it preserves the crystallographic orientation of the host, as indicated by external form or ghost twinning. Orthoclase is also found lining microscopic fissures, especially where these cut microcline crystals. Tiny, euhedral crystals are found within a few kaolinite aggregates. Universal stage measurements show that the optic plane is parallel to $(10\bar{1})$, and gamma is normal to (010). The indices of refraction are somewhat variable: $\alpha = 1.516 - 1.519$; $\gamma = 1.523 - 1.527$; $2V(-) = 40° - 42°$.

WOODHOUSEITE: A phosphate of the svanbergite-goyazite group was mentioned by Lovering in his work on the Boulder County tungsten veins (Lovering, 1941, p. 249). It appears as pale-yellow, tiny cuboid crystals disseminated especially in hydromica but also in the vein-filling microcrystalline ("horn") quartz. Clay aggregates containing the alunite-like phosphate may show yellowish tint. The refraction indices on some of the largest rhombohedrons were: $\alpha = 1.646$; $\gamma = 1.654$: B = 0.008.

These values fit well with those of the mineral woodhouseite.

JAROSITE: Jarosite is found in small quantities, chiefly in the innermost (hydromica) zone of alteration, both as an alteration product of biotite and as a superficial coating. In the first case it is probably hydrothermal, since it shows the same type of occurrence as the iron carbonates; the superficial jarosite was probably reprecipitated at a supergene stage.

QUARTZ AND OPAL: Outside the vein filling, quartz is present in small to moderate amounts in the wall rock as replacing mineral. At the Wellington mine, Breckenridge, vein no. 2 shows considerable silicification accompanying the hydromica replacement. Small quantities of quartz and opal associate with the kaolinite replacing plagioclase in the Cold Spring mine; quartz occurs in small, equant grains with marginal intergrowth with the clay, whereas opal forms tiny vesicles.

Description of Individual Patterns

PATTERN I: Pattern I was found in the southwestern end of the belt, in the only mines active at the time of this study—the Wellington mine at Breckenridge and the Silver King mine at Montezuma. It also extends to the Argentine district, where it has been recognized in the Grizzly mine. The ores are essentially lead and zinc sulfides in carbonate gangue. At Wellington, pyrite and quartz are also abundant. The country rock in the Wellington mine is a quartz latite porphyry with abundant, small andesine and biotite phenocrysts in a fine-grained groundmass of quartz, potassium feldspar, and little orthoclase. Pre-Laramide (?) alteration is represented by some sericite and chlorite replacement of, respectively, plagioclase and biotite. At Silver King, the country rock is quartz-oligoandesine amphibolite schist with layers of fine-grained tonalite and granodiorite, probably metasomatic; coarser, more granitic areas are also present.

The Laramide alteration is basically the same in both mines. There is a single, symmetrical bleached zone, where plagioclase has been replaced by hydromica to a distance of about 15 times the width of the vein. Iron-rich carbonate is a common associate of hydromica. Biotite is altered to kaolinite, quartz, and siderite in the porphyry, and to phlogopite and siderite in the schist. These assemblages are typical of the entire mineral belt. Silicification is common but irregularly distributed at Wellington; it attacked only the groundmass, which otherwise is generally less altered than the phenocrysts. The bleached zone grades into the fresh rock as hydromica disappears. Kaolinite is present erratically in the outer edge of the hydromica zone at Wellington and is also mixed in small quantities with the hydromica in the pseudomorphs after plagioclase. Nontronite occurs in the border zone at Silver King. Pyrite is widely though unevenly disseminated in the bleached zone in both mines, and iron carbonates replaced hornblende in the amphibolite schist.

Outside the southwest end of the belt, pattern I was found only at the Quaker City vein in Gordon Gulch, near Nederland. A profile studied just west of the caved crosscut tunnel showed a single zone, extending as much as 100 feet from the vein, where the predominant alteration product is hydromica. The plagioclase is not wholly altered throughout the zone, and the granite texture is well preserved, but in a zone about 2 feet wide enclosing the vein the wall rock has been replaced by white-gray, fine-grained, moderately soft material composed of quartz, hydromica, and sericite. The formation of this zone seems to have been favored by shearing and brecciation of the wall rock.

PATTERN II: Pattern II zoning is predominant in the Georgetown-Silver Plume-Argentine and the Ward lead-zinc-silver districts. The wall rock is injected schist, gneiss, and amphibolite of the Idaho Springs formation (Georgetown and Argentine), Silver Plume granite (Ward), and Laramide quartz monzonite (Ward). The alteration here is not so clearly related to the veins as in the other patterns and shows as an intensive replacement of plagioclase in wide

PLATE 1.—VEINS SHOWING PATTERN VI OF HYDROTHERMAL ALTERATION

FIGURE 1.—Pyritic gold vein. Gardner tunnel, Emancipation mine, Gold Hill district. V, vein; *hm*, hydromica zone; *or*, orthoclase zone; *ka*, kaolinite zone. Iron staining between hydromica and orthoclase zones. *mf*, montmorillonite and fringe zones (not distinguishable on the picture). Kaolinite zone is partly covered by dust coating. Width of alteration profile, about 2 feet.

FIGURE 2.—Rock specimen showing alteration zoning. Vasco 6 mine, Nederland (tungsten). V, vein (quartz); HM, hydromica zone; Or, orthoclase zone; Ka, kaolinite zone; Ph, zone of total phlogopitization of biotite, occupying the inner part of hydromica zone. Note absence of ferruginous bands. Height of specimen, 4 inches.

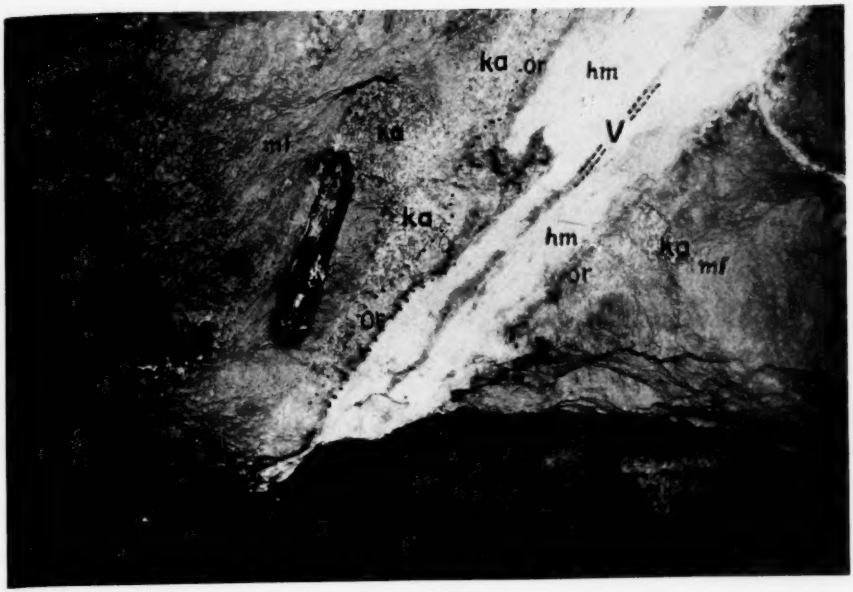

FIGURE 1

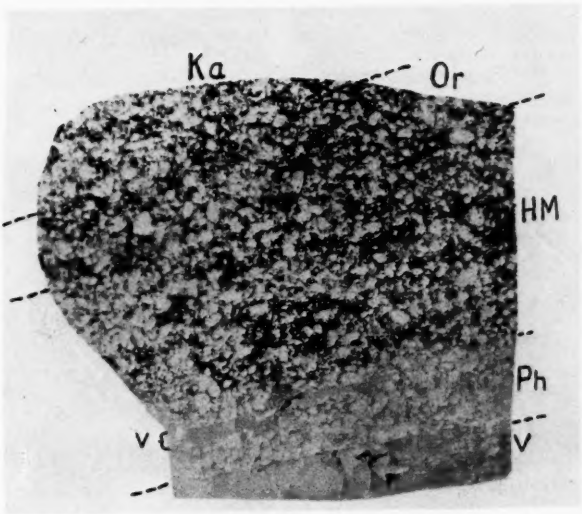

FIGURE 2

VEINS SHOWING PATTERN VI OF HYDROTHERMAL ALTERATION

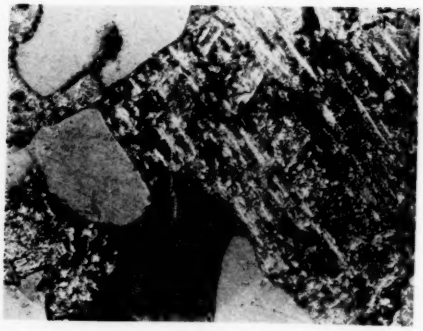

FIGURE 1

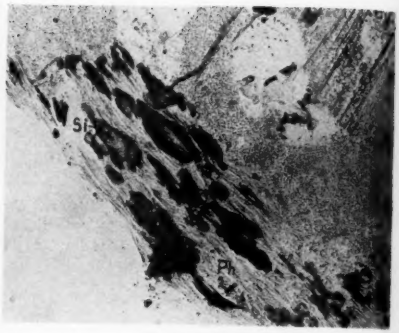

FIGURE 2

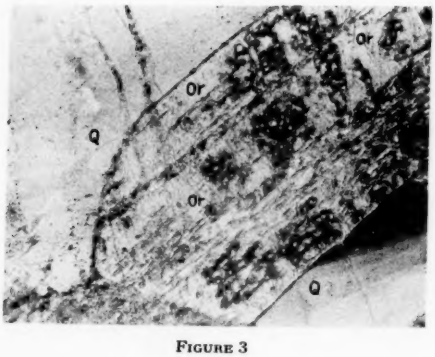

FIGURE 3

FIGURE 4

FIGURE 5

FIGURE 6

MICROSCOPIC FEATURES OF HYDROTHERMAL ALTERATION

areas enclosing one or more veins. The replacing material is an intimate mixture of hydromica, kaolinite, and montmorillonite. Biotite appears only slightly bleached, and carbonate is abundant. In the White Raven mine, near Ward, the sulfide veins show no conspicuous alteration halo, whereas one unmineralized fissure was found with well-developed alteration zoning: a main, inner zone with the clay mixture, and a less altered, grayer outer zone with kaolinite replacing plagioclase phenocrysts of the quartz monzonite porphyry, and montmorillonite predominating in the groundmass.

East of Ward the vein alteration changes gradually into that of the Gold Hill type. About 2 miles southeast of Ward, on Lefthand Canyon road, an abandoned tunnel shows both types of veins—that is, sulfide veins surrounded by an indefinite, weak hydromica-kaolinite alteration halo, and pyrite-quartz veins showing pattern V or VI, recognized by the ferruginous bands.

PATTERN III: Pattern III, found in the Jamestown district, includes four types of veins (Lovering and Goddard, 1950, p. 260–265): lead-silver, fluorspar, pyritic gold, and telluride, in order of decreasing age. No lead-silver veins were sampled by the writer. Generally, the alteration consists of a single zone of hydromica, quartz, and orthoclase, in places superimposed on a mild greisenlike replacement of the granite, characterized by poikilitic muscovite and abundant secondary orthoclase and quartz. Fine-grained, well-crystallized biotite is common, generally in veinlets associated with muscovite, quartz, and other secondary minerals. Secondary is distinguished from primary orthoclase—which it partly replaces—by its finer grain and association with other secondary minerals and by its smaller optic angle (40° as against 60°–70°). Fluorite is a common associate, as well as pyrite; topaz is uncommon. The greisenlike alteration is found all over the Jamestown area and is apparently related to the fluoride mineralization. It is not restricted to the area of productive fluorspar veins, having been found as far east as Springdale (Gladiator mine). The quartz monzonite porphyry of the Jamestown stock also shows replacement by orthoclase (as patches within the plagioclase), fluorite, hydromica or sericite, and fine-grained biotite. Secondary biotite has replaced primary biotite and hornblende, or forms veinlike aggregates.

The wall rock of the fluorspar veins shows little apparent alteration, though the microscope reveals more secondary orthoclase and hydromica than the average. Hydromica and sericite or hydromica are abundant in the fine-grained fluorite veins.

The alteration in the Jamestown district can be summarized as follows: (1) a widespread, greisenlike replacement of the granite, represented by poikilitic white mica, milky quartz, orthoclase, a little fluorite, fine-grained biotite, and in a few places topaz; (2) a restricted alteration zone of hydromica and orthoclase replacing plagioclase, related mainly to the gold telluride pyritic veins; orthoclase and fine-grained fluorite aggregates replaces the rock almost indiscriminately in places. Veins with a zone of almost exclusively hydromica (or sericite) alteration are also found (Grand Central telluride mine).

The Jamestown district deserves more detailed studies to establish more precisely the structural and petrographic relations between the different phases of alteration.

PATTERN IV: The alteration associated with the galena-sphalerite-pyrite veins in the Idaho tunnel of the Caribou mine (Smith, 1938) near

PLATE 2.—MICROSCOPIC FEATURES OF HYDROTHERMAL ALTERATION

FIGURE 1.—Hydromica pseudomorphs after plagioclase. Note twinning reflected in the arrangement of clay individuals. Unaltered individuals are quartz. Snowbound mine. Crossed nicols, ×110.

FIGURE 2.—Phlogopite (Ph) and iron carbonate (Si) replacement of biotite. Adjacent plagioclase is replaced by hydromica. Logan mine. ×80.

FIGURE 3.—Orthoclase (light gray, *Or*) and kaolinite (dark-gray aggregates) in pseudomorph after plagioclase. Some hydromica marks the original plagioclase twinning. *Q*, quartz. Eureka mine (tungsten). Crossed nicols, ×100.

FIGURE 4.—Orthoclase (light gray, *Or*) and kaolinite (dark-gray aggregates) pseudomorphic after plagioclase. Orthoclase veins, containing some hydromica, are optically iso-oriented. Crevices in the middle of veins suggest that replacement progressed from cracks in the host. Eureka mine (tungsten). Crossed nicols, ×110.

FIGURE 5.—Kaolinite (dark-gray aggregate) and hydromica (light gray) replacement of plagioclase. Note relict twinning in hydromica. *Q*, quartz inclusion. Clay-rich area in the orthoclase zone. Eureka mine. Crossed nicols, ×100.

FIGURE 6.—Montmorillonite veinlets in plagioclase. Montmorillonite zone, Cold Spring mine. Crossed nicols, ×130.

Nederland, Boulder County, represents pattern IV. This was the only working to which the writer had access, since the mine was closed down at the time of his visit. The alteration lets. The kaolinite pseudomorphs contain subordinate hydromica and sericite; some enclose also thin veinlets of potassium feldspar. The thickness of the zone averages 8 inches.

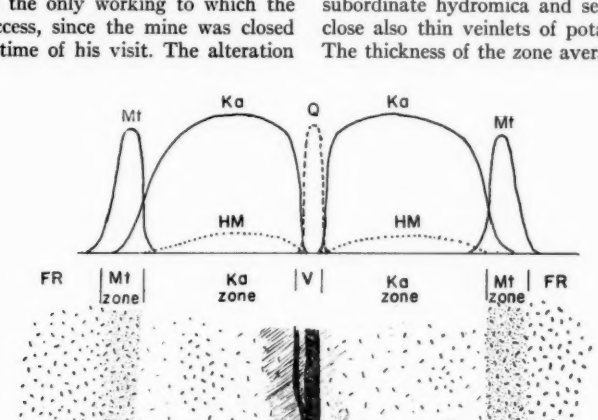

FIGURE 8.—CROSS SECTION OF ALTERATION ZONES AT CARIBOU MINE, IDAHO TUNNEL
Pattern IV. HM, hydromica; Ka, kaolinite; Mt, montmorillonite; Q, quartz; V, vein; FR, fringe zone. Total width of profile, 3 feet. Curves in upper part of figure show approximate proportions of secondary minerals.

here consists of a bleached, moderately coherent, kaolinite inner zone, and a narrower, crumbly montmorillonite-kaolinite outer zone (Fig. 8).

Two veins, the Caribou and the Poorman, were sampled at several places. The wall rock (Wright, 1954) is a fine-grained monzonite to quartz monzonite with variable proportions of biotite, hornblende, and—in lesser amounts—augite. In the area sampled, the total proportion of mafic minerals varies widely within a few feet or inches. In the monzonite stock, the rock outside the range of the Laramide alteration is very fresh.

The veins consist of brecciated rock replaced by microcrystalline quartz and iron-rich carbonate. Sulfides are discontinuous along the veins. Banded texture is common, generally with microcrystalline quartz and carbonate in the middle and coarse-grained ankerite on the sides.

The bleached, inner zone is characterized by kaolinite pseudomorphs after plagioclase. Biotite is replaced by kaolinite and siderite, but areas of slightly altered biotite are present. The other mafic minerals are replaced by iron-rich carbonate, which is also common in veinlets. The kaolinite pseudomorphs contain subordinate hydromica and sericite; some enclose also thin veinlets of potassium feldspar. The thickness of the zone averages 8 inches.

The montmorillonite-kaolinite outer zone is 1–2 inches wide and is softer and grayer than the inner zone. All plagioclase crystals have been altered into montmorillonite and kaolinite mixed in similar amounts. Some biotite plates have been replaced by a mixture of phlogopite, siderite, and quartz. As in the inner zone, potassium feldspar, quartz, and apatite are fresh, but magnetite is oxidized. Hornblende and augite are less altered in the outer zone. The zone limits are sharp.

Wright (1954) described in detail the wall-rock alteration related to a uranium-bearing vein in the 1040-foot level of the same mine, 540 feet below the Idaho tunnel level. His findings coincide only partially with the writer's. Outward from the vein, he finds on one side three zones: (1) sericite-kaolinite zone, bleached, hard; (2) montmorillonite-kaolinite zone, gray green, crumbly; (3) sericite (kaolinite) zone, white, compact. On the other side there is only a sericite zone analogous to (1) and (3). In the kaolinite pseudomorphs of the writer's inner zone hydromica or sericite reach in places 20 per cent, thus approaching the composition of Wright's inner zone. Zone 3 is not represented in the veins here described. Rock fragments

found in the mine dump show, however, sulfide veinlets surrounded by sericitized wall rock. Apparently, two separate phases of alteration are partially superimposed in this deposit.

In the Idaho tunnel, the granite-injected schists of the Idaho formation show a widespread argillic alteration similar to that found in the Georgetown area (pattern II).

PATTERN V: Pattern V may be considered as an underdeveloped pattern VI, from which it departs only by the absence of the orthoclase zone. It has been found only in the Corning tunnel near Gold Hill and the Lily tunnel near Nederland. Since only one vein was accessible in each mine, pattern V may be typical of the whole mine or of only the vein sampled. It may also be present in deposits where pattern VI is predominant. Pattern V corresponds to the zoning described by Lovering (1941) and Lovering and Tweto (1953) from the same area, and by Sales and Meyer (1948) from Butte, Montana. Its megascopic and microscopic characteristics are identical, with the above exception, to those of pattern VI.

The Corning tunnel, located half a mile northeast of Gold Hill, cuts the Iowa vein 200 feet from the portal. The wall rock is a medium-grained biotite granodiorite (Boulder Creek granite). The vein belongs to the pyritic gold type and consists here of fine-grained quartz stringers, each of which shows its own alteration zoning where separation is sufficient. Thin fissures filled by dolomite show the same pattern. The width of the zones is roughly proportional to that of the veins. Ferruginous bands parallel the veins at a distance within the inner zone; the inner part of this zone has been bleached by probably supergene solutions that dissolved the iron-rich carbonates and precipitated the iron hydroxides near the outer boundary of the zone, generally leaving a light-green-gray margin of the unbleached hydromica zone. The kaolinite zone is well developed and characterized by white clayey pseudomorphs that contrast with the relatively unaltered biotite.

In the Lily tunnel (Lovering and Tweto, 1953) there is access only to a thin quartz ferberite vein about 50 feet from the portal. The zoning, that is obscured by ferruginous staining and pre-Laramide sericitization, is asymmetrical; the zones are wider and better defined in the hanging wall and contain in the outer part of the kaolinite zone abundant illite-montmorillonite regular mixed-layer clay, which is absent in the foot wall.

PATTERN VI: Pattern VI represents the most complex zoning in the mineral belt and is found in the Nederland tungsten and Gold Hill pyritic gold districts, Boulder County. More than 12 mines[1] were studied; the alteration zoning is consistent, and a description of each therefore will not be given here. The only difference in the alteration of tungsten and pyritic gold veins is a ferruginous staining (Pl. 1, fig. 1) that is either absent or weak in the tungsten veins, in accordance with the relative absence of pyrite. The mode of occurrence of the different secondary minerals can be taken as representative of the entire mineral belt and will therefore be described in some detail.

Most of the veins cut Boulder Creek granite (Lovering and Tweto, 1953), a highly migmatitic rock ranging from medium-grained granite to biotite-hornblende tonalite gneiss. The most common facies is a medium-grained gneissoid biotite-adamellite. Masses of fine-grained and aplitic facies are abundant (*e.g.*, Hurricane Hill), as are pegmatite dikes. The plagioclase (calcic oligoclase) is generally replaced by 10–20 per cent of sericite of pre-Laramide age.

There are three clearly visible alteration zones (Pl. 1, fig. 1). The innermost zone is textureless, grayish white with yellowish jarosite staining, and moderately friable; biotite is discolored. The middle zone, less conspicuous and narrower than the other two, is greenish gray and of normal hardness; it grades into the inner zone, whereas its outer boundary is marked by a sharp decrease in hardness. The third zone is friable and characterized by white argillic pseudomorphs after plagioclase, contrasting with the moderately fresh biotite; it grades into the fresh rock. This zone corresponds to Lovering's argillic zone, and the middle zone is roughly what he called "hard casing" (Lovering, 1941). To each zone corresponds a different mineral assemblage: inner zone, hydromica-phlogopite-iron carbonate; middle zone, orthoclase-kaolinite-hydromica; outer zone, kaolinite-montmorillonite. In many veins a closer study reveals a fourth zone in which montmorillonite,

[1] Sample localities include: tungsten: Chance mine, Nederland, first level; Clark tunnel, Nederland, Barker 1 vein; Clyde tunnel, Nederland, Footwall vein; Cold Spring mine, Nederland, fifth and seventh level; Crackerjack tunnel, Millionaire Gulch; Eureka tunnel, Middle Boulder Creek; Hoosier-Hummer mine, 225-foot level; Prospect tunnel, Nederland. Pyritic gold: Emancipation (Gardner) tunnel, Gold Hill; Ingram tunnel, 120-foot level, Gold Hill; Logan and Grand Republic mines, Gold Hill, tunnel level; Poorman mine, Gold Hill, tunnel level; Snowbound tunnel, Gold Hill.

lying between the kaolinitic zone and the fresh wall rock, is the only clay mineral. A fifth, outermost zone may be distinguished in which the only alteration is a partial replacement of the mafic minerals by phlogopite and carbonate.

orthoclase, and barite. Cavities filled with opal and kaolinite are common. The "dark horn" (Lovering, 1941) contains abundant interstitial ferberite.

The hydromica zone coincides partially with

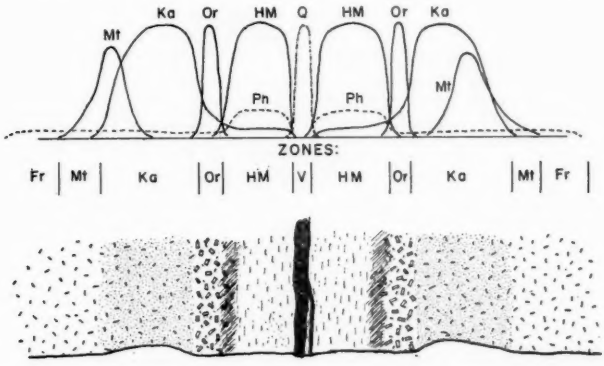

FIGURE 9.—IDEALIZED CROSS SECTION OF A VEIN SHOWING ALTERATION PATTERN VI
See Figure 8 for definition of symbols. Ph, phlogopite-siderite alteration of biotite. Iron-staining bands between hydromica and orthoclase zones.

Figure 9 shows an idealized section of a vein and its alteration zoning. The curves indicate the relative abundance of the main secondary minerals. The zoning was studied, wherever possible, on both sides of the veins and was found to be essentially symmetrical in most veins. In the following description, each zone is designated by its critical secondary mineral. Thus, the successive zones, outward from the vein, are: hydromica zone, orthoclase zone, kaolinite zone, montmorillonite zone, and fringe zone. Figure 10 shows the type and degree of replacement for each of the main primary constituents of the wall rock. Alteration zones are generally described in the veinward sequence, a procedure that is based on the belief that the zones have developed successively from the fresh rock toward the vein. The writer believes that this assumption is unjustified because the zones may develop simultaneously, each under a particular physicochemical environment. This is thought to be the case of the zone patterns described in this paper.

The veins are formed by microcrystalline quartz ("horn quartz", Lovering, 1941); in places they have drusy cavities lined by quartz, kaolinite, and, in tungsten veins, ferberite. Pyrite is fine-grained and disseminated. The microscope shows interstitial carbonate, woodhouseite, kaolinite, and hydromica, scanty shear zones in many veins; cataclasis, in addition to the discoloration of biotite, causes the texturelessness of this zone (Pl. 1, fig. 1). In a few veins, completely altered biotite does not occupy the entire width of the zone (Pl. 1, fig. 2). Yellowish jarosite staining is generally present. In the pyritic veins, staining by iron (and manganese) hydroxides hides the transition with the orthoclase zone. This staining, very conspicuous in most places, is banded and forms a veneer on old exposed surfaces; on fresh surfaces the hydroxides appear in the intergranular interstices of the rock. Gypsum also coats the wall rock in this zone.

Mineralogically, the inner zone is characterized by the replacement of plagioclase by hydromica (Pl. 2, fig. 1), and—generally—the discoloration of biotite to pale-green phlogopite (Pl. 2, fig. 2). Iron-rich carbonate (both siderite and ankerite have been detected) appears as lenses in the phlogopite and also forms irregular aggregates and veinlets; these are scarce in the bleached part of the zone. The hydromica pseudomorphs enclose granules of iron carbonate and woodhouseite; the phosphate may produce a yellowish tint. If pre-Laramide sericite is present, its well-defined lamellae contrast with the smaller, fluffy individual crystals of hydromica. Quartz and opal are present in the pseudomorphs in certain veins (*e.g.*, Cold

Spring mine). X rays reveal small quantities of kaolinite intimately mixed with the potassic clay.

The width ratio of hydromica zone to vein is about 5:1. Maximum thickness was found in the Clyde tunnel, where the zone extends almost 25 feet (Fig. 16).

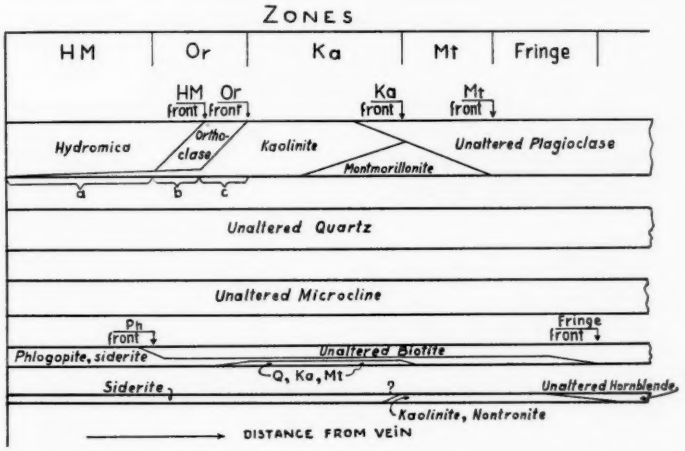

FIGURE 10.—DIAGRAM SHOWING DEGREE AND TYPE OF ALTERATION OF MAIN PRIMARY MINERALS IN THE PATTERN VI VEINS

The relative abundance of the primary minerals is indicated by the width of the blocks. a, range of rapid expansion of the hydromica front during the initial stage; b, c, expansion of hydromica and orthoclase fronts, respectively, during the main stage of alteration.

The orthoclase zone retains in part the hardness of the fresh rock because of the presence of the feldspar in pseudomorphs after plagioclase, in contrast with the exclusively argillic alteration of the adjacent zones. Secondary orthoclase preserves the crystallographic orientation of the host, whether it replaces the whole or only veinlike parts of it (Pl. 2, figs. 3, 4). The pseudomorphs contain also kaolinite (Pl. 2, fig. 5) and hydromica. Orthoclase is easily distinguished from the microcline by the lack of twinning and abundance of inclusions and appears in places to have replaced plagioclase along cracks (Pl. 2, fig. 4). Hydromica follows cleavage and twinning planes, whereas kaolinite forms compact aggregates which do not reflect the structure of the host. Most of the biotite is preserved in the orthoclase zone, though its plates are paler and less straight than normal and lack their characteristic luster. Many mica plates show partial phlogopite carbonate alteration that appears to the naked eye as pale-green-gray flat lenses intercalated in the cleavage planes. Near the kaolinite zone, kaolinite and quartz take partially the pace of phlogopite and carbonate (Fig. 11). The orthoclase zone is from 2 to 6 inches wide in most of the veins studied by the writer.

The kaolinite zone has a sharp inner boundary and transitional outer boundary. The white argillic pseudomorphs have almost exclusively kaolinite, in places with some orthoclase stringers, near the inner boundary. In most of the zone, however, montmorillonite is also present, amounting to about 50 per cent of the pseudomorphs in some veins. Pseudomorphs with abundant montmorillonite are grayer and more crumbly (*e.g.*, Logan group; Snowbound mine). Montmorillonite forms interstitial films between kaolinite individuals. In this zone biotite shows the type of alteration present in the orthoclase zone, but the quartz-kaolinite-montmorillonite assemblage (Fig. 11) is here more abundant. In the Chance and Prospect mines, the kaolinite in the biotite is fibrous. The kaolinite zone is about as thick as the hydromica zone (average, 1 foot) and roughly 4–5 times thicker than the orthoclase zone.

The montmorillonite zone, as defined in this paper, begins where kaolinite becomes negligible; in this zone montmorillonite is the only clay mineral replacing plagioclase. Since this replacement is partial, the total amount of montmorillonite may be, and commonly is, less in this zone than in most of the kaolinite

zone (Fig. 9). The transition between the two zones begins with the appearance of unreplaced areas in plagioclase, separated by argillic veinlets of decreasing width. The veinlets show a kaolinite-rich argillic mixture in the middle and a wall zone of montmorillonite. The dis-

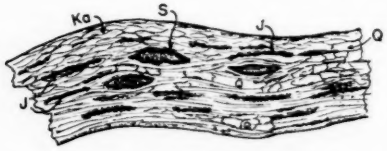

FIGURE 11.—ALTERATION OF BIOTITE IN THE KAOLINITE ZONE
Ka, kaolinite, with intercalated montmorillonite films. Q, quartz; S, siderite; J, jarosite.

appearance of the kaolinitic middle part marks the beginning of the montmorillonite zone. The alteration in this zone is shown in Figure 6 of Plate 2. The only megascopic sign of this alteration is a dull luster in the cleavage surfaces of the plagioclase. Biotite lacks the quartz-kaolinite-montmorillonite replacement typical of the kaolinite zone; otherwise it shows the dull luster and interleaved phlogopite carbonate layers that characterize the latter zone. Hornblende (Cold Spring mine) is partially or totally altered into an intimate mixture of iron carbonate, kaolinite, and nontronite.

In about half of the veins studied (Ingram, Logan, Poorman, Hoosier, Chance, and Crackerjack) montmorillonite and kaolinite disappear at nearly the same distance from the vein; the montmorillonite zone is therefore lacking here. This zone is everywhere much narrower than the kaolinite zone.

The fringe zone lies beyond the last trace of montmorillonite in plagioclase, where the only hydrothermal alteration is the partial phlogopitization of biotite and (at Cold Spring) the iron carbonate kaolinite-nontronite replacement of hornblende. This zone is equivalent to the propylitic zone of other areas (Sales and Meyer, 1948).

SUBPATTERNS VIa AND VIb: In variations of pattern VI montmorillonite enters as a regularly interstratified constituent of hydromica either in the outer part or the whole of the innermost zone (Fig. 2). The first, pattern VIa, was found in the Crackerjack (Fig. 12) and Prospect tunnels; pattern VIb is represented by the Chance mine and the Clark tunnel.

The presence of the mixed-layer clay mineral cannot be established without laboratory examination, but in places it can be suspected from some of the physical properties of the clay. Rocks containing the mixed-layer clay disaggregate more easily than those containing hydromica; where the two clay minerals occur

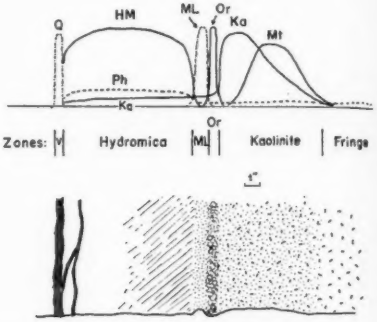

FIGURE 12.—CROSS SECTION OF THE ALTERATION ZONES AT CRACKERJACK TUNNEL
Subpattern VIa. *See* Figure 8 for definition of symbols. Ph, phlogopite-siderite alteration of biotite; ML, mixed-layer 1:1 illite-montmorillonite.

in adjacent zones, as in the Crackerjack tunnel, this difference may show up very clearly. In the Crackerjack mine, in a little more than 2 inches the alteration of the plagioclase passes successively from hydromica to mixed-layer clay, orthoclase, and kaolinite.

Some veins with pattern VI zoning may show an incipient development of subpattern VIa, as the randomly interlayered montmorillonite in the hydromica becomes more abundant toward the outer part of the hydromica zone. In the Cold Spring mine (fifth level) for instance, the content of montmorillonite in the hydromica increases from about 13 per cent in the main part of the zone to about 20 per cent in the outer part. This is accompanied by a decrease in the refraction indices from about 1.582 to about 1.570 for gamma.

CHEMICAL CHANGES

Table 4 shows the chemical composition of five samples from the vein and four successive zones of the Chance mine. This mine was chosen because the fine grain ahd homogeneous composition of the wall rock ensures more nearly representative samples than in most other mines. The variation curves (Fig. 13) have been calculated correcting for the bulk density of the rock as given in Table 4. It may be pointed

out here, however, that the bulk density measured on argillized rocks is likely to be misleading if no consideration is given to the increase in porosity that takes place in contact with atmosphere. Expansion occurs at the face of the workings by relief of pressure and hydration. Bulk-density values close to 2.0, as reported in some papers, must be abnormal and probably do not represent the density of the rock immediately after alteration.

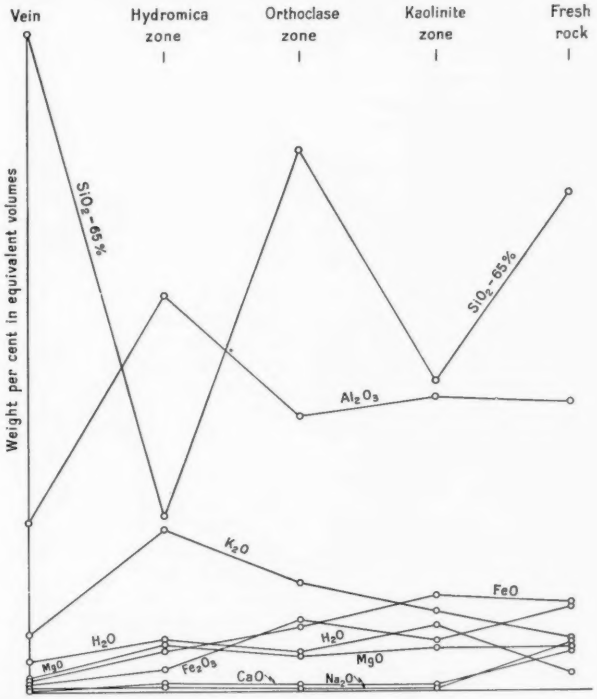

FIGURE 13.—CHEMICAL CHANGES IN THE ALTERATION ZONES, CHANCE MINE

Bulk chemical changes in the successive zones are moderate and probably indicate a limited transfer of matter. Only plagioclase and, to a lesser degree, the mafic minerals were affected by the alteration. In Figure 14 the gains and losses have been calculated with respect to the fresh rock. Solid blocks represent gains, ruled blocks represent losses; the height of the blocks is proportional to the percentage of the constituent in the fresh rock divided by its percentage in the altered rock, plotted on a logarithmic scale.

The gains of K_2O and Al_2O_3 and the loss of SiO_2 in the hydromica zone are due to replacement of plagioclase by the clay mineral, which in this mine is a mixed-layer species with 50-50 illite-montmorillonite. The gain of MgO must be attributed to both phlogopitization and formation of the clay mineral. The orthoclase zone shows a gain of K_2O, which has been limited by the presence of kaolinite in the pseudomorphs after plagioclase. The kaolinite zone lost SiO_2 and gained Al_2O_3 and K_2O; the alkali may be accounted for by the presence of fine veinlets of orthoclase in the clay pseudomorphs. With the alteration of plagioclase Na_2O and CaO have been strongly leached from all zones. The proportion of H_2O follows closely the clay content of the zones.

The broken lines in Figure 14 represent qualitatively the variations in the oxide concentration in the hydrothermal liquids as they migrated through the various zones. A gain in the rock corresponds to a loss in the solution and vice versa. The slope of the curve is qualitatively proportional to the magnitude of the

gain or loss in each zone, assuming that the solutions travel away from the vein.

The chemical changes in the Chance mine

TABLE 4.—CHEMICAL ANALYSES OF THE ALTERED WALL-ROCK ZONES, CHANCE MINE, NEDERLAND, BOULDER COUNTY, COLORADO

Doris Thaemlitz, analyst for FR155a, FR155b, FR158, FR159; Eileen H. Oslund, analyst for FR157; Rock Analysis Laboratory, University of Minnesota.

	Vein FR155a	Hydromica zone FR155b	Orthoclase zone FR157	Kaolinite zone FR158	Fresh rock FR159
SiO_2	88.97	74.96	80.85	78.29	79.55
Al_2O_3	5.23	12.38	8.02	9.09	8.45
Fe_2O_3	0.28	0.68	2.07	1.50	2.48
FeO	0 35	1.26	1.89	2.94	2.57
MgO	0.43	1.45	1.02	1.29	1.25
CaO	0.09	0.20	0.11	0.15	1.21
Na_2O	0.13	0.14	0.07	0.06	1.36
K_2O	1.79	5.06	3.13	2.42	1.37
H_2O+	1.07	1.73	1.35	2.17	0.69
H_2O-	0.82	1.18	0.45	0.57	0.12
TiO_2	0.22	0.28	0.49	0.56	0.62
P_2O_5	0.08	0.03	0.03	0.03	0.02
MnO	0.01	0.03	0.03	0.05	0.03
	99.47	99.38	99.76*	99.12	99.72
Bulk density	2.48	2.45	2.49	2.48	2.62

* Includes CO_2, 0.23; BaO, 0.01; S, 0.01

are very close to those found by Lovering in the Cold Spring vein (Lovering, 1941, p. 242, Table I). Unfortunately, analyses of the orthoclase zone of the latter vein are not available. The hydromica zones show a gain in MgO in the Chance mine and a loss in the Cold Spring mine. This may be attributed to the composition of the clay mineral, that at Cold Spring has only little interlayered montmorillonite.

ORIGIN OF HYDROTHERMAL ALTERATION

General Statement

The following discussion refers—unless otherwise stated—to pattern VI and its variations, although it can in general be applied to the other patterns.

Alteration and Vein Formation

Study of the veins in the Front Range mineral belt indicates that wall-rock alteration and vein filling took place in two separate phases. This conclusion is based on the following:

(1) Fissures containing no vein filling but showing a well-developed alteration zoning are common. These fissures were reached by the thin, gaseous altering fluids but not by the more viscous, less strongly propelled vein-filling solutions.

(2) Contemporaneity of the phases would mean that the altering fluids escaped into the wall rocks directly from the silica-rich, vein-forming liquids that filled the veins. Under such conditions the escaping phase would be expected to have carried substantial amounts of silica into the wall rocks. In general, no such silicification is found. If fractionation was incomplete, and the vein liquids still carried volatile constituents, some degree of silicification might have taken place (*e.g.*, at Breckenridge).

(3) Vein filling tends to seal off the fissures. Therefore, the altering phase must have arrived before the vein-forming liquids.

The contrasting physicochemical behavior of the two phases becomes apparent if the pervasive character of the wall-rock alteration is compared with the restricted, sharply bounded vein filling.

Lovering (1941) discussed in detail the formation of the tungsten and related veins of Boulder County, Colorado, and concluded that the argillic (kaolinite-montmorillonite) alteration preceded ore deposition, but that sericite (the writer's hydromica) and adularia were the product of a post-ore, alkaline phase (Lovering, 1941, p. 267, Fig. 17). He finds that the veins are genetically related to biotite latite dikes. Hydrothermal solutions would have escaped from the latite magmas as an acid, gaseous phase which later condensed and became alkaline by reaction with the wall rocks (Lovering, 1941, p. 274–279).

The present writer believes that the above-mentioned secondary minerals were formed in the same stage, before the formation of the ore veins.

Hydrothermal Differentiation

On separation of a hydrothermal phase including compounds of wide range of solubility and volatility, further differentiation may have

taken place with separation of a gaseous phase out of the liquid phase. The gaseous phase, containing a large part of the water and most

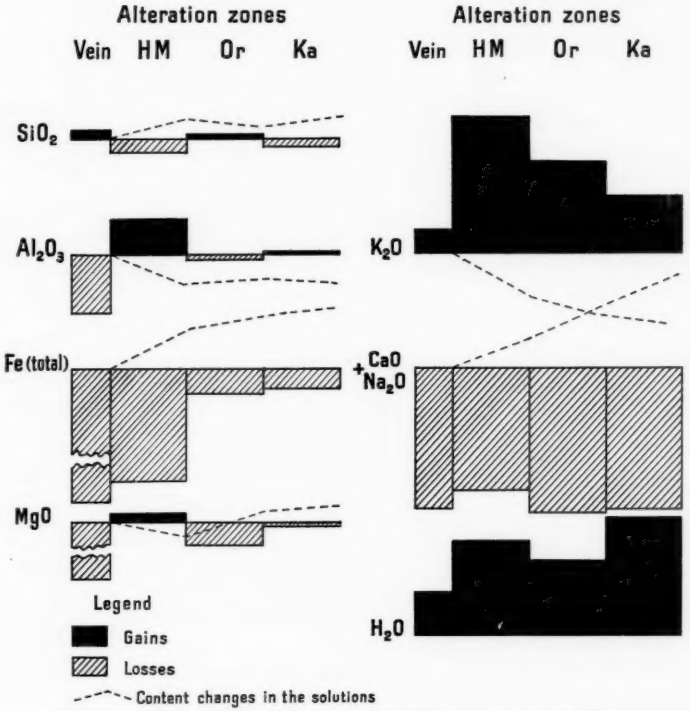

FIGURE 14.—DIAGRAM OF GAINS AND LOSSES, CHANCE MINE
HM, hydromica zone; Or, orthoclase zone; Ka, kaolinite zone. Dashed curves represent qualitative concentration changes in the fluids.

of the acid radicals including CO_2 and appreciable alkali chlorides, would have advanced ahead of the liquid phase. The liquid phase contained most of the silica and carbonate, as well as the ore metals.

The relatively high volatility of the ore-metal halides seems to indicate that the metals belonged to the gaseous phase. In the veins here studied, however, it is evident that most were deposited with the late silica-rich, vein-forming liquids. (*See* Lovering, 1941, p. 247–279.) Ferberite, for instance, is contemporaneous with at least much of the "horn" quartz, particularly with the coarser, subhedral variety. Drusy ferberite is common. Thus, the ore metals did not in any considerable extent escape with the vapor phase upon fractionation. The reason for this may be that in a silica-rich solution fluorine would escape as SiF_4, the boiling point of which is 178.3°K at 1 atm. (Kelley, 1935) rather than as WF_6, the boiling point of which is 290.4°K at 1 atm. (Kelley, 1935). The same would hold for the chlorine compounds.

The degree of fractionation of the "mother liquor" would depend upon the pressure gradient and the distance traveled. Lovering (1941, p. 277) states that "relatively open channels were available and, therefore, the pressures driving the solutions upward were not abnormally large". These conditions would have favored the separation of the two phases.

On the way upward the gaseous phase would have diffused into the wall rocks and caused alteration. Alteration could have lasted only until arrival of the vein-forming liquid which sealed off the fissures. If the liquids arrived at a given point at an early stage of fractionation the lateration halo would be narrow. Veins formed under these conditions would show no

constant relation between thickness of the vein and that of the alteration halo. The fact that such a relation exists in most veins of pattern VI indicates that fractionation has taken place, since the volume of the gaseous phase must be roughly proportional to that of the vein-filling column. A time gap probably separated the wall-rock alteration from the vein formation; because of differences in mobility, this gap would widen upward.

Probably no important change took place in the hydrothermal fluids as they traveled along the fissures. The portion not penetrating into the walls moved along too fast for any considerable reaction with the wall rocks. Many geologists have postulated that acid solutions ascending along fissures would gradually turn neutral or alkaline by reaction with the walls, on the assumption that the dissolved matter diffuses inward into the fissures. Assuming that the alteration progresses outward from the conduits it seems more logical to expect a pH decrease caused by gradual insulation of the wall rock by the alteration sheath. According to the hypothesis presented in this paper, no significant change of pH has taken place in the ascending solutions during the development of zoning in the Front Range, because the dissolved matter was carried away from the fissures through the successive zones and into the fresh wall rock by the bodily diffusing fluids. The writer believes that alteration progressed simultaneously in all zones, and that no totally altered, insulating sheath was therefore formed until the end of the process.

Mechanism of Zone Development

Sequential versus simultaneous origin of zones.—The zoning of the hydrothermal alteration has been attributed to one or more of the following mechanisms:

(1) Waves of hydrothermal solutions invading the rocks in separate phases or stages. Most workers using this concept (Lovering, 1949; Kerr, 1950; Kerr *et al.*, 1950; Peterson *et al.*, 1946; Schwartz, 1947; 1953; Stringham, 1953) imply definite time intervals between the waves or at least between their peaks. Chemical and/or physical properties of the fluids would vary from wave to wave. The stage concept has been applied mainly to porphyry copper deposits, where the spatial relationships of the zones are somewhat obscure.

(2) A single wave, the composition of which changed as the solution circulated along the channels (Lovering, 1941; 1950). Except for the continuity of the fluid invasion, this process may be theoretically considered similar to the one above. In both processes the zones are formed in a time sequence.

(3) Zones formed simultaneously by physical and/or chemical fronts as the solutions migrated away from the conduits into the wall rocks (Sales and Meyer, 1948).

Mechanism (2), as generally applied to veins (Lovering, 1941; 1950), provides for the formation of each zone at the expense of the inner part of the preceding one, so that the zone closest to the vein is the youngest.

The case for mechanism (3), simultaneous formation of the zones, has been convincingly stated by Sales and Meyer (1948, p. 32) with regard to the veins at Butte, Montana. Their chief argument is that the same arrangement of zones is found throughout the district "around every ore-bearing fracture, regardless of size, attitude or relative age. . . ." A separate origin of the zones would require "that the invading zone of sericitization never advanced completely through the argillized zone to attack fresh rock directly." A zone pattern produced by successive, encroaching waves of alteration must depart considerably from the regular arrangement invariably found at Butte.

Zoning at Butte is almost identical to the writer's pattern V, and Sales and Meyer's reasoning can just as properly be applied to the veins studied by the present writer. The strongest argument in favor of a simultaneous origin seems to be the striking persistence of the relative thickness of the zones and the lack of transgressive boundaries. There are clear indications in the veins of the Front Range mineral belt, that the formation of each zone was the direct consequence of the processes taking place during the formation of the next innermost zone. The changes in composition must have taken place as the fluids migrated through the wall rocks away from the veins, rather than during their ascent along the fissures.

The theory of simultaneous, parallel fronts seems to be the most logical explanation for the structural features of the multiple zoning in the Front Range mineral belt. The behavior of the fronts during the alteration presents several possibilities. Sales and Meyer (1948, p. 33) believe that at Butte "each zone migrated away from the fissure, that is, it grew at its outer edge and simultaneously receded at its inner edge because of encroachment by the next innermost zone." This means that when the sericite front reached a given plagioclase crystal the latter

had already been replaced by kaolinite. As far as the Boulder County deposits are concerned, the evidence is contrary to the idea of front migration.

Figures 1–5 of Plate 2 show the typical textural relationships found in the hydromica and the orthoclase zones. Hydromica seems to have replaced only plagioclase; the aggregates generally reflect the polysynthetic twinning. The inherited optical orientation of orthoclase indicates the same for this mineral; in one instance, relict albite twinning was observed in the secondary feldspar. No textural indication of replacement of kaolinite by either of the other two secondary minerals has been found. Kaolinite forms massive aggregates which do not reflect the structure of the host and contrast with the more ragged, structurally controlled hydromica or sericite, thus giving in places a false impression of mutual replacement (*See* Sales and Meyer, 1948, Fig. 4.) The intermingled kaolinite and montmorillonite show strong indications of having crystallized together. These facts oppose the idea of displacement of zone fronts as expressed by Sales and Meyer and indicate that the zones developed simultaneously and the alteration fronts became nearly stabilized early in the process. As the origin of the alteration is discussed in more detail, it will be evident, however, that a limited expansion of the fronts did take place.

Nature of alteration fronts.—The formation of the zone pattern VI can be described in terms of six fronts. Four represent the alteration of plagioclase; the other two correspond to the alteration of biotite:

Fronts for plagioclase:

(1) Hydromica front: outer boundary of the zone of stability of hydromica; inner boundary of the orthoclase stability zone

(2) Orthoclase front: outer boundary of the stability zone of orthoclase; inner boundary of the kaolinite zone

(3) Kaolinite front: outer boundary of the stability zone of kaolinite

(4) Montmorillonite front: outer boundary of the stability zone of montmorillonite (and of the instability zone of plagioclase), in places coincides with the kaolinite front

Fronts for biotite:

(1) Fringe front: outer boundary of the partial alteration of biotite (to phlogopite-siderite)

(2) Phlogopite front: outer limit of the complete decomposition of biotite. This is much sharper than the fringe front and generally coincides approximately with the hydromica front

There is also an instability front for hornblende, roughly coincident with that of biotite, or fringe front.

Fronts may be determined by one or more of the following factors: (1) temperature, (2) pH, and (3) chemical composition of the fluids. The temperature gradient in the wall rocks has been investigated by Lovering (1950) who concluded that, for a period of 10,000 years, the alteration takes place in "an almost isothermal environment" (p. 251). Although nothing is known of the duration of the process in this instance, the gradient probably could not have been steep enough to account for the formation of as many as four or five fronts within a distance of a few feet or even inches, even though the differences in the temperature fields of the minerals involved were larger than they seem to be, as well as in right order for the zone sequence—a doubtful condition. In a region of steep geothermal gradient, as in the mineral belt during Laramide times, the difference in temperature between hydrothermal fluids and wall rock must have been slight . The writer concludes, therefore, that temperature was a subordinate factor in the formation of the alteration zoning.

Changes in pH cannot explain the zoning. If other factors are constant, the passage from hydromica to orthoclase to kaolinite requires first an increase of alkalinity, followed by a sharp turn into acidity. Such changes would be difficult to explain.

Chemical gradients, determined by changes in composition of the hydrothermal fluids during their course through the wall rocks, remain the only major factor in the formation of zones. Temperature may have affected the position of the fronts or the width of the alteration halo; pH, a significant factor, must be considered in connection with the chemical gradient.

Development of alteration fronts.—The fluids permeating the wall rocks contained, as far as can be ascertained from the alteration products, H_2O, CO_2, $S^{=}$, $PO^{=}$, Cl^{-}, F^{-}, K^{+}, Mg^{++}. Their temperature was well above the lower limit of stability of sericite in acid solutions, which Gruner's (1944) experiments put at about 350°C., and was probably between 400° and 500°C. within the conduits. The fluids were probably supercritical and moderately acid. In this environment, plagioclase, biotite, and hornblende were unstable; other minerals, such as quartz, potassium feldspar, and most accessories, were either stable or metastable. As the concentration of the different chemical constituents changed by reaction with the wall

rock, chemical fronts were established, and the alteration zones began to form.

Figure 15 shows the stability fields of the main hydrothermal minerals involved, plotted against the Si/Al ratio as the ordinate and the change of K^+ and $Na^+ + Ca^{++}$ concentrations as the abcissa. The latter also corresponds to an increasing distance from the conduit; therefore, the course of differentiation of the fluids as they migrated away from the conduits can be followed through the successive stability fields. Field boundaries and variation curves have purely qualitative significance and have been traced according to the following premises:

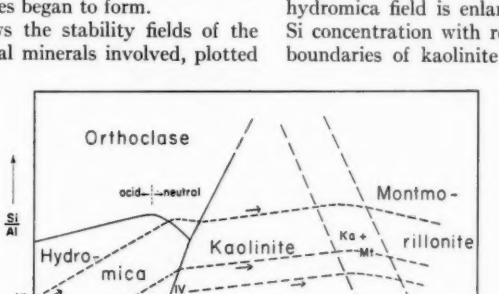

FIGURE 15.—STABILITY FIELD OF HYDROTHERMAL MINERALS IN THE WALL-ROCK ENVIRONMENT DURING ALTERATION

Short-dashed lines represent courses of differentiation of the fluids migrating through the wall rocks. Numbers IV, V, and VI indicate patterns.

According to Gruner (1944), hydromica (or sericite) is formed out of feldspar by potassium-bearing solutions in acid environment above 350°C. Below this temperature kaolinite is the stable phase, except in neutral or alkaline environment where, as shown by Noll (1936), either hydromica or potassium feldspar will form. Noll also demonstrated that an increase in the Si/Al ratio favors the formation of potassium feldspar instead of hydromica from solutions within the system $(Ca,Mg)O$—$(K, Na)_2O$—Al_2O_3—SiO_2—H_2O. Although kaolinite forms preferably in acid medium, Noll's investigations show that with very low K concentration it will also form from silica-alumina-water solutions under mildly alkaline conditions, in which circumstances it is accompanied by montmorillonite.

In the system represented by Figure 15, the hydromica field is enlarged by an increase of Si concentration with respect to Al. The field boundaries of kaolinite with respect to both orthoclase and hydromica are determined chiefly by the K content, but an increase in Al enlarges the field of kaolinite—more with respect to orthoclase than with respect to hydromica. Kaolinite and montmorillonite fields overlap along a wide area, for which the boundaries depend principally upon the pH (or the Na + Ca concentration) and secondarily upon the Si/Al ratio. The pH variation curve in Figure 15 corresponds to pattern VI.

HYDROMICA ZONE: The fluids entering the wall rock from the fissures reacted with plagioclase and formed hydromica in its place; they also attacked biotite, in which Mg was substituted for Fe without destroying the mica. The volume-to-volume replacement of oligoandesine by hydromica represented an addition of Al_2O_3 of about 15 per cent, and a subtraction of about 10 per cent of the SiO_2 contained in the plagioclase. Therefore, an increase in the ratio of Si to Al took place in the fluids as they moved away from the conduits into the wall rocks (Figs. 14, 15).

Most of the iron released by the alteration of biotite was fixed as carbonate without significant transport, because of the diminished acidity. The iron and magnesium released by

hornblende became also fixed as carbonate, and Si and Ca were carried away.

ORTHOCLASE ZONE: After traveling a certain distance the Si/Al ratio in the fluids decreased to a value below which orthoclase instead of hydromica was formed at the expense of plagioclase. At this point, the pH had risen to about neutrality by incorporation of Na and Ca from plagioclase. This incorporation overbalances the loss of K gone into the hydromica. As indicated above, neutralization must have had a strong effect in bringing about the formation of orthoclase. The orthoclase ceased to form at a distance from the conduit where the concentration of potassium descended below a critical value; that is, at the orthoclase front.

KAOLINITE ZONE: As they crossed the orthoclase front, the fluids began to form kaolinite instead of feldspar. In agreement with experimental data (see above), montmorillonite was formed with kaolinite in most of the kaolinite zone of patterns V and VI. Montmorillonite began to appear a little beyond the orthoclase front, increased as the fluids crossed the zone, and decreased at a rate either smaller than or equal to that of kaolinite. In a few veins the expanding clay equals or outweighs kaolinite in part of the zone. The amount of montmorillonite probably depended on the Na and Ca concentration in the fluids. Kaolinite ceased to form where the pH and base content became too high.

MONTMORILLONITE ZONE: As Na + Ca concentration increased and the pH rose, plagioclase became less susceptible to the attack by the fluids, which affected only the walls of cracks in the plagioclase, and deposited montmorillonite. The influence of microgradients is shown by the banding of many veinlets, in which kaolinite occupies the middle and the expanding clay lines the walls. The place where the fluids ceased to attack the plagioclase at all represented the montmorillonite front.

PHLOGOPITE ZONE: The zone of intense phlogopite-carbonate replacement of biotite coincides roughly with the hydromica zone. The exceptions (Pl. 1, fig. 2) show that the two fronts were partly independent of one another. The front was the place where the migrating fluids ceased to attack biotite on a large scale. Beyond it the attack decreased suddenly from 100 to 5–10 per cent of the mica; in the kaolinite zone, this limited attack was more radical because it produced in parts a mixture of kaolinite, quartz, and montmorillonite (Fig. 11) that replaced the mica and destroyed its crystalline framework. The stability field of phlogopite extended to at least the outermost, or fringe, front, but the ability of the hydrothermal fluids to decompose biotite dropped abruptly at a place near the hydromica front. This drop was apparently due to neutralization of the fluids. In the presence of Mg-bearing fluids, the reaction biotite → phlogopite may take place much faster in acid than in neutral or alkaline conditions. Neutralization was also probably a contributing factor in the formation of orthoclase and therefore in the setting of the hydromica front. Consequently, the hydromica and the phlogopite fronts must have been partially related to one another.

Problem of front migration.—Hydromica and kaolinite generally extend into the orthoclase zone and may even overlap one another slightly. The coexistence of the three secondary minerals (Pl. 2, figs. 2, 3) may be tentatively explained by one of the three following processes: (1) simultaneous crystallization, (2) successive replacement of the secondary minerals by one another, and (3) successive crystallization without mutual replacement.

Simultaneous formation of the three minerals out of the same solution seems unlikely on phase-rule considerations. As to process (2), it has been shown above that no signs of mutual replacement are found in the aggregates and that all three minerals appear to have formed by replacement of the same host, *i.e.*, plagioclase. Process (3) seems to be the logical conclusion, but it requires a shift of the fronts to produce the overlapping. An explanation of the shift may be as follows: Early in the process, the hydromica front was established near its final position, between the outer boundaries of hydromica and orthoclase zones (*see* Fig. 10) as the flow across the wall rock became stabilized. After this, the gas pressure continued to increase at a slower rate, and the increasing flow pushed the fronts outward, over-riding the next outer zone but replacing only the remaining areas of plagioclase. As the hydromica front reached the former position of the kaolinite front, the three secondary minerals—kaolinite, orthoclase, and hydromica, in this order—would have formed side by side.

The zone boundaries, as arbitrarily defined by the writer, do not wholly coincide with the final position of the fronts. For instance, whereas the outer boundaries of the montmorillonite, kaolinite, and orthoclase zones represent the fronts at their maximum expansion, the outer limit of the hydromica zone corresponds to the initial front.

The stages in the evolution of the fronts can

be summarized as follows: (1) Initial stage. Irruption of gases in the fissures, followed by a short period of rapid increase in the rate of flow through the wall rock, and then rough stabilization. During this period, the fronts moved rapidly outward from the conduits to assume their respective positions in the wall rock. This sweeping displacement was too fast to leave any marked effect on the rocks; the sort of effect to be expected is exemplified by the kaolinite present in small amounts within the hydromica zone (Fig. 10), which record the path of the kaolinite front.

(2) Main stage. After partial stabilization, the fronts continued to expand slowly, as the rate of flow increased to culmination. Most of the alteration took place at this stage.

(3) Waning stage. Decline in the rate of flow may have occurred by simple exhaustion of the channel fluids, by decrease of permeability, or by irruption in the conduits of the vein-filling liquids. If, as believed, a time gap existed between the alteration and the vein formation, the last cause should be ruled out. During the decline the fluids had little, if any, effect upon the previously formed alteration zones, as every alteration mineral was either stable or metastable in the field of the others.

During the main stage, the alteration of plagioclase took place simultaneously and at approximately the same rate in the three inner zones. Therefore, it was completed about the same time in all three zones. Assuming that this occurred before the flow began to decline, there would have taken place a sudden outward shift of the fronts to new positions into the fresh rock, and a new set of zones could have begun to form adjacent to the outermost zone. No such double zoning, however, was found in the veins studied by the writer. A reason for this may be a decrease in the flow rate caused by a drop in permeability as a result of the presence of an argillic zone which may have acted as a barrier for the fluids.

Transfer of matter during alteration.—The problem of the transport of chemical constituents during the alteration has been discussed by several authors. Two opposite mechanisms may have active in a wall rock next to a fissure: (1) diffusion of ions through a static pore-filling solute, and (2) bodily movement of the solutions through pores and cracks, away from the channel. Diffusion is conceived as a two-way transport and responds to various concentration gradients built up during the chemical reaction between wall rock and altering fluids. According to Lovering (1950, p. 249–260) diffusion predominates in wall-rock alteration. Sales and Meyer (1948) attribute the alteration at Butte to the same process. Other authors (Burbank, 1950; Schmitt, 1950) favor the bodily movement of solutions.

If the pore solvent is static, ionic diffusion may accomplish the required transfer to bring about the zoning. However, concentration gradients built up by chemical exchange between rocks and solvent would have been too weak for any considerable matter transport, because of the low solubility of most of the constituents involved (Si, Al). The rise in concentration of, for example, silica in the kaolinite zone would produce gradients sloping in opposite directions—toward the vein as well as toward the fresh rock. Apparently even a modest rate of outward fluid migration should overcome ionic diffusion. Actually, the strongest concentration gradient established in the wall rock during the circulation of fluids in the channel is that of the solvent itself.

The only advantage of ionic diffusion over bodily movement of fluids is that it apparently provides a simple mechanism for disposal of the excess matter. In the writer's opinion, however, the problem of matter disposal is not a serious one in the Front Range veins. First, the total transfer during alteration was not large, as can be seen from Table 4 and Figure 14. The total SiO_2 gained by the solutions from both the hydromica and kaolinite zones (disregarding the orthoclase zone, where there was a slight loss) in the Chance mine amounts to 0.18 gram per cubic cm, or 5.4 grams per square cm through an integrated thickness of 30 cm, making due allowance for the bulk densities (Table 4). Secondly, as the fluids traveled away from the fissure their silica-transporting power increased substantially with the pH and the concentration of sodium. When the fluids reached the fresh rock they contained mainly a sodium silicate solute which must have been disposed of by bodily diffusion in the wall rocks.

Nature of the Replacement Mechanism

As far as can be ascertained from microscopic observations, the replacement of the plagioclase by the various secondary minerals in the veins studied by the writer was generally a volume-to-volume process. This generalization is wholly valid only for plagioclase, because the replacement of biotite by the phlogopite-iron carbonate assemblage involved some volume

increase, indicated by the growth of the carbonate between cleavage planes.

In a general sense the mineralogical nature of the alteration depends largely on the composition of the host rock, but some qualifications are necessary for the veins discussed in this paper. The different alteration of plagioclase and biotite in most zones expresses the influence of the host. The difference is, however, not only chemical but also structural; hydromica represents a complete rearrangement and substitution of plagioclase; phlogopite is an exchange of one type of cation for another within the same crystalline framework. Where complete reworking of the biotite has taken place, as it has partly in the kaolinite zone, biotite and plagioclase were replaced by nearly the same minerals. Direct precipitation of hydromica and kaolinite in open fissures also occurred in places, showing that the solutions contained all the necessary ingredients.

The writer believes that the composition of the host was essential for localizing the alteration, but most of its effect on the type of alteration was indirect. Secondary minerals formed where solution of a primary constituent had occurred, mainly because free space was there available and because crystallization of the secondary mineral was triggered and sustained by the loss of energy spent in the attack. The nature of the mineral was determined primarily by the over-all composition of the fluids, secondarily by the composition of the replaced mineral. The dissolution of the host affected the chemical nature of the fluids and determined the formation of fronts as described above. The writer believes that the above conclusion can be applied to other areas. The basic idea is that the altering solutions are more important in determining the nature of the secondary product than the composition of the host. Sericite replacing both plagioclase and potassium feldspar in the inner zone at Butte (Sales and Meyer, 1948) is an example of the limitations in the influence of the host mineral. Where the composition of the replaced mineral contrasts strongly with that of the altering fluids, local, steep chemical gradients may originate crystal phases which—though in disequilibrium with the solution as a whole—can persist throughout the process if the rate of solution is sufficiently slow. It is, therefore, largely a question of degree of equilibrium between the fluids and the wall rock. The writer believes that the degree of equilibrium was relatively high in the Front Range mineral belt.

Origin of Other Patterns of Alteration

The above discussion refers to pattern VI. However, the processes outlined should also be valid for other patterns in the Front Range mineral belt. The discussion of the remaining patterns will follow approximately the order of increasing departure from pattern VI.

SUBPATTERNS VIa AND VIb: The chemical analyses in Table 4 correspond to subpattern VIb, in which the clay of the innermost zone is a mixed-layer mineral. A straight pattern VI would show a somewhat greater gain of potassium and a smaller gain of magnesium in the innermost zone. With hornblende present, magnesium might have shown a loss (Cold Spring). The formation of interstratified illite-montmorillonite clays is explained in terms of a lower K/Mg ratio in the fluids. This ratio decreased (*see* Fig. 15) away from the fissures and reached the critical value before arriving at the orthoclase zone; hydromica then gave way to the mixed-layer clay, thus forming pattern VIa.

PATTERN V: Pattern V differs from pattern VI by the lack of orthoclase zone. The fluids that gave rise to pattern V probably had a slightly lower potassium content. Thus the depletion of the alkali would have come before the Si/Al ratio reached the adequate value for the formation of feldspar. Such fluids should have also been more acid, thus reducing the orthoclase field. (*See* Fig. 15, curve V.) Increased free-acid content would also have had the effect of eliminating the feldspar zone. In the diagram this would be indicated by shrinkage of the orthoclase field, in which case curve VI also fails to enter it. The ratio of acid radicals to potassium may have increased, for instance, by a greater-than-ordinary distillation of the hydrothermal solutions.

PATTERN IV: The formation of predominant kaolinite in the innermost zone may be due to low temperature, high acidity, or low potassium content, or a combination of these factors—referring to pattern VI solutions as standards. An evaluation of these factors will not be attempted here. Curve IV in Figure 15 shows the interpretation based on either one or both of the two last factors.

PATTERN III: Alteration at Jamestown seems to have started with a pervasive, high-temperature replacement of the country rock (greisen-like alteration). As this stage declined, the lagging less penetrative part of the hydrothermal column could advance through better defined channels; some fissures tapped fluorine-

rich segregations, whereas others, perhaps at a slightly more advanced stage of differentiation, served as channelways for sulfide and telluride-bearing liquids. Within these liquids further differentiation seems to have taken place; a light, probably gaseous phase separated and caused most of the replacement of plagioclase by hydromica, whereas the development of orthoclase and silicification occurred at a somewhat later stage, upon arrival of the heavier, ore-bearing portion of the differentiated solution. Apparently the wall-rock altering phase was rich in potassium and probably of neutral-to-alkaline character, as indicated by the absence of kaolinite.

PATTERN II: Pattern II shows best the separation between the altering phase and the vein-forming phase. The sulfide veins are not generally accompanied by conspicuous alteration zones, although argillic replacement is widespread in the surrounding rocks. Some non-mineralized fissures show intense argillization. The interpretation of this pattern is handicapped by the lack of information on the horizontal and vertical distribution of the alteration. The hydrothermal phase probably was potassium-poor. The presence of intimately mixed hydromica, kaolinite, and montmorillonite cannot be due to simultaneous crystallization but is probably due to successive replacement, first by hydromica, then by kaolinite-montmorillonite. These stages were not separate waves of alteration but probably represented differentiation of the fluids as they migrated in different directions. Apparently each altered crystal has been affected by solutions coming from different local sources (fissures) and at various stages of differentiation.

PATTERN I: The problem of pattern I is what prevented the altering phase from following the normal course of differentiation after it had formed the hydromica zone. The writer has stressed the point that wall-rock alteration depended upon two conditions: (1) chemical composition of the fluids, in so far as it determined the minerals with which they were saturated; (2) the dissolving power, essentially related to the free-acid content. A solution may be saturated with a given clay mineral, but precipitation may not occur if the solution does not react with the wall rock. Precipitation would also fail to occur if the solution, though able to dissolve the primary minerals, is undersaturated of the ions needed to form the secondary products. This solution will leach the rock and leave behind open spaces. In pattern I, the writer believes that the reacting capacity of the fluids became neutralized before leaving the hydromica field, and the saturated phase went on without further crystallization of secondary minerals.

Silicification

Silicification of the wall rocks was a restricted phenomenon in the veins of the Front Range mineral belt. Excluding brecciated areas, where silica is related to the vein-filling phase, and a little quartz and opal present in argillic pseudomorphs in some veins (*e.g.*, Cold Spring), the only appreciable silicification was found at Breckenridge (Wellington). Silica is here somewhat irregularly distributed but concentrates near the veins. The association of silicification with pattern I may perhaps be explained in terms of degree of differentiation of the hydrothermal column. If a high proportion of the volatile compounds remained in the siliceous, vein-forming liquid as it arrived at a given place, the vapor pressure would greatly facilitate the introduction of silica into the wall rock. This interpretation fits with that proposed above with regard to the formation of a single hydromica zone in pattern I. In effect, poor reacting ability (low acidity) in the altering phase may be attributed also to lack of differentiation in the hydrothermal column.

Alteration Pattern and Wall-rock Type

The range of petrographic variation of the wall rock in the Front Range mineral belt is wide, but the mineralogy is monotonous: plagioclase, quartz, potassium feldspar, and mica (mainly biotite) represent more than 95 per cent of the total composition. This is valid for the igneous as well as for the metamorphic rocks. Some hornblende-bearing facies of granite gneisses and schists are also present. Plagioclase is the most affected by the alteration, followed by biotite and hornblende; potassium feldspar and quartz are practically inert to hydrothermal attack. The proportion of plagioclase is therefore a main factor in the development of zoning.

Patterns V and VI are within the area of the Boulder Creek batholith. Most facies in this body are rich in plagioclase, and the zoning shows exceptionally well. Where the veins cut zones of plagioclase-poor, schistose rocks the zones are weakly developed, as in the Georgetown-Argentine area. Since most of these rocks, however, are granite-injected schists with appreciable amounts of plagioclase, the pattern

differences cannot be attributed solely to wall-rock influence.

Pattern I was studied in three different wall-rock types. In the Wellington mine the rock is a quartz latite porphyry; at Silver King it is a banded quartz-biotite-hornblende rock with abundant metasomatic tonalite, and at Oregon-Quaker City it is a granite. The zoning is formed essentially at the expense of plagioclase, and the three places show no fundamental differences.

The effect of wall rock on the width of the zones was noticed in a vein at Cold Spring, fifth level, where the wall rock on one side is a biotite- and plagioclase-poor leucocratic granite and on the other side a biotite-rich granodiorite. The zones are nearly twice as wide on the leucocratic side as they are on the granodiorite side, which is explained by the lower rate of chemical change of the fluids traveling through the plagioclase-poor rock.

Alteration Pattern and Ore Type

The zone pattern in the mineral belt bears a definite relationship to the type of ore in the veins. The most complex zoning (patterns V, VI) is related to the pyritic gold and ferberite veins of Boulder County. Pattern III is found in the pyrite telluride gold veins of the northeastern end of the belt, which are spatially and genetically related to fluorite deposits. Pattern IV, also associated with lead-silver-zinc mineralization seems to be localized in a small area west of the tungsten district. The simplest zoning (patterns I and II) is generally restricted to the lead-silver-zinc veins predominating in the southwestern part of the belt but is also present in scattered deposits along the western side of the belt up to Ward and Jamestown.

As a broad generalization, then, the simple patterns (I–III) are associated with sulfide ores along the western border of the mineral belt, whereas the more complex patterns (V–VI) are related to the sub-belt situated to the southeast of the former where pyritic gold or tungsten predominates over sulfides. The latter includes the ores of the Central City area, which belong to the complex type (Tooker, 1955; 1956).

Alteration Pattern and Laramide Intrusions

The petrography and sequence of the Laramide igneous intrusions of the mineral belt have been thoroughly studied by Lovering and Goddard (1938; 1950). The intrusions progressed in general from southeast to northeast; simultaneously, the magmas became slightly more alkalic. Correspondingly, the pyritic gold telluride veins as well as the tungsten veins are related genetically to the more alkalic types (latite porphyries) (Lovering and Goddard, 1938). The sulfide ores seem to be located preferably within or close to the stocks, whereas most of the pyritic gold, telluride, and tungsten veins are in the zone of dikes along the southeastern side of the mineral belt.

Summary and Conclusions of Relation of Wall-rock Alteration to Laramide Intrusions and Ores

Alteration patterns I and II are generally associated with lead-silver-zinc sulfides and older igneous Laramide bodies. Patterns V and VI are related preferably to tungsten and gold pyrite telluride veins and to relatively alkalic, Laramide dikes. Pattern III is related to gold telluride and fluorspar veins and partly alkaline composite stock. The alkalic (potassic) nature of the alteration increases northeastward and is at a maximum in the Jamestown district.

The significance of these relationships is unknown to the writer. Perhaps the increasing potassium content in the alteration of the northeastern part of the belt is related to the more alkaline character of the intrusives. This correlation, however, is not clear. The most intense potassium replacement (Jamestown) is associated with calc-alkalic and sodic igneous bodies. (*See* Lovering and Goddard, 1950, p. 256–257.) The more complex patterns were probably related to acidic hydrothermal fluids. This may have some connection with younger age and greater distance from the igneous stocks, which in turn may be favorable conditions for a greater hydrothermal differentiation. Pattern VI seems to have been formed by solutions with high free-acid and potassium content.

The ore type seems to have no direct connection with the wall-rock alteration. This conclusion is supported by the fact that in other districts (*e.g.*, Butte) a zoning similar to that of pattern V is found in association with sulfide ores (Sales and Meyer, 1948). In the Front Range mineral belt the alteration is fairly homogeneous in the individual districts, although the mineralization may change considerably, as in the Boulder County tungsten and pyritic gold deposits. The above conclusion is in accordance with the idea that alteration

and ore formation belong to different phases of the process.

No simple, direct relationship between wall-rock alteration and Laramide igneous bodies may be derived from the available data. The writer believes that the character of the hydrothermal alteration is only broadly related to the nature of the magmas and that the differences found within the mineral belt depend principally upon the evolution of the fluids after they left the source areas. Structural conditions would, therefore, have considerable influence on the nature of the alteration.

Before these and other problems related to the origin of the alteration in the Front Range can be satisfactorily answered, much more study is necessary. Specifically, the mapping of the alteration patterns should be carried to a much greater detail than shown in this paper. Pattern II should be investigated more thoroughly, with the purpose of establishing the spatial relationship between the diffuse, argillic alteration and the addition directly associated with the veins.

Comparison with Alteration in Other Areas

Although potassium feldspar is an alteration product in many districts, it had never been found in definite zones around veins as in pattern VI. Among the few vein deposits where alteration studies have been made, the deposit at Butte, Montana (Sales and Meyer, 1948), offers the closest similarity with the deposits described in this paper, and in particular with pattern V. Minor differences are: (1) silica is an important constituent of the inner zone at Butte, whereas it is subordinate or nonexistent in Boulder County; (2) primary potassium feldspar was replaced by sericite in the same zone as Butte; (3) At Butte, biotite is slightly chloritized in the montmorillonite zone, recrystallized into fine-grained biotite in the kaolinite zone, and replaced by sericite in the sericite zone. Fine-grained, secondary biotite is not found in patterns V or VI but in the area of pattern III (Jamestown). Despite these differences, the alteration at Butte and in Boulder County are similar enough to warrant the assertion that they must have had essentially the same origin.

Most alteration studies in the literature refer to deposits with complex structural histories (Lovering, 1949; Kerr *et al.*, 1950; Kerr, 1951; Peterson *et al.*, 1946; González Bonorino, 1949; Schwartz, 1947; 1953; Leroy, 1954; Stringham, 1953). Schwartz (1956) presents an excellent summary of the alteration in various areas. The avenues for the altering solutions are ill-defined at best. Most authors believe that the alteration took place in all instances in several separate stages, each stage corresponding to a new inflow of solutions. Although the number of stages may be as many as seven (Stringham, 1953) and the general picture of the alteration is complex, a sericite-quartz zone or area surrounded by an argillic (kaolinite, hydromica, montmorillonoid) zone is present almost everywhere (Schwartz, 1956). A propylitic zone, characterized by the alteration of the mafic minerals alone and equivalent to the fringe zone, is also found around the argillic zone. The close analogy of this sequence with that of the veins at Butte and Boulder County suggests a common basic mechanism of alteration.

The main grounds for the "stage" hypothesis are: (1) the irregular contours of the zones or areas covered by each "stage", and (2) the replacement relationships between the minerals of the adjacent zones.

(1) The front mechanism may produce zones that are nonparallel at the surface if the fronts were concentric with respect to irregular channelways always located below the present surface. Furthermore, solutions traveling in wide areas are likely to find differences in composition and permeability (*i.e.*, fissures) that affect the extension of the zones.

(2) Encroachment of one stage or zone by the adjacent one is not precluded by the front hypothesis, since it generally occurs during expansion of fronts. This encroachment does not necessarily entail mutual replacement of the secondary minerals but rather a successive replacement of the common host. The criteria generally used to recognize replacement are based on textural relationships of the aggregates and are highly unreliable. Even criteria such as veining must be used with caution. The various clay minerals form aggregates with peculiar habits, from which no "mutual boundary" relationships can be expected in general. For instance, if kaolinite and hydromica (or sericite) are present in a pseudomorph the former will make, whatever their relative age, compact aggregates surrounded by an irregular, unevenly textured hydromica mass that appears to penetrate into the kaolinite. Many clear-cut replacement textures could be relict or inherited textures, resulting from the replacement of a host that has already been replaced by another. This happens when an alteration front overrides the adjacent zone.

Although the writer believes that the front hypothesis can also be applied to porphyry copper bodies, it is also probable that repeated upsurges of hydrothermal fluids were operative. An excellent example of multistage alteration—although not a porphyry copper deposit—is the East Tintic district, Utah (Lovering, 1949). However, complexity in the alteration can be brought about even by a single phase of alteration if adequate structural conditions are present. For instance, solutions radiating from a dispersion center may find fissures that allow them to reach outer zones without further change in composition. A zoning will develop along the fissures in apparent independence of the diffuse alteration that surrounds it and that is forming more or less simultaneously. Such a relation could be interpreted as produced in two stages.

In conclusion, the front theory of alteration can be applied, in greater or lesser extent, to almost any hydrothermally altered body, especially after the tridimensional picture and the stricture of the country rock have been taken into account. After the alteration pattern has been analyzed with the front theory in mind, the presence of more than one stage of alteration can be ascertained.

Supergene Alteration

The relative importance of hydrothermal and supergene alteration in mineral deposits has been a matter of disagreement among investigators. Lindgren (1915) considered that supergene waters carrying sulfuric acid from the oxidation of pyrite were the main agent of kaolinization, but later work (Burbank, 1932; Graton and Bowditch, 1936; Lovering, 1941) established the predominantly hydrothermal origin of argillization. The problem remains, however, of determining to what extent, if any, supergene processes affect the hydrothermal alteration products in ore deposits Kerr (1950) concluded that in porphyry copper deposits the "argillic and sericitic minerals formed by hydrothermal alteration suffer little change during later supergene processes." The present writer agrees with this conclusion with regard to the Front Range mineral belt.

The distinction between the two types of alteration is not always apparent. In the last phases of hydrothermal processes the solutions must behave like heat-activated vadose waters. Intermingled vadose and juvenile solutions would also give rise to a series of transitional alteration phases. In environments of moderate-to-high-temperature hydrothermal processes, however, the effect of supergene solutions should be readily distinguished. The difference lies mainly in their CO_2 and H_2O pressures, which are the main factors in their dissolving power. In the mineral belt, cold, low-pressure vadose liquids dissolved and precipitated interstitial matter but could not attack the primary or secondary silicates.

The most noticeable supergene phenomenon in the mineral belt is the formation of ferruginous bands on both sides of the veins. These bands are especially well developed in the pyritic veins of the Gold Hill district (Pl. 1, fig. 1). Iron and manganese hydroxides are concentrated in fissures and intergranular spaces in the outer part of the hydromica zone; exposed surfaces are covered by the hydroxides that migrated out of the interstices and formed conspicuous red-brown to bluish-black bands with concretionary and mammilary structure The iron staining is attributed to iron-bearing, acid solutions formed by oxidation of pyrite at high levels. Because of its sheared texture, the zone next to the vein is favorable for the circulation of the supergene solutions, which bleached the inner part of the zone as they dissolved part of the siderite and ankerite out of the altered mafic minerals. The hydroxides were precipitated as the solutions sought to migrate laterally through the less permeable outer part of the zone and into the orthoclase zone. Jarosite, gypsum, and barite were also formed out of the sulfate-bearing supergene solutions. Gypsum is in places abundant and relatively widespread (*e.g.*, Clyde tunnel).

Supergene transportation of opal and kaolinite from hydrothermal veinlets into younger fissures seems to have occurred in many places.

Alteration as a Guide to Ore

The use of the wall-rock alteration in prospecting for ore has been discussed principally by Lovering (1949) and Schwartz (1955). No systematic technique has been developed, although miners have long used rock alteration as an indication of a vein. The only contribution that alteration studies can give to prospecting is the recognition of hidden alteration features bearing a systematic relation to ore or at least to the vein. If, as the writer believes, the wall-rock alteration and the vein formation belong to separate phases of the hydrothermal process, the chances of finding such systematic relationships are indeed few.

In the Boulder County tungsten and pyritic gold deposits, the recognition of the complex zoning and, in particular, of the orthoclase zone might have been of some use in guiding the exploration work. In the widest veins, where

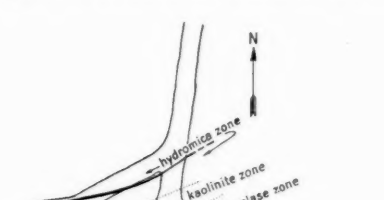

FIGURE 16.—MAP OF ALTERATION ZONES, FOOTWALL VEIN, CLYDE TUNNEL

the zones may be several feet thick, the rock on either side of the kaolinite zone seems similarly fresh. Microscopic examination discloses, however, that on one side plagioclase is preserved, whereas on the other side it has been replaced by orthoclase. The vein would be on the latter side. A good example of a wide orthoclase zone that is not outwardly different from the fresh rock is found in the Clyde tunnel, a mile north of Nederland (Fig. 16). The country rock is the fine-grained, biotite granodiorite or adamellite that characterizes Hurricane Hill and vicinity (Hoosier-Hummer, Clyde, and Lily mines). The kaolinite zone is recognized by the "salt and pepper" texture that results from the contrast between biotite and the white argillic pseudomorphs. The hydromica zone shows similar pseudomorphs, but the alteration of biotite to phlogopite makes the texture less contrasting. The orthoclase zone looks much like the fresh rock. The identification of this zone could have helped during the exploration work.

GENERAL CONCLUSIONS

The writer attempts in this paper to develop a "front" theory that explains the alteration zoning found in the veins of the Front Range mineral belt. The theory is developed with regard to the most complex zoning, pattern VI, and extended therefrom to the other patterns. The conclusions can be summarized as follows:

(1) Wall-rock alteration and vein formation are two separate phases of the hydrothermal process. The alteration was accomplished by a moderately acidic, gaseous phase that separated by distillation from the hydrothermal solution. The remaining less volatile, silica-rich, alkaline, liquid portion arrived later, filling the fissures with the gangue and most of the ore minerals. This conclusion is based mainly on the presence of wall-rock alteration around fissures that have not been reached by the vein-filling solutions, and of veins with no alteration halo.

(2) Zoning like that found in patterns IV to VI is the result of a one-stage process in which the fluids changed in composition as they migrated through the wall rocks away from the fissures. This is strongly supported by the parallelism and lack of transgression of the zone boundaries, as well as by the constant relative thickness of the zones.

(3) The change in chemical composition of the migrating fluids as a result of the effects of the wall rock gave rise to several fronts which represented the stability limits of the various secondary minerals. In the setting of these fronts the hydrogen-ion concentration was a contributing factor whereas temperature was of subordinate importance. The maximum number of fronts (pattern VI) is six: hydromica, orthoclase, kaolinite, montmorillonite, phlogopite, and fringe. The first four are defined on the basis of the alteration of plagioclase, the last two on that of the biotite and other mafic minerals. The hydromica and the phlogopite fronts are coincident in many places.

(4) Chemical analyses indicate a significant increase of the Si:Al ratio in the migrating fluids within the innermost zone. Hydromica ceased to form where the above ratio reached a critical value (hydromica front). The field of orthoclase was thus reached, with the help of a rise in pH. Neutralization also reduced radically the attacking power of the solutions with respect to biotite, which thereafter is only partially altered. The phlogopite front represents this abrupt change in the alteration of biotite.

As the fluids traveled away from the fissure dissolving plagioclase and forming orthoclase in its place, the potassium content diminished to a critical concentration (orthoclase front) beyond which the feldspar ceased to crystallize and gave way to kaolinite, joined later by montmorillonite. The introduction of mont-

morillonite was forced by the alkalinization of the fluids, mainly as a result of the incorporation of Na and Ca.

Kaolinite and montmorillonite continued to crystallize together until the solutions became too alkaline for the former (kaolinite front). In some veins the power of the fluids to attack plagioclase was also lost at this point, and the two clay minerals ceased to form here. In others, montmorillonite continued to form for a short distance, and a montmorillonite zone was thus originated. In these veins the respective fronts were separated.

After the alteration of plagioclase stops, the only effect of the fluids on the wall rock is the partial phlogopitization of biotite and replacement of hornblende by siderite, kaolinite, and nontronite, until the partial pressure of CO_2 becomes too low even for this alteration (fringe front).

(5) Petrographic evidence shows that no mutual replacement has taken place to any significant extent among the various secondary minerals. These replaced only the primary constituents of the rock, chiefly plagioclase. More than one alteration mineral can be present in the same pseudomorph because of simultaneous or successive replacement of the common host. For instance, the association of hydromica, orthoclase, and kaolinite in the orthoclase zone is due to expansion of fronts and encroachment of zones before the complete alteration of plagioclase. Simultaneous crystallization is exemplified by kaolinite and montmorillonite.

(6) The process of zone formation is based upon the hypothesis of outward migration of the fluids, as opposed to ionic diffusion in a static solute. The pressure gradient that drove the fluids away from the conduits was stronger than the concentration gradients of the individual ions.

Siliceous, alkaline residual solutions leaving the alteration halo could travel long distances in the country rock and present no problem of disposal.

(7) Formation of other patterns of zoning can be explained by differences in the composition of the original fluids, which depended largely on the degree of hydrothermal fractionation. Low potassium content may be the cause of the absence of the orthoclase zone (pattern V) or of the orthoclase and hydromica zones (pattern IV). The simpler patterns, where the kaolinite-montmorillonite alteration is poorly developed or missing, may be the result of lesser fractionation of the hydrothermal column. Pattern II requires further study. The hypothesis of limited fractionation agrees with the fact that the simpler patterns are more closely related to Laramide igneous stocks. A phase of greisenlike alteration was found in the Jamestown district, associated with pattern III.

(8) No clear-cut relationship has been recognized between hydrothermal alteration and ore type and Laramide intrusions. In general, patterns I and II are associated with lead-silver-zinc deposits and also with somewhat older intrusives. Patterns V and VI are related to pyritic gold telluride and tungsten veins and to slightly alkalic dikes. Pattern III is related to gold telluride and fluorspar deposits and to a partly alkaline (saturated) composite stock. The alkalic (not alkaline) character of the alteration increases toward the northeast; this roughly parallels a similar change in the Laramide intrusions (Lovering and Goddard, 1950).

No direct connection was detected between ore type and wall-rock alteration. This is in agreement with the conclusion that the two represent different phases of the hydrothermal processes. The type of ore may be largely a matter of availability of a particular metal at the moment of the process. No difference in pattern of alteration was found in districts where more than one ore type was present, as shown in the Boulder County tungsten and gold district.

(9) The writer believes the explanation here offered for the origin of the zoning in the Front Range mineral belt can be applied to other districts, not only to those with similar characteristics, such as the Butte district, but also perhaps to others with more complex alteration such as the porphyry copper deposits. In these deposits, however, complicating structural features have to be taken into account.

(10) The only supergene phenomena detected in relation to the hydrothermal alteration are transport and precipitation of iron and manganese hydroxides in the pyritic veins, precipitation of sulfates and carbonates, and clay transportation. No supergene clay formation was found.

Addendum

This paper had been submitted for publication before the writer became aware of Tooker's recent publication (1956). Since Tooker's work deals with the Central City—Idaho Springs area within the Front Range mineral belt, a brief review of its conclusions and a comparison with those given in this paper follow:

The host rocks in the Central City—Idaho Springs area are quartz feldspar gneisses and granites of Precambrian age. Tooker distinguishes four alteration zones: (1) least altered (fresh) rock; (2) weakly altered; plagioclase partly or totally replaced by montmorillonite; (3) moderately altered, soft clay-mineral rock with primary textures preserved or indistinct; subdivided according to the predominant clay mineral in (a) montmorillonite-rich rock, (b) kaolinite-rich rock, and (c) illite-rich rock; (4) intensely altered wall rock, original textures obliterated, sheared; silicified, sericitized, and pyritized.

This zone sequence corresponds fairly well with that of the Nederland-Gold Hill area. Zone 2 resembles the present writer's montmorillonite zone, whereas subzones 3a and 3b correspond to the outer and inner parts, respectively, of the kaolinite zone, which in many veins of the Boulder County area contains abundant montmorillonite in the outer half. Zone 3c is the hydromica zone. The silicified, innermost zone 4 is lacking in the Nederland-Gold Hill district (exception, Quaker City vein), unless the wall rock crisscrossed by siliceous veinlets next to the main vein may be considered as such. Zone 4 may perhaps be interpreted as a late-stage feature related to vein filling rather than to the argillic alteration stage. The orthoclase zone has not been recognized in the Central City-Idaho Springs area, the zone sequence thus corresponding to the present writer's pattern V. In partial agreement with Sales and Meyer's (1948) findings at Butte but contrary to the rule in the portion of the Front Range mineral belt studied by the present writer, potassium feldspar "is altered to kaolinite and perhaps other clay minerals" and "quartz is in part corroded and recrystallized" in zone 3 (Tooker, 1956, p. 351).

Tooker concludes that in the Central City-Idaho Springs district most wall-rock alteration preceded the sulfide phase of hydrothermal activity.

References Cited

Bradley, W. F., 1950, The alternating layer sequence of rectorite: Am. Mineralogist, v. 35, p. 590–595

Bradley, W. F., and Weaver, C. E., 1956, A regularly interstratified chlorite-vermiculite clay mineral: Am. Mineralogist, v. 41, p. 497–504

Brown, George, and McEwan, D. M. C., 1951, X-ray diffraction by structures with random stratification, p. 138–154 *in* Brindley, G. W., *Editor*, X-ray identification and crystal structures of clay minerals: Mineralog. Soc., London, 345 p.

Burbank, W. S., 1932, Geology and ore deposits of the Bonanza district, Colorado: U. S. Geol. Survey Prof. Paper 169, 166 p.

Earley, J. W., Brindley, G. W., McVeagh, W. J., and Vander Heuvel, R. C., 1956, A regularly interstratified montmorillonite-chlorite: Am. Mineralogist, v. 41, p. 258–267

González Bonorino, Félix, 1949, Diferenciación magmática y alteración hidrotermal en Agua Tapada, Catamarca: Asoc. Geol. Argentina Rev., v. 4, p. 181–217

——1956, Hydrothermal alteration in tungsten and gold-pyrite veins of Boulder County, Colorado (Abstract): Geol. Soc. America Bull., v. 67, p. 1699

Graton, L. C., and Bowditch, S. I., 1936, Alkaline and acid solutions in hypogene zoning at Cerro de Pasco: Econ. Geology, v. 31, p. 651–698

Grim, R. E., and Rowland, R. A., 1942, Differential thermal analysis of clay minerals and other hydrous materials: Am. Mineralogist, v. 27, p. 746–761, 801–818

Gruner, J. W., 1944, The hydrothermal alteration of feldspars in acid solutions between 300° and 400°C.: Econ. Geology, v. 39, p. 578–589

Heystek, H., 1954, An occurrence of a regular mixed-layer clay mineral: Mineralog. Mag., v. 30, p. 400–408

Kelley, K. K., 1935, Contributions to the data in theoretical metallurgy: U. S. Bur. Mines Bull. 383, p. 1–132

Kerr, P. F., 1950, Discussion of alteration and its application to ore search: Colo. School Mines Quart., v. 45, p. 328–336

——1951, Alteration features at Silver Bell, Arizona: Geol. Soc. America Bull., v. 62, p. 451–480

Kerr, P. F., Kulp, J. L., Patterson, C. M., and Wright, R. J., 1950, Hydrothermal alteration at Santa Rita, New Mexico: Geol. Soc. America Bull., v. 61, p. 275–348

Leroy, P. G., 1954, Correlation of copper mineralization with hydrothermal alteration in the Santa Rita porphyry copper deposit, New Mexico: Geol. Soc. America Bull., v. 35, p. 739–768

Lindgren, Waldemar, 1915, The origin of kaolin: Econ. Geology, v. 10, p. 89–93

Lippman, F., 1954, Uber einen Keuperton von Zaisersweiher bei Maulbronn: Heidel. Beitz. Min. u. Petrol., v. 4, p. 130–134

Lovering, T. S., 1941, The origin of tungsten ores of Boulder County, Colorado: Econ. Geology, v. 36, p. 229–279

——1949, Rock alteration as a guide to ore—East Tintic district, Utah: Econ. Geology Mon. 1, 65 p.

——1950, The geochemistry of argillic and related types of alteration: Colo. School Mines Quart., v. 45, no. 1B, p. 231–260

Lovering, T. S., and Goddard, E. N., 1938, Laramide igneous sequence and differentiation in the Front Range, Colorado: Geol. Soc. America Bull., v. 49, p. 35–68

——1950, Geology and ore deposits of the Front Range, Colorado: U. S. Geol. Survey Prof. Paper 223, 319 p.

Lovering, T. S., and Tweto, Ogden, 1953, Geology and ore deposits of the Boulder County tungsten district, Colorado: U. S. Geol. Survey Prof. Paper no. 245, 199 p.

Noll, W., 1936, Uber die Bildungsbedingungen von Kaolin, Montmorillonit, Sericit, Pyrophyllit und Analcim: Min. petr. Mitt., v. 42, p. 210–247

Peterson, N. P., Gilbert, C. M., and Quick, G. L., 1946, Hydrothermal alteration in the Castle Dome copper deposit, Arizona: Econ. Geology, v. 41, p. 820–840

Sales, R. H., and Meyer, Chas., 1948, Wall rock alteration at Butte, Montana: Am. Inst. Min. Metall. Engineers Tech. Pub. 2400, 25 p.

——1950, Interpretation of wallrock alteration at Butte, Montana: Colo. School Mines Quart., v. 45, no. 1B, p. 261–273

Schmitt, Harrison, 1950, The fumarolic-hot spring and "epithermal" mineral deposit environment: Colo. School Mines Quart., v. 45, no. 1B, p. 209–228

Schwartz, G. M., 1947, Hydrothermal alteration in the "porphyry copper" deposits: Econ. Geology, v. 42, p. 319–352

——1953, Geology of the San Manuel copper deposits, Arizona: U. S. Geol. Survey Prof. Paper 256, 65 p.

——1955, Hydrothermal alteration as a guide to ore: Econ. Geology, 50th Anniversary Volume, p. 300–323

——1956, Argillic alteration and ore deposits: Econ. Geology, v. 51, p. 407–414

Smith, W. C., 1938, Geology of the Caribou stock in the Front Range, Colorado: Am. Jour. Sci., 5th ser., v. 36, p. 161–196

Stringham, Bronson, 1953, Granitization and hydrothermal alteration at Bingham, Utah: Geol. Soc. America Bull., v. 64, p. 945–991

Sudo, Toshio, Takahashi, Hiroshi, and Matsui, Haruhiko, 1954, Low spacing of about 30 kX confirmed from a fireclay: Nature, v. 173, p. 261–262

Tooker, E. W., 1955, Investigation of wall-rock alteration, Central City and Idaho Spring districts, Gilpin and Clear Creek counties, Colorado (Abstract): Geol. Soc. America Bull., v. 66, p. 1682

——1956, Altered wall rocks along vein deposits in the Central City-Idaho Spring region, Colorado: Clays and Clay Minerals, Natl. Acad. Sci. Nat!. Res. Council Pub. 456, p. 348–361

Weaver, C. E., 1956, The distribution and identification of mixed-layer clays in sedimentary rocks: Am. Mineralogist, v. 41, p. 202–221

Wright, H. D., 1954, Mineralogy of a uraninite deposit at Caribou, Colorado: Econ. Geology, v. 49, p. 129–174

Departamento de Geología, Universidad de Buenos Aires, Argentina

Manuscript Received by the Secretary of the Society, January 16, 1957

BULLETIN OF THE GEOLOGICAL SOCIETY OF AMERICA
VOL. 70, PP. 91–106, 12 FIGS. JANUARY 1959

GEOMETRY OF SUPERPOSED FOLDING

BY L. E. WEISS

ABSTRACT

Two simple kinematic models of folding in tectonites have been adopted and diagrams prepared to show ideal geometrical transformations of a set of parallel surfaces (S) as a result of superposition of one generation of folds on another.

It was found for both models of folding that a second generation does not necessarily form folds with constant trend and plunge. These folds depend for their axial orientation on the attitude of S in which they form. It was found also that cylindroidal folds of a second generation are necessarily smaller and less persistent in axial direction than those of an earlier generation.

Geometry of rotation of early formed B lineations by later folding is different for the two models of folding adopted. Where the second folding is by flexural slip of S, the earlier lineations follow small-circle paths in projection, as described by Sander. Where S is slip-folded by the second deformation, earlier lineations ideally follow great-circle paths in projection. Some departures from this ideal geometry to be expected in nature are listed.

CONTENTS

TEXT

	Page
Introduction	91
Folds in tectonites	92
Models of folding	92
Kinematic geometry of the two models	92
Geometry of cylindroidal fold systems	92
Superposed deformations	93
Interfering or superposed systems of folds	93
Geometry of superposition of folds	95
Geometry of rotation of B structures by flexural slip folding	98
Geometry of rotation of B structures by slip folding	100
Departures from ideal geometry which may be expected in nature	102
Conclusions	105
References cited	106

ILLUSTRATIONS

Figure	Page
1. Kinematic geometry of flexural slip and slip folding	93
2. Geometry of a cylindroidal fold system	94
3. Relationship between S' and πS maxima in folded rocks	95
4. Structural geometry of a field of cylindroidal folding	96
5. Geometry of superposition of later folds on earlier cylindroidal folds	97
6. Geometry of superposition of β' folds on the β folds of Figure 4	99
7. Geometry of rotation of a linear structure by later folding	100
8. Geometry of superposition of slip folds on a cylindroidal fold (axis $\beta = B$) by nonaffine slip on S' normal to B'	101
9. Diagrammatic projection of field in Figure 8	102
10. Synoptic diagrams for data from Figure 9	103
11. Geometry of intersection of a group of tautozonal S' surfaces with S on a cylindroidal β' fold	104
12. Rotation of plane of rotation of an earlier linear structure (B) where nonaffine slip on S' is accompanied by elongation along either B' or a'	105

INTRODUCTION

Some recently published papers, many of them dealing with the Scottish Highlands, have drawn attention to the widespread complex and superposed folds in tectonites (*see*, for instance, Sutton and Watson, 1954; King, 1955; King and Rast, 1955; Ramsay, 1956; Rast and Platt, 1957; Clifford, 1957; Clifford *et al.*, 1957; Weiss and McIntyre, 1957). This paper examines the special problems arising where a single set of parallel S surfaces (bedding or foliation) contains more than one generation of folds.

Successive generations of folds may result

from different phases of one orogenic movement or from unrelated deformations separated widely in time. In the following discussion of geometry, no distinction is drawn between these. Examples are considered in which two fold systems are formed in two successive acts; however no genetic relationship between the acts is implied. Excluded from the following discussion of ideal geometry are complex fold systems of the type described by Clifford *et al.* (1957), who considered them products of essentially inhomogeneous deformation caused by mutual interference, during formation, of large folds.

Geometrical transformations shown in the figures of this paper are ideally simplified and therefore may not correspond in detail to natural deformations. However, the close resemblance between ideal and natural geometry observed by the writer has encouraged him in the belief that a detailed study of the ideal cases will increase understanding of less regular natural geometry. In particular, such a study will help separate the relationships between axes of superposed folds which are geometrically possible from those which are geometrically impossible. All projections illustrated are from the lower hemisphere of an equal-area projection.

The writer gratefully acknowledges the helpful criticism and advice received from Dr. Iris Borg of Princeton and Dr. F. J. Turner of the University of California.

Folds in Tectonites

Models of Folding

Most geologists recognize two mechanisms of folding in tectonites and believe that most folds probably are formed by a combination of these mechanisms together with mechanisms less easily defined. The two principal models of folding are as follows:

(1) Folds in a body with layering S are formed by flexure or buckling of individual competent layers combined with simultaneous slip of layer over layer. This type of folding corresponds to the generally accepted model of flexural slip folding (*see* Knopf and Ingerson, 1938, p. 155; Turner, 1948, p. 173–174).

(2) Folds in a body with layering S are formed by nonaffine laminar flow or slip on a second set of surfaces inclined to S. Such a mechanism implies that, under certain conditions of deformation, layers in rocks lack cohesion and become incapable of transmitting stresses, and that surfaces between individual layers do not act as surfaces of preferential slip. Carey (1954) has outlined features of "rheid" behavior in rocks which resemble features of the generally accepted model of slip folding, as this second type of folding is sometimes termed (*see* Knopf and Ingerson, 1938, p. 157–158; Turner, 1948, p. 165–166). Ideally, slip folding, like rheid folding, has geometrical features like those of laminar flow in a fluid, and therefore it is sometimes termed flow folding or flowage folding; but these terms can denote a less homogeneous type of deformation—more akin, perhaps, to turbulent flow in a fluid—with a correspondingly less regular geometry (Bain, 1931).

It is not suggested that all folds in tectonites are of one of the two kinds just described. Most folds, where considered in successive layers of different competence, combine features of both kinds and are formed by the two mechanisms acting together. In particular, neither mechanism by itself accounts for the elongation along fold axes that is so common in tectonites.

Kinematic Geometry of the Two Models

The geometry of flexural slip folding is projected in Figure 1*a*. The slip surface is S, the axis of slip is B (kinematic B axis), and the direction of slip is a (kinematic a axis). For opposing senses of external rotation of S about the fold axis (β), S_1 and S_2 are attitudes of S. In S_1 and S_2 the directions of slip are respectively a_1 and a_2. For flexural slip folds, β is parallel to B ($\beta = B$).

The geometry of slip folding of S by nonaffine slip on S' is projected in Figure 1*b*. The internal rotations of S for opposing senses of slip on S' are given by S_1 and S_2. S is folded about its line of intersection with S' (β') irrespective of the axis of slip in S' (B') or the direction of slip in S' (a'). In slip folding, for all but special cases of deformation (for instance, where S intersects S' either parallel to B', so that $\beta' = B'$, or parallel to a', so that no folding occurs), β' is not parallel to B' ($\beta' \neq B'$).

Geometry of Cylindroidal Fold Systems

The ideal concept of a fold axis as the rectilinear generator of a fold (Clark and McIntyre, 1951, p. 594) is only statistically fulfilled, because even regular folds do not persist unchanged in profile for a great distance along

their axes. But, whether it is a flexural slip fold or a slip fold, and however complicated it may be in profile, a fold may be described as cylindroidal within a given field if the folded

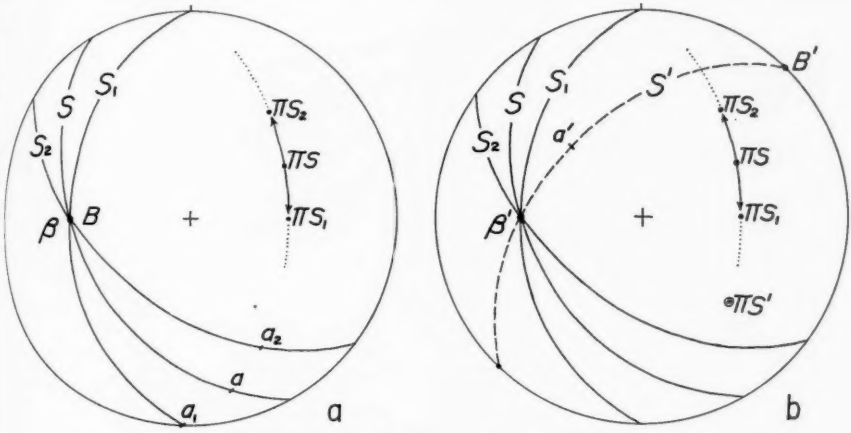

FIGURE 1.—KINEMATIC GEOMETRY OF FLEXURAL SLIP FOLDING AND SLIP FOLDING

set of S surfaces is statistically tautozonal about a rectilinear axis. Such a statistically defined fold axis is termed a β axis by Sander (1948, p. 132–146). The geometry of such a fold and its associated B lineations is summarized in Figure 2.

In most fields of cylindroidal folding, axial planes of individual folds are subparallel. Where present, this parallelism is demonstrated in projection by a symmetrical disposition of poles of S (πS) within the πS diagram (Fig. 2). In the plane of the girdle of πS there may be one elongated maximum (Fig. 3*a*, upper) denoting a considerable appression of the folds (Fig. 3*a*, lower). The center of gravity of this maximum defines the pole of the axial plane ($\pi S'$) for the field as a whole. In most tectonites where folding is advanced, geometry approximates this example. But, where folds are less appressed (Fig. 2), limbs of folds may fall into two sets, so that πS for each set forms a distinct maximum in the πS girdle (Fig. 3*b*). The axial plane for the whole field (S') is one of the symmetry planes of the πS diagram. Most folds found in tectonites have hinges of much smaller extent than limbs (the folds are similar rather than parallel or concentric), so that fewer measurements of attitudes in the field are gathered from hinges than from planar limbs. But the geometry of πS girdles can vary greatly in nature, especially where folds are consistently overturned and have limbs of unequal length.

Extension of a field such as that shown in Figure 2 may result in patterns of preferred orientation of S and B (B lineations, mullions, small folds, and so on) of decreased regularity. Where, for instance, the poles of S do not lie in a clearly defined girdle, or B structures do not lie in a single maximum, the field can be considered noncylindroidal, and the field must be divided into subfields in which folding is cylindroidal. Only by such a procedure can the geometry of noncylindroidal fields be established. Mapping of contacts alone is inadequate.

The geometrical features of most systems of cylindroidal folds can be summarized as follows: (1) The axes of folds in the system are statistically rectilinear (this is implicit in the term cylindroidal). (2) Less common, but of more fundamental significance, is a statistical parallelism of axial planes of folds in the system. In slip folds this plane is the flow or slip surface.

SUPERPOSED DEFORMATIONS

Interfering or Superposed Systems of Folds

Mutually interfering fold systems have long been recognized in some greatly deformed bodies of rock. They have been attributed to superposition of folds either in independent orogenies or in successive phases of one deformation. (For recent discussion of the geometry of layered bodies so folded, *see* Ramsay, 1956; Clifford *et al.*, 1957; Weiss and McIntyre, 1957.)

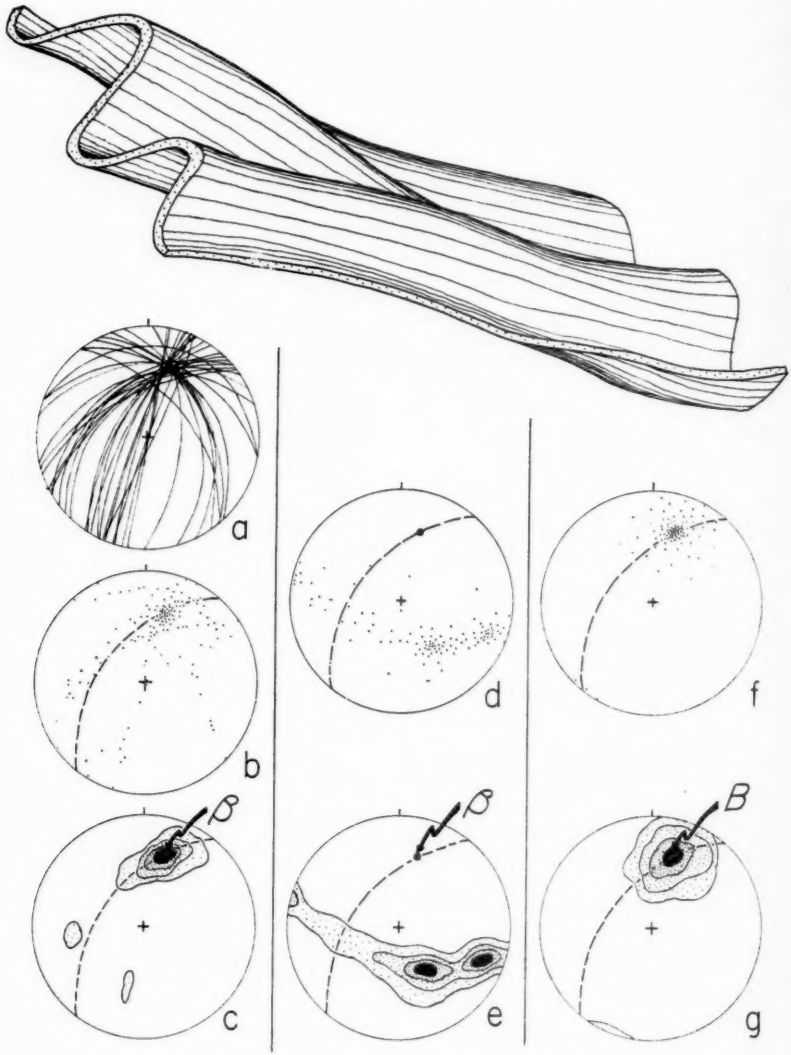

FIGURE 2.—GEOMETRY OF A CYLINDROIDAL FOLD SYSTEM
Figures 2*a*, 2*b*, 2*c*—projections of S; Figures 2*d*, 2*e*—projections of πS; Figures 2*f*, 2*g*—projections of B. The lower projection in each column is the contoured equivalent of the one above.

Some geometrical features of surfaces affected by mutually interfering fold systems are discussed with reference to idealized examples in which the following conditions are assumed:

(1) The first folding is cylindroidal and is the result of flexural slip (Fig. 4). The left-hand portion of Figure 4 is a map of a large fold with plunging axis (β) and a dipping axial plane. In subfields I-IV (outlined on the map by broken lines), S is macroscopically planar, as shown by the strong single maximum in each of the πS diagrams inset on the map. In each of these fields weak folding about β is shown by elongation of the maximum into a partial girdle with axes respectively β_1 to β_{1V}. Where data from these four diagrams are compiled into a

synoptic diagram (Fig. 4*e*), a pronounced girdle appears with axis β. Likewise the four statistically defined attitudes of S in fields I-IV (respectively S_{I} to S_{IV}) intersect in β as shown in

faces (S') oblique to β. For both models of folding, axial planes of individual folds of the second generation are assumed to be subparallel. Such a relationship has been observed in

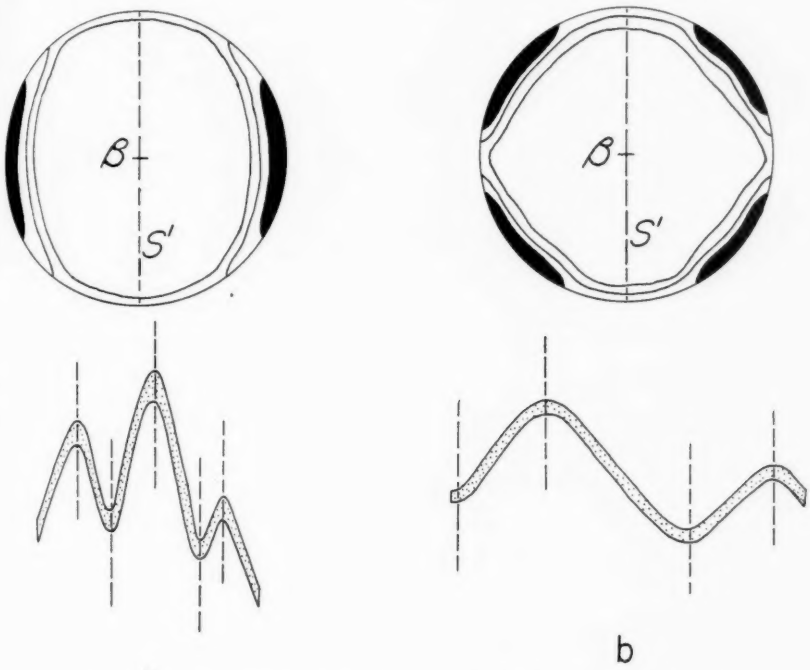

FIGURE 3.—RELATIONSHIP BETWEEN S' AND πS MAXIMA IN FOLDED ROCKS
Figure 3*a* shows symmetrical folds with closely appressed limbs; 3*b* shows "open" symmetrical folds.

Figure 4*g*. Because deformation is by flexural slip, small-scale linear structures (small folds, mullions, B lineations, and so on) are present parallel to $B = \beta$. In each subfield these lie in a maximum coincident with the corresponding β (respectively β_{I}–β_{IV} in Figs. 4*a*–4*d*) and elongated in the plane of the statistically defined S for that subfield (respectively S_{I}–S_{IV} in Figs. 4*a*–4*d*). Where plotted synoptically for the whole field, these B structures lie in a nearly equidimensional maximum (B in Fig. 4*f*) coincident with β.

(2) The geometry of superposition of a second generation of folds in S is investigated by geometrical operations in projection. The two cases considered are where the second generation forms, first, by flexural slip of S, and second, by nonaffine slip on a set of surnatural examples of superposed folds (*see* Sander, 1948, p. 177–178; Clifford *et al.*, 1957, p. 17–19; Weiss and McIntyre, 1957, p. 596–600).

Geometry of Superposition of Folds

A second deformation of a body in which S is folded generally does not form a new generation of folds with rectilinear subhorizontal fold axes. For each subfield in which S is planar after the first folding, a rectilinear fold axis can form; but none of these axes is subhorizontal because for the general case of a plunging first fold (Fig. 4), no horizontal attitudes of S remain anywhere in the field. The geometry of superposition of one generation of folds on another is shown in Figure 5; in Figure 5*a*,

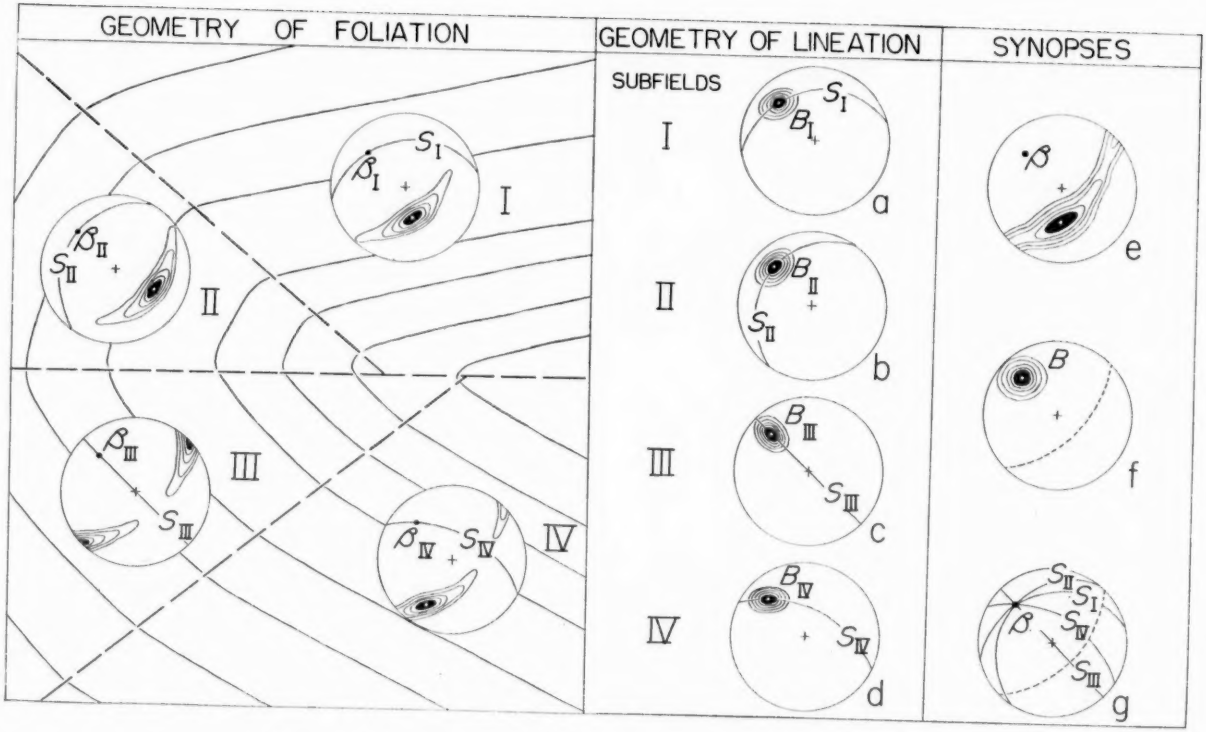

FIGURE 4.—STRUCTURAL GEOMETRY OF A FIELD OF CYLINDROIDAL FOLDING

FIGURE 4.—STRUCTURAL GEOMETRY OF A FIELD OF CYLINDROIDAL FOLDING

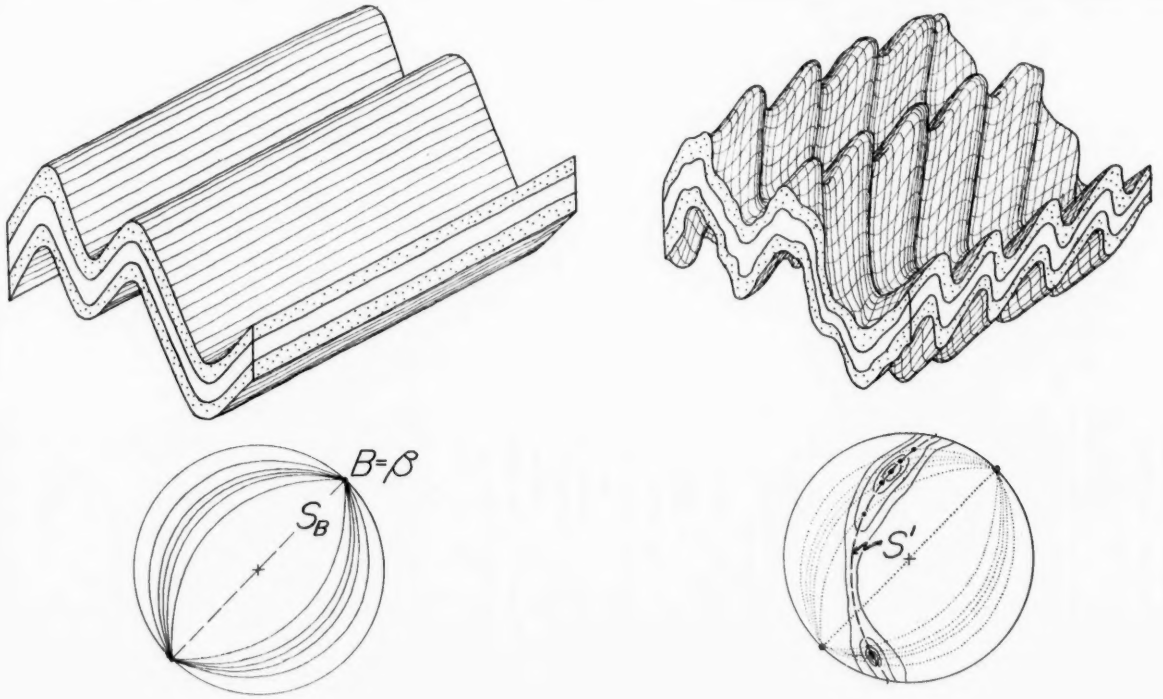

FIGURE 5.—GEOMETRY OF SUPERPOSITION OF LATER FOLDS (AXES β') ON EARLIER CYLINDROIDAL FOLDS (AXES β)

upper, S is folded about a subhorizontal axis (β). The geometry of this folding is projected in Figure 5*a*, lower, in terms of several attitudes of S measured on opposite limbs and hinges of folds. Because folding is relatively open, two attitudes of S predominate, corresponding to the two kinds of fold limb. The axial planes of the folds (S_B) are shown vertical. Figure 5*b*, upper, shows the geometry of the β folds after superposition of a new generation of folds (either flexural slip or slip folds) with subparallel axial planes (S'). The axes of the second generation of folds (β') lie in S'; but the orientation of β' in a particular subfield is parallel to the intersection of S with S' and cannot be rectilinear. Figure 5*b*, lower, projects the geometry of this structure. No vestige remains of the β axis in Figure 5*a*, lower, because all attitudes of S in the field have changed, and previous β intersections have been dispersed. The β' axes and associated lineations and small folds are rectilinear in subfields where S was planar after the first folding, but for the field as a whole, there are two maxima of β' structures, corresponding to the intersections of S' with the two planar preferred orientations of S (Fig. 5*a*, lower), spreading into a girdle in the plane of S', as shown by the diagrammatic contours in Figure 5*b*, lower (*see* Weiss and McIntyre, 1957, Fig. 12). These two maxima correspond to β' axes with greatly different trend and appreciably different plunge, although they belong to the same generation of folds.

The geometrical operations just described can be performed also on the plunging fold shown in Figure 4. Superposition on this structure of a second generation of folds with subparallel axial surfaces (S') gives rise to the geometry shown in Figure 6. In subfields where S was planar (subfields I–IV), cylindroidal folds with axes respectively β_I to β_{IV} are formed (*see* diagrams inset on map). These axes are oriented differently in each subfield, reflecting the differently oriented intersections between S and S'. For the sake of simplicity, folds of the second generation are assumed to have closely appressed limbs, so that πS defines a single maximum within each girdle subnormal to S' (Fig. 3*a*). The pattern of preferred orientation of πS for the whole field does not define a rectilinear β'. There must be a strong maximum of πS at $\pi S'$; but the presence of girdles in different planes for subfields I–IV produces an irregular pattern in which no β' axis for the whole field can be determined, and in which the previously existent β maximum is distorted or, where folding is advanced, completely dispersed. This condition is shown diagrammatically in Figure 6*i*, in terms of the planes of the four πS girdles intersecting in $\pi S'$.

Small-scale structures parallel to β'_I to β'_{IV} are B' structures only where the second deformation is by flexural slip. Whatever their kinematic significance, however, these structures lie as shown in Figures 6*a*–6*d* respectively for the four subfields. The maximum in each subfield coincides with the corresponding β' axis. For the whole field, the small-scale structures lie in a girdle with maxima at the lines of intersection of S' with the planar S in subfields I to IV (Fig. 6*j*).

A general rule that can be established from Figure 6 with respect to the scale of successive generations of folds is that the largest folds of the second generation, where cylindroidal, must be smaller than those of the first generation, because they can be formed only on planar limbs of the first generation. In a field with two generations of folds, it is therefore to be expected that the largest or major structures are the first formed, the second-generation folds take the form of smaller-scale or minor structures superposed on the limbs of the large folds. Such structural relationships are widespread in the Scottish Highlands and occur in many other parts of the world.

The geometry of S outlined holds equally well for folds formed by flexural slip and by slip, but, where the geometry of rotation of early formed B structures (in particular, lineations and small folds) is considered, significant theoretical differences can be seen for the two models of folding.

Geometry of Rotation of B Structures by Flexural Slip Folding

The geometry of rotation of an older lineation by flexure of the surface in which it lies is well known as a result of the work of Sander (1948, p. 171–172). Let a B lineation lie in a planar S. Then, flexure of S about another axis β' (Fig. 7*a*) rotates B as shown. On the attitudes of S resulting from the folding (S_1, S_2, and so on), B maintains a constant angle with β' and so follows a small-circle[1] path on the projection with β' as its center (B_1, B_2, and so on). In each of the subfields I to IV in Figure 6, the angle between B ($= \beta$) and β' has a different value,

[1] The term small circle is used in this paper to denote any path (other than a great circle) that is circular on the sphere of projection, regardless of the attitude of this circle.

FIGURE 6.—GEOMETRY OF SUPERPOSITION OF β' FOLDS ON THE β FOLDS OF FIGURE 4

so that the small circle of rotation of B structures about β' is different for each subfield. These circles are shown respectively by C_I to C_{IV} in Figures 6*e*–6*h*. In Figure 6*k* they are shown superposed. For the field as a whole there is no simple path of movement of B structures. Thus, the second deformation by flexural slip folding tends to disperse the initial maximum of B structures (Fig. 4*f*) irregularly. In each subfield, B structures can be "unrolled" about the respective β' in the manner outlined by Sander (1948, p. 174–178); but no single axis of unrolling will serve for the field as a whole. Also, in order to reconstruct their initial preferred orientation, B axes should not be unrolled to a horizontal orientation as suggested by Sander, but only to the point of intersection of the small circles of rotation. This point coincides with the initial preferred orientation of B structures shown in Figure 4*f*. A simultaneous unrolling of the attitudes of S in which individual B structures lie should restore these to their preferred orientation before the second folding.

It can be seen from Figure 6 that a second deformation by flexural slip must be, on the scale of the whole field, triclinic. In individual subfields, deformation can be monoclinic or orthorhombic, but the planes of symmetry for the subfields are mutually inclined, so that none hold for the field as a whole.

Geometry of Rotation of B Structures by Slip Folding

Figure 8*a* shows a body containing a simple open fold in S with B lineation parallel to its axis (β). In Figure 8*b* the same body is shown after nonaffine slip on S' (one of the vertical sides of the body) in direction a', normal to B' (one of the horizontal edges of the body). Different attitudes of S become slip-folded according to the geometry shown in Figure 3*b*, and cylindroidal folds form on the limbs of the β folds with axes (β') parallel to the intersections of S' with the effectively planar attitudes of S. The geometry of rotation of B in one such cylindroidal field is shown in Figure 7*b*. As S is internally rotated to S_1 or S_2 by opposite senses of slip, B moves respectively to B_1 and B_2. The geometry of this deformation has been discussed elsewhere (Weiss, 1955, Fig. 1). B moves along a great-circle path of the projection passing through a'. This path remains constant for any field in which S' is planar and B is rectilinear before deformation.

The geometry of a field such as that in Figure 8 is projected in Figure 9. The folded S of Figure 8*a* is shown in Figure 9*a*. S_1 to S_6 correspond to six subfields in which S is effectively planar on the first fold with axis β. The surface of nonaffine slip induced by the second deformation is S'. In each of the six subfields,

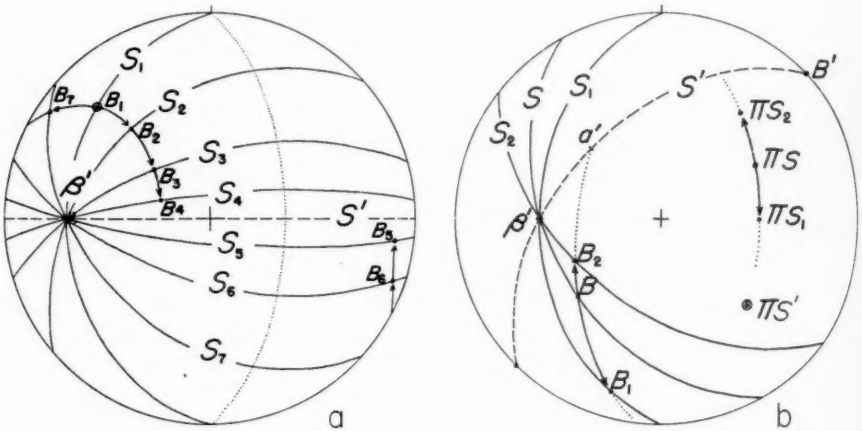

FIGURE 7.—GEOMETRY OF ROTATION OF A LINEAR STRUCTURE (B) BY LATER FOLDING
Figure 7*a* shows flexural slip folding with axis $\beta = B$; 7*b* shows slip folding by nonaffine slip on S' with axis $\beta' \neq B'$.

cylindroidal slip folds are formed with axes (β'_1 to β'_6 respectively in Figs. 9*b*–9*g*) parallel to the intersections of the respective planar preferred orientations of S with S'. In this fashion the initially homogeneous field of Figure 9*a* becomes divided into six homogeneous subfields (F_1 to F_6) with geometry as shown respectively in Figures 9*b*–9*g*. In each subfield the poles of S (circled dots) come to lie in a girdle normal to the corresponding β'. This geometry is independent of the direction of slip (a') in S'.

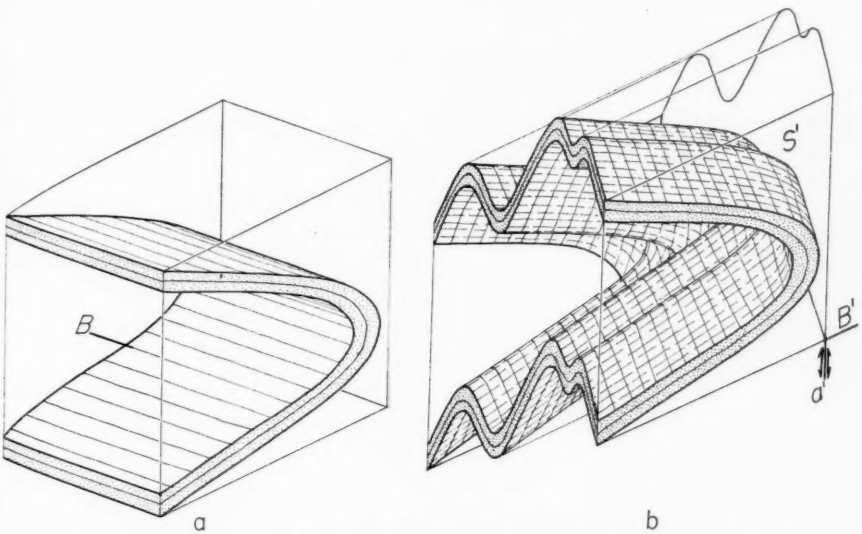

FIGURE 8.—GEOMETRY OF SUPERPOSITION OF SLIP FOLDS ON A CYLINDROIDAL FOLD (AXIS $\beta = B$) BY NONAFFINE SLIP ON S' NORMAL TO B'

Internal rotation of S in each subfield is accompanied by internal rotation of minor linear structures (B) initially parallel to β (Fig. 9*a*). In each of the subfields F_1 to F_6, B rotates toward a'. The unique plane defined by B and a' is constant for the whole field, so that the path of rotation of B is along the same great circle of the projection in all subfields and is independent of the orientation of β'. The amount of rotation of B in any subfield depends upon the amount of internal rotation of the S in which it lies (crosses in Figs. 9*b*–9*g*).

The data from Figure 9 are compiled into synoptic diagrams in Figure 10. Figure 10*a* shows all planar attitudes of S from Figures 9*b* to 9*g*. In Figure 10*b* the intersections of these attitudes are plotted, and in 10*c* these intersections are contoured to give a β' diagram. Plainly, the single maximum in this diagram is an oversimplification of geometry and conceals the true relation of β' axes in the whole field. Only by preparing β' diagrams for the six subfields in which folding is cylindroidal can the true geometry of S be established. Figure 10*d* is a plot of all small-scale B structures (dots) and all small-scale β' structures (circles) from Figures 9*b* to 9*g*. For the field as a whole, these small-scale structures lie in two distinct girdles intersecting in a'. Because the β' structures lie in the plane of S', the orientation of B' (lying in S' normal to a') can be found.

The results of this analysis can be applied to the field shown in Figure 6. The great circles of rotation of B must be the same for all subfields as shown by G_I to G_{IV} respectively in Figures 6*e*–6*h*. These girdles intersect S' at a', thereby fixing the orientation of B' in each subfield. The girdle of B structures for the field as a whole (Figure 6*l*) coincides with girdles for individual subfields.

Comparison of Figures 6*k* and 6*l* shows that geometry of rotation of older lineations by flexural slip folding is markedly different from geometry of rotation by slip folding. Unrolling

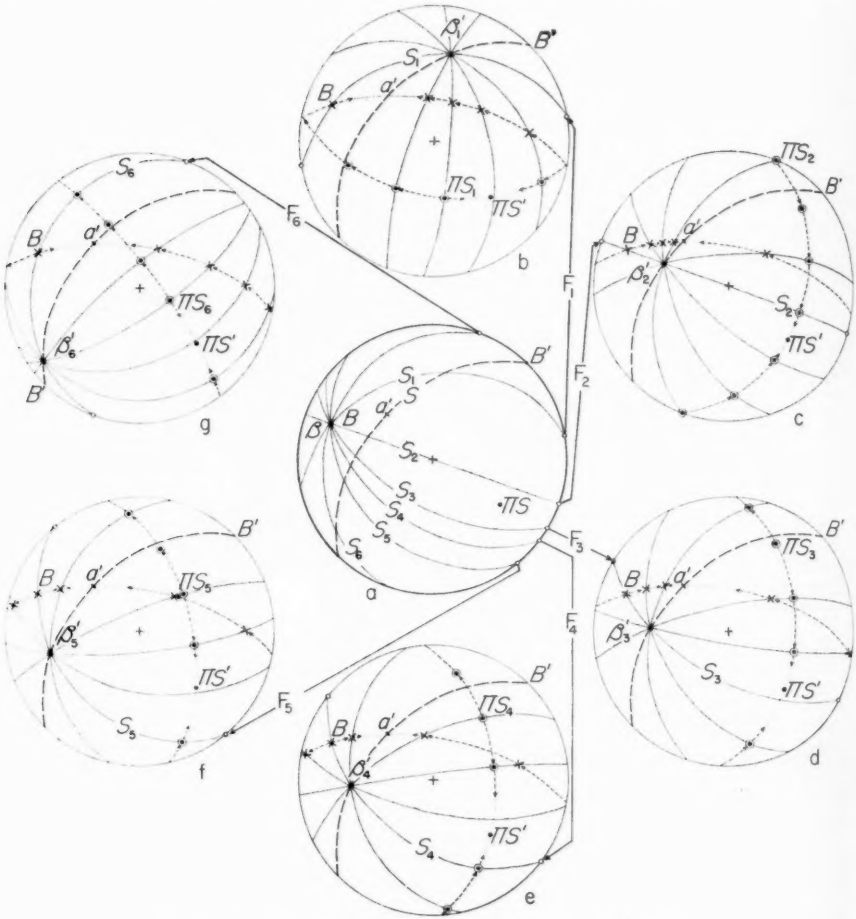

FIGURE 9.—DIAGRAMMATIC PROJECTION OF FIELD IN FIGURE 8

of older lineations after slip folding is perhaps possible, because the path of movement is known; but, as can be seen from Figure 6*l*, no clue remains to the initial preferred orientation of *B*.

Departures From Ideal Geometry Which May Be Expected In Nature

The geometry discussed is ideally perfect. Obvious departures from this geometry can be predicted in natural fabrics, as follows:

(1) It has been assumed in this study that the slip surface (*S'*) is planar. In structures of this kind at Loch Leven (Weiss and McIntyre, 1957, p. 590) *S'* surfaces vary slightly in orientation, so that poles of the axial planes lie in a girdle with one very strong maximum. This range in orientation can be explained in two ways: in a large field *S'* is more correctly represented by a set of intersecting surfaces with a limited but marked range in orientation. Where such a set of surfaces intersects pre-existent folds, as shown in Figures 11*a*–11*d*, the intersections of *S'* with *S* lie in a sheaf-shaped girdle narrowest at *B'* (Fig. 11*d*). A sheaf-shaped girdle of this kind observed at Loch Leven was interpreted in this fashion (Weiss and McIntyre, 1957, Fig. 13). According to the second explanation slip on *S'* has developed

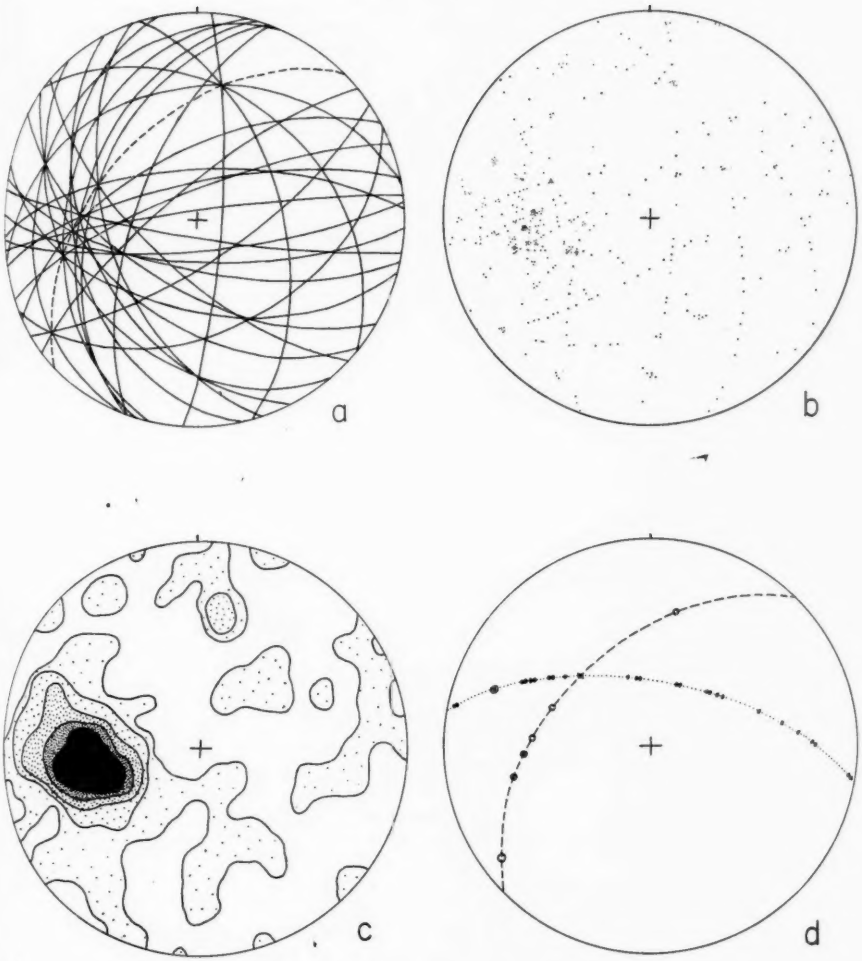

FIGURE 10.—SYNOPTIC DIAGRAMS FOR DATA FROM FIGURE 9

Figure 10*a* shows S planes (full lines) and S' (broken line); 10*b* shows intersections of S planes; 10*c* shows intersections contoured, contours 1-2-3-4-5 per cent per 1 per cent area, 10*d* shows girdles of B (dots) and β' (circles).

into flexural slip of S' (*cf.* Carey, 1954, p. 93–95). In this way an element of external rotation about B' is added to all structural elements. Such rotations follow small circles of the projection and have the geometry shown in Figure 7*a*.

(2) The field at the end of the first deformation may be noncylindroidal, so that a second deformation by slip folding could not reproduce the ideal geometry of Figure 7. Axial planes of β' folds are still subparallel, but geometry of internal rotation of B structures is not constant throughout the field, because the initial preferred orientation of B is not everywhere the same. This difficulty should be overcome by dividing such a field into smaller subfields.

(3) Slip on S' may not be constant in direction throughout a field in which S' is planar.

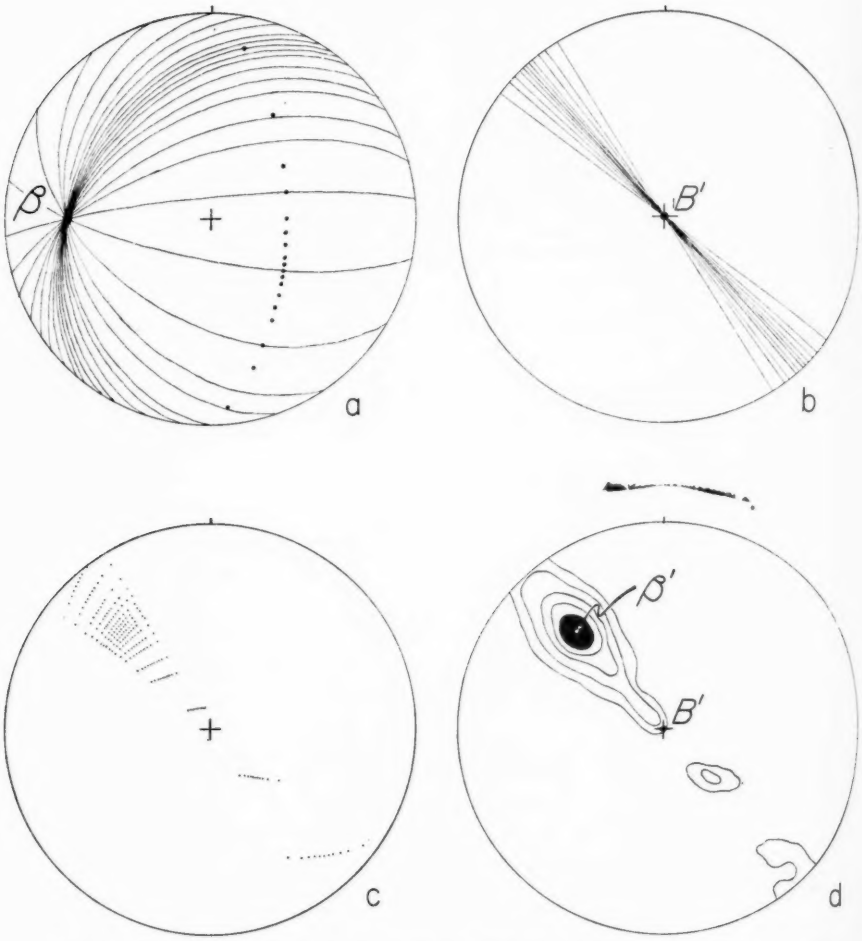

FIGURE 11.—GEOMETRY OF INTERSECTION OF A GROUP OF TAUTOZONAL S' SURFACES WITH S ON A CYLINDROIDAL β FOLD

Figure 11*a* shows geometry of S in β fold (dots are πS); 11*b* shows S' surfaces with a limited range of orientation, intersecting in B'; 11*c* shows intersections of S and S' (200); 11*d* shows β' diagram, contours, 2½-5-10-15-20 per cent per 1 per cent area.

Geometry of internal rotation of B is different for different directions of slip (a' axes). Axial planes of β' folds remain parallel to S', and β' axes remain parallel to the intersections of S and S'. Deformation is triclinic.

(4) As De Sitter (1956, p. 97) has pointed out, a shortening normal to S' is probably associated with slip on S' in the natural equivalent of slip folding. For deformation to remain monoclinic, this shortening must be accompanied by an elongation of the deformed body in the plane of S', either in a' or B'. Such subsidiary elongations do not significantly affect the geometry of internal rotation of S. They result in a more pronounced appression of fold limbs than could be achieved by the simplified model of slip folding. Similarly, the effects of these elongations on the geometry of rotation of B are minor so long as deformation is effectively homogeneous. Whether elongation is

along a' or B' is immaterial; the effects are the same—namely, that the plane of rotation of B structures approaches parallelism with S' by rotation about a'. The geometry of rotation is shown in projection in Figure 12. BP_1 is the plane of rotation of B by nonaffine slip on S' without elongation along a' or B'. Where such an elongation occurs, the plane of rotation of B rotates about a', occupying successively such positions as BP_2 and BP_3 as it approaches parallelism with S'.

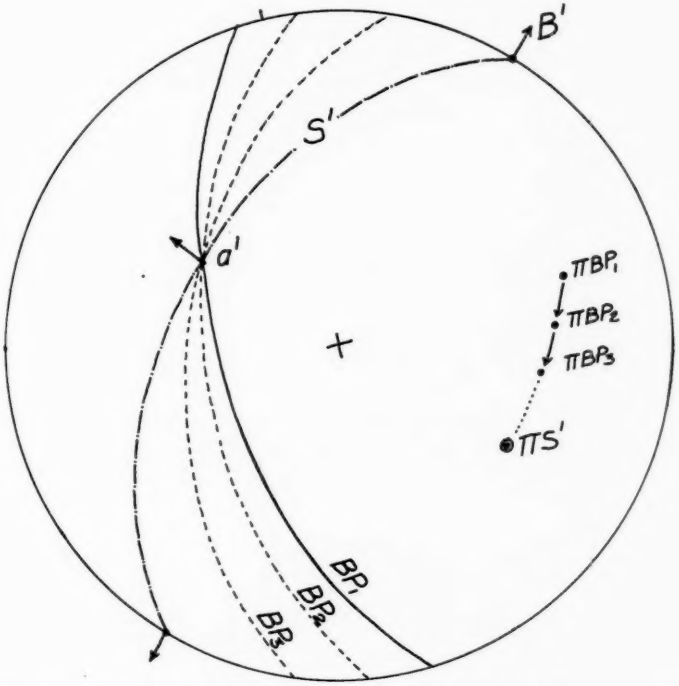

FIGURE 12.—ROTATION OF PLANE OF ROTATION OF AN EARLIER LINEAR STRUCTURE (B) WHERE NONAFFINE SLIP ON S' IS ACCOMPANIED BY ELONGATION ALONG EITHER B' OR a'

Any of these complicating factors may operate in natural fabrics, thereby contributing toward divergence from ideal geometry.

CONCLUSIONS

The ideal geometry of folding adopted in the analyses discussed must occur rarely in nature. Most folds in tectonites probably have an intermediate kinematic geometry combining elements of the two models. From the analyses, the following general conclusions can be drawn:

1. Where one generation of folds is superposed on an earlier generation, the geometry of S ceases to be expressible in terms of a rectilinear axial trend of folding, because the earlier folds are bent, and the later folds develop with variable trend and plunge.

2. In general, cylindroidal folds of a later generation are on a smaller scale than those of an earlier generation, because they form only in fields where S remains planar after the earlier folding.

3. The geometry of rotation of earlier linear structures by later folding depends upon the kinematics of the later folding. For most kinds of folding a lineation in projection follows a path intermediate between a small circle and a great circle. Kinematics of folding may be indicated by the resemblance of the natural path to either of the two ideal paths.

4. The diagrams show that fields affected by

superposed folding show a high degree of geometrical regularity which is capable of being established and interpreted.

References Cited

Bain, G. W., 1931, Flowage folding: Am. Jour. Sci., v. 22, p. 503–530

Carey, S. W., 1954, The rheid concept in geotectonics: Geol. Soc. Australia Jour., v. 1, p. 67–117

Clark, R. H., and McIntyre, D. B., 1951, The use of the terms pitch and plunge: Am. Jour. Sci., v. 249, p. 591–599

Clifford, T. N., 1957, The stratigraphy and structure of part of the Kintail district of southern Ross-shire: Geol. Soc. London Quart. Jour., v. 113, p. 57–92

Clifford, P., Fleuty, M. J., Ramsay, J. G., Sutton, J., and Watson, J., 1957, The development of lineation in complex fold systems: Geol. Mag., v. 94, p. 1–23

De Sitter, L. U., 1956, Structural geology: N. Y., McGraw-Hill Book Co., 552 p.

King, B. C., 1955, The tectonic pattern of the Lewisian around Clashnessie Bay near Stoer, Sutherland: Geol. Mag., v. 92, p. 69–80

King, B. C., and Rast, N., 1955, Tectonic styles in the Dalradian and Moines of parts of the Central Highlands of Scotland: Geol. Assoc. Proc. v. 66, p. 243–266

Knopf, E. B., and Ingerson, E., 1938, Structural petrology: Geol. Soc. America Mem. 6, 270 p.

Ramsay, J. G., 1956, The structural geology of a double fold system at Loch Monar, Inverness-shire and Ross-shire: Geol. Soc. London Proc., no. 1541, p. 121–125

Rast, N., and Platt, J. I., 1957, Cross-folds: Geol. Mag., v. 94, p. 159–166

Sander, B., 1948, Einführung in die Gefügekunde der geologischen Körper: I: Vienna and Innsbrück, Springer—Verlag, 215 p.

Sutton, J., and Watson, J., 1954, The structure and stratigraphical succession of the Moines of Fannich Forest and Strath Bran, Ross-shire: Geol. Soc. London Quart. Jour., v. 110, p. 21–54

Turner, F. J., 1948, Mineralogical and structural evolution of the metamorphic rocks: Geol. Soc. America Mem. 30, 342 p.

Weiss, L. E., 1955, Fabric analysis of a triclinic tectonite and its bearing upon the geometry of flow in rocks: Am. Jour. Sci., v. 253, p. 225–236

Weiss, L. E., and McIntyre, D. B., 1957, Structural geometry of Dalradian rocks at Loch Leven, Scottish Highlands: Jour. Geology, v. 65, p. 575–602

Department of Geology, University of California, Berkeley 4, California

Manuscript Received by the Secretary of the Society, February 6, 1958

Short Notes

BULLETIN OF THE GEOLOGICAL SOCIETY OF AMERICA
VOL 70, PP. 107-110, 1 FIG. JANUARY 1959

FAULTED RUNDLE (MISSISSIPPIAN) SECTION AT CROWSNEST PASS, ALBERTA, CANADA

BY SAMUEL J. NELSON

The abnormally thick carbonate section of the Rundle group at Crowsnest Pass, Alberta, has interested geologists for many years. The Rundle here attains an apparent thickness of more than 5000 feet in contrast to near-by sections most of which are less than 3000 feet. Although no obvious faults occur in this section, some geologists attribute the thickness to repetition, while others consider basinal deposition as the answer. J. R. Cundill (1955) outlined stratigraphic evidence illustrating faulting in the section, and the writer here presents paleontologic evidence in support of Cundill's interpretation.

The section discussed is exposed on the north side of Crowsnest Lake at Crowsnest Pass in the southern Canadian Rockies immediately east of the Alberta-British Columbia boundary. The Rundle here is a westward-dipping, superficially undisturbed sequence of carbonates underlain on the east by the Banff and overlain on the west by the Rocky Mountain formation.

The Rundle group at Crowsnest Pass, as in most areas of the southern Canadian Rockies, can be divided into three formations which, in ascending order, are the Livingstone, Mount Head, and Etherington. In other areas these three formations generally aggregate between 2000 and 3000 feet: the Livingstone (1000–1500 feet), of resistant light-colored crinoidal limestones and interbedded finer-grained carbonates, of Osagean age; the Mount Head (600 feet), a recessive unit of Meramecian age consisting of dark limestone, dolomite, and shaly beds; and the Chesterian Etherington formation (700 feet or less) of resistant light-weathering dolomites and limestones. The reader is referred to Warren (1927), Beales (1950), Douglas (1953), Norris (1957), and Bostock, Mulligan, and Douglas (1957) for details of Rundle stratigraphy.

Dawson (1886), who made the first reference to the Rundle of Crowsnest Pass, considered that complex folding was the cause of the extraordinary thickness. Warren (1928; 1933) and McKay (1932) thought that their measured thicknesses of between 5000 and 5300 feet were caused by deposition and not structural complications. Cundill (1955) concluded, from lithologic studies, that the succession was repeated by three faults and possibly a fourth, and indicated that the true stratigraphic thickness is about 2700 feet.[1] The section was recently briefly referred to by Bostock, Mulligan, and Douglas (1957), who stated that the maximum thickness is 3900 feet. Faulting was not mentioned.

In 1955 the writer with J. R. Cundill and two assistants spent 10 days making detailed fossil collections from the section. A study of faunas has shown that Cundill's three main faults are probably correct, and that the fourth which he tentatively proposed is also present. Faunal evidence indicates that the stratigraphic thickness of the Rundle is between 2900 and 3000 feet (Fig. 1). Thus Cundill's excellent stratigraphic analysis is confirmed by paleontology.

The writer wishes to express his gratitude to officials of The British American Oil Company, Ltd., Calgary, for financial backing of this project. Dr. P. S. Warren, of the University of

[1] Cundill placed only the Livingstone and Mount Head formations in the Rundle group and stated that their combined stratigraphic thickness was about 2100 feet. If the Etherington (his Tunnel Mountain formation) is included in the group then the above figure of 2700 feet is obtained. Some confusion has been caused by the fact that his diagram shows a total thickness of 2750 feet for the Livingstone and Mount Head in contrast to the stated figure of 2100 feet. Cundill (Personal communication) mentioned that the latter figure was derived by assuming an arbitrary value for repetition on the fourth fault. Faunal evidence (Fig. 1) suggests that the figure is closer to 2300 feet.

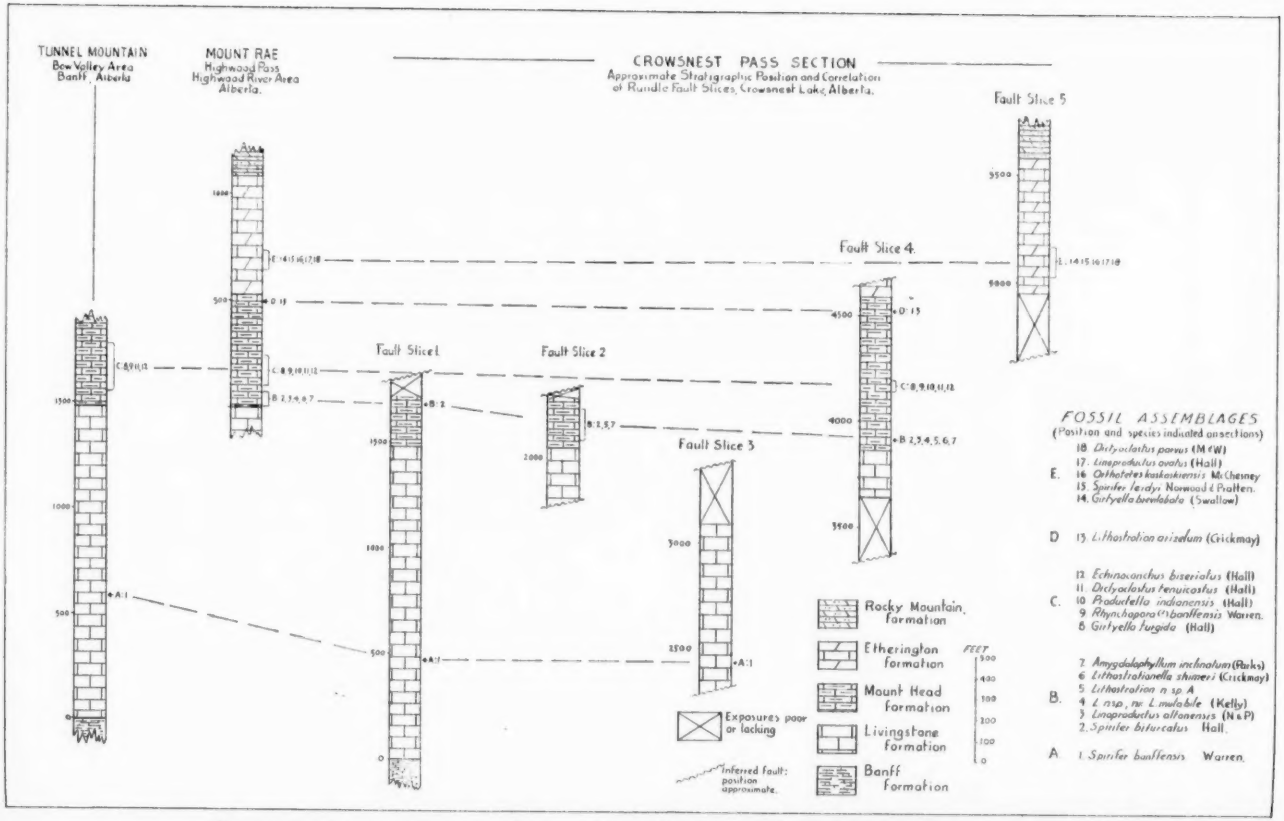

FIGURE 1.—CORRELATION OF THE RUNDLE GROUP (MISSISSIPPIAN) OF CROWSNEST PASS, ALBERTA

Alberta, has guided the writer through most phases of this study.

Figure 1 shows the stratigraphic correlation of the fault slices diagnosed for the Rundle limestone of Crowsnest Lake with two well-known sections in Alberta—Mount Rae (Storm Creek), about 65 miles north of the Pass, and Tunnel Mountain, 45 miles farther northwest. Footages for the last section are those of Beales (1950); those of Mount Rae are the writer's. Portions of sections not pertinent to this discussion are omitted; their deletion is indicated by jagged lines on columnar sections in the figure.

Lithologic divisions and footages of the Crowsnest Pass Rundle (Fig. 1) are those of Cundill (1955). The base of the Mount Head formation in this paper has been raised 200 feet above that of Cundill so that the lithologies conform more closely with the formation at Tunnel Mountain and Mount Rae. Cundill's "Tunnel Mountain formation" is here called the Etherington formation (*see* Norris, 1957; Bostock, Mulligan, and Douglas, 1957) to conform with more recent nomenclature.

Five diagnostic fossil assemblages are recognized in sections portrayed on Figure 1 and are designated as assemblages A to E, respectively. *Spirifer banffensis* Warren is the only fossil present in assemblage A. This easily recognizable species occurs 585 feet above the base of the Livingstone on Tunnel Mountain, suggesting a middle Livingstone correlation for assemblage A in fault slices 1 and 3. Species of assemblage B, geographically widespread in the Canadian Rockies, are characteristic of lower Mount Head strata. Cundill's (1955) lithologic evidence has been used in determining the fault position at the top of fault slice 1, for the stratigraphic interval between assemblage B in this slice and in superjacent slice 2 could represent the fossil assemblage range rather than repetition by faulting. Assemblage C is characteristic of the lower part of middle Mount Head although *Echinoconchus biseriatus* (Hall) and *Dictyoclostus tenuicostus* (Hall) are known to range some distance higher. Assemblage D consists of *Lithostrotion arizelum* (Crickmay). The holotype of this species is from basal Mount Head strata at Lake Minnewanka (Crickmay, 1955). Specimens almost identical with the type are abundant in uppermost Mount Head at Mount Rae. The writer considers that these stratigraphically higher specimens are either homeomorphs developing out of *L. whitneyi* Meek of middle Mount Head, or an expression of a reintroduced zonule useful for local mapping. The stratigraphic position of the Crowsnest Pass *L. arizelum* with respect to assemblage C suggests that the containing strata probably correlate with uppermost rather than lowermost Mount Head. An interval of about 500 feet separates assemblages D and E, while in other nearby sections this interval is 140–200 feet. Thus the enlarged interval suggests repetition by faulting. No diagnostic fossils occur above assemblage E, but the 400-foot section between E and the base of the Rocky Mountain formation is similar to that of normal sections and suggests that faulting is absent.

FIGURE 1.—CORRELATION OF THE RUNDLE GROUP (MISSISSIPPIAN) OF CROWSNEST PASS, ALBERTA

REFERENCES CITED

Beales, F. W., 1950, The Late Palaeozoic formations of southwestern Alberta: Geol. Survey Canada Paper 50-27, 72 p.

Bostock, H. S., Mulligan, R., and Douglas, R. J. W., 1957, The Cordilleran region: p. 283–392, Pls. 30–36, Figs. 61–78; *in* Geology and economic minerals of Canada: Geol. Survey Canada, Econ. Geology, ser. 1, 4th ed., 517 p.

Crickmay, C. H., 1955, The Minnewanka section of the Mississippian: published by the author, Imperial Oil Co., Calgary, Alberta, 15 p. 2 pls., 3 charts

Cundill, J. R., 1955, Notes on faulted Mississippian section at Crowsnest Pass: Alberta Soc. Petroleum Geologists Jour., v. 3, no. 8, p. 138–139

Dawson, G. M., 1886, Preliminary report on the physical and geological features of that portion of the Rocky Mountains between latitudes 49° and 51° 30′: Geol. Nat. History Survey Canada, pt. B, Ann. Rept. 1885, p. 1B-169B

Douglas, R. J. W., 1953, Carboniferous stratigraphy in the southern Foothills of Alberta: Alberta Soc. Petroleum Geologists Third Ann. Field Conf. and Symp., p. 68–88, Figs. 1–9, 9A

McKay, B. R., 1932, The Mesozoic-Palaeozoic contact and associated sediments, Crowsnest district, Alberta and British Columbia: Geol. Survey Canada Summ. Rept. 1931, pt. B, p. 1B–25B, Figs. 1–2

Norris, D. K., 1957, The Rocky Mountain succession at Beehive Pass, Alberta: Alberta Soc. Petroleum Geologists Jour., v. 5, no. 10, p. 248–254, Figs. 1–2

Warren, P. S., 1927, Banff area, Alberta: Geol. Survey Canada Mem. 153, 94 p., 7 pls.

——1928, The Palaeozoics of the Crowsnest Pass, Alberta: Roy. Soc. Canada Trans., v. 22, sec. 4, p. 109–119, 1 Pl.

——1933, Geological section in Crowsnest Pass, Rocky Mountains, Canada: Roy. Canadian Inst. Trans., v. 19, pt. 2, p. 145–160

DEPT. GEOLOGY, UNIVERSITY OF ALBERTA, EDMONTON, ALBERTA, CANADA

MANUSCRIPT RECEIVED BY THE SECRETARY OF THE SOCIETY, MAY 13, 1958

BULLETIN OF THE GEOLOGICAL SOCIETY OF AMERICA
VOL. 70, PP. 111-114 JANUARY 1959

AGE OF THE SAMARSKITE OF KISHENGARH, RAJASTHAN, INDIA

By U. Aswathanarayana

There are three orogenic belts in Rajasthan (also known as Rajputana), India—the Gneissic complex, the Aravalli orogenic belt, and the Delhi orogenic belt. "Each of the three orogenic cycles of Rajputana ends with a display of pegmatites, and, since the younger pegmatites also occur in the older rocks, it is not always easy to assign its proper age to any particular occurrence" (Holmes *et al.*, 1949, p. 291). Apparently there are marked differences in the characteristics of pre-Delhi and post-Delhi pegmatites. The former are medium-grained, foliated, and disturbed by later movements; they contain few, if any, radioactive minerals. The post-Delhi pegmatites are coarse-grained, massive, and unfoliated and have yielded radioactive minerals. Holmes *et al.* (1949, p. 293, 296) determined the ages of uraninite from Bisundni (735 ± 5 m.y.) and monazite from Soniana (700–865 m.y.) in Rajasthan, both of which belong to the post-Delhi group.

The present investigations extend the earlier work reported by the author (1956) and aim to date the samarskite and feldspar from the pegmatite of Bajrang mine located 13 miles east of Kishengarh town along the Kishengarh-Jaipur road (75° 2′; 26° 36′). This pegmatite is coarse-grained, massive, and contains radioactive minerals and is considered post-Delhi. It strikes N. 70° W. and dips 70° N. It consists of quartz, pink feldspar, usually microcline, muscovite, beryl, samarskite, and monazite. The feldspar does not occur in conspicuously large crystals. There is no evidence of segregation of minerals in any particular zone.

Spectrochemical and X-ray analyses have been made to supplement megascopic identification of the radioactive mineral (samarskite).

The following are the spectrochemical data in terms of the elements and their concentration in ppm.:

Ba—145; Ce—4250; Co—240; Cr—29; Cu—40; La—400; Mn—630; Nd—2000; Pb—2000; Sc—215; Th—18500; Zr—2650; Sr—320; V—121.

Y and Yb are present as minor elements. The spectrochemical analysis was not conclusive. X-ray-diffraction analysis using goniometric set-up clearly indicated that the mineral is noncrystalline and metamict. This observation coupled with the data on the *d* spacing of the X-ray powder pattern suggests that the mineral is samarskite.

Elaborate precautions were taken to avoid contamination in the process of powdering. In the case of feldspar, the diamond mortar and pestle, hammer, chisel, and stainless-steel sieve were first cleaned with triple-distilled water, immersed in nitric acid, rinsed with quadruple-distilled water, and tested for the absence of acidity. The crushing is done in a dust-free room and on a table top vacuum-cleaned and covered with clean paper.

The core of the mineral is separated from the rest, untouched by hand, crushed and sieved with a 60-mesh sieve. The minus 60 mesh powder is used in the investigation.

Similar precautions were taken for powdering samarskite. The precautions described by Tilton *et al.* (1955) to avoid contamination from reagents, apparatus, and laboratory air have been scrupulously followed. Whenever possible, lead-free teflon beakers and hoods have been used in preference to pyrex glassware, and it is hoped that this step contributes to the accuracy of the data. The nature of the laboratory studies undertaken are given in the following schematic arrangement:

Feldspar	Unwashed—Dissolution	Isotopic composition	Two aliquots from the same solution
		Total lead concentration	
	Washed—Dissolution	Isotopic composition	
Samarskite	Dissolution	U concentration	Two aliquots from the same solution
		Pb concentration	
	Dissolution	Pb isotopic composition	

The concentrations of uranium and lead in samarskite and the concentration of lead in the feldspar were determined by using isotope-dilution techniques (Tilton *et al.*, 1955). Because of the large quantities of lead in samarskite, about a milligram of the sample only was used for the analysis.

The mass-spectrometric procedures employed by Tilton *et al.* (1955) for the isotopic analysis of uranium and lead have been utilized in the present investigation too. The isotopic composition of lead was computed from about 40 sets of peaks in each case. The concentrations of lead and uranium were calculated from about 25 sets of peaks. The limits for the acceptable data were the following: (1) 3×10^{-11} amps. in ion beam for more than 2 hours, with less than about 0.5 per cent of intensity change per minute, and (2) the deflection on the data chart above 50 per cent of full scale (Chow and Patterson, unpublished). The probable absolute accuracy is within $\sim \pm 0.5\%$ for Pb^{206}/Pb^{204} ratio, $\sim \pm 0.2\%$ for Pb^{206}/Pb^{207} ratio, and $\sim \pm 0.3\%$ for Pb^{206}/Pb^{208} ratio.

TABLE 1.—SAMARSKITE—LEAD AND URANIUM

Isotopic composition of toal lead	Concentration of Pb^{206}	Concentration of total uranium
$Pb^{206}/Pb^{204} = 5942$	9.694 μg per 1.2 mg of sample	119.2 μg per 1.2 mg of sample
$Pb^{206}/Pb^{207} = 16.28$		
$Pb^{206}/Pb^{208} = 22.65$		

The atomic percentages of Pb^{206}, Pb^{207}, Pb^{208}, and Pb^{204} were computed from the ratios in Table 1 and corrected for nonradiogenic Pb^{206} and Pb^{207}. The nonradiogenic lead ratios in the unwashed feldspar lead (Table 2) ($Pb^{206}/Pb^{204} = 16.47$; $Pb^{207}/Pb^{204} = 15.58$) were used in the calculations. The isotopic composition of nonradiogenic lead is, however, not critical as the Pb^{204} atomic per cent is extremely low. The corrected atomic per cents were then converted into weights using the Pb^{206} content of the sample, as estimated by the use of isotope-dilution technique.

Ages have been computed from the standard equations (Faul, 1954, p. 282, 294), and the following constants have been used in the calculations:

$\lambda 238 = 0.1537 \times 10^{-9}\ Yr^{-1}$;
$\lambda 235 = 0.972 \times 10^{-9}\ Yr^{-1}$;
$K = 137.8$

The age spread is given below:

Pb^{207}/Pb^{206} age = 579 m.y.
Pb^{206}/U^{238} age = 587 m.y.
Pb^{207}/U^{235} age = 578 m.y.

The data in Table 2 can be used to calculate the hypothetical time at which the lead was isolated from its uranium and thorium environment and was introduced into the feldspar lattice. Assuming that the lead in the feldspar had a normal evolutionary history, one can either calculate the time required to go from a normal lead today back into time into the feldspar lead or the time required to go from the primordial earth lead to the feldspar lead. In the first calculation, two expressions from Collins *et al.* (1953) were used to obtain two ages. The values for constants a (= 18.69) and b (= 38.82) in the above calculations were provided by T. J. Chow (unpublished). In the second calculation, the expression and constants of Patterson (1956, p. 231, 235) were used.

TABLE 2.—ISOTOPIC COMPOSITION (ATOMIC RATIOS) OF FELDSPAR LEAD

Sample	Pb^{206}/Pb^{204}	Pb^{206}/Pb^{207}	Pb^{206}/Pb^{208}	Total lead conc. in ppm.
Washed feldspar	16.58	1.055	0.4267	N.D.
Unwashed feldspar	16.47	1.057	0.4285	68.3

The calculated ages are as follows:

$$t\frac{206}{204} = 1200 \text{ m.y.}; t\frac{208}{204} = 200 \text{ m.y.}; t\frac{207}{204}, \frac{206}{204} = 1400 \text{ m.y.}$$

Samarskite has given an unusually closely spaced age spread, and hence an age of 580 ± 20 m.y. can be given to it with confidence. It is believed that the errors in chemical determinations define the errors in the ages. Eckelmann and Kulp (1957, p. 1121) listed lead isotopic data on five samarskites. The low abundance of Pb^{204} in the present sample is of interest as it is among the lowest concentrations reported, if not the lowest.

The gross discrepancy among the feldspar lead ages and the samarskite age can be best explained in the following way: The lead contained in the feldspar is abnormal in that its isotopic composition does not correspond to that of ore lead of the same age. The abnormality consists in its having marked deficiency in Pb^{206} and marked excess of Pb^{208}.

The similarity in the isotopic composition of lead obtained from the acid-washed and

unwashed feldspars indicates that neither leaching subsequent to the formation of the feldspar nor the presence of trace quantities of galena could have modified the isotopic composition of feldspar lead. The unwashed feldspar is inactive when radiometrically assayed, but, considering the statistical fluctuations in the background, it is computed that the sample could (but need not necessarily) contain a maximum of 1 ppm of U or 3 ppm of Th. Thus, even if it is assumed that the sample is radioactive and the activity is due to thorium, the concentration of thorium is still about 15 times less than that required to account for the excess of Pb^{208}.

Data on the isotopic composition of lead isolated from three feldspars, drawn from three distinct environments, are available. Tilton *et al.* (1955) reported that, although the feldspar component of the granite they analyzed has an abnormal excess of radiogenic Pb^{206} and Pb^{208}, the feldspar in the pegmatite which intruded the granite has an isotopic composition which corresponds to that of "normal" ore lead of the same age. Patterson (unpublished) found "normal" lead in the Southern California batholith granite of Cretaceous age. The lead in the feldspar under study, with its deficiency of Pb^{206} and excess of Pb^{208}, apparently constitutes a new and distinct type.

The age data, given earlier, permit the following explanation: Both samarskite and feldspar crystallized 580 m.y. ago. The feldspar, however, drew into its lattice lead evolved in a region which, for long periods in the past, contained abnormally high concentrations of thorium and low concentration of uranium relative to lead. It remained "frozen" with this abnormal lead as there was practically no subsequent contribution of lead from the negligible amounts of U and/or Th contained in the feldspar.

The age of the samarskite indicates that the Kishengarh pegmatite is very young Precambrian or earliest Paleozoic; it is younger than the pegmatites of Bisundni and Ajmer-Merwara dated by Holmes *et al.* (1949) and Holmes (1955). This finding is consistent with geological evidence as it is not necessary to suppose that pegmatites intruded at the same time all along the immense synclinorium (Heron, 1953, p. 368).

I am deeply grateful to Dr. Claire Patterson under whose supervision this work was carried out. Dr. T. J. Chow and Judith Kawafuchi have been of immense help to me in my laboratory work. I wish to thank Prof. Harrison S. Brown and Prof. Robert P. Sharp who kindly permitted me to work in the laboratories of the Geological Division of the California Institute of Technology. The financial assistance of the State Department of the United States of America, and the Andhra University, India, which enabled me to work at the California Institute of Technology for a short period, is thankfully acknowledged.

References Cited

Aswathanarayan, U., 1956, Absolute ages of the Archaean orogenic cycles of India: Am. Jour. Sci., v. 254, p. 19–31

Collins, C. B., Russell, R. D., and Farquhar, R. M., 1953, The maximum age of the elements and the age of the earth's crust: Can. Jour. Physics, v. 31, p. 402–418

Eckelmann, W. R. and Kulp, J. L., 1957, Uranium-lead method of age determination, pt. II: Geol. Soc. America Bull., v. 68, p. 1117–1140

Faul, H., 1954, Nuclear geology: New York, John Wiley, p. 1–414

Heron, A. M., 1953, The geology of Central Rajputana: Geological Survey India Mem., v. 79, p. 1–389

Holmes, A., 1955, Dating the Precambrian of Peninsular India and Ceylon: Geol. Assoc. Canada Proc., v. 7, pt. II, p. 81–106

Holmes, A., Smales, A. A., Leland, W. T., and Nier, A. O., 1949, The age of uraninite and monazite from the post-Delhi pegmatites of Rajputana: Geol. Mag., v. 86, p. 288–302

Patterson, C. C., 1956, Age of meteorites and the earth: Geochim. et Cosmochim. Acta, v. 10, p. 230–237

Tilton, G. R., Patterson, C., Brown, H., Inghram, M., Hayden, R., Hess, D., and Larsen, Jr., E., 1955, Isotopic composition and distribution of lead, uranium and thorium in a Precambrian granite: Geol. Soc. America Bull., v. 66, p. 1131–1148

Department of Geology, Andhra University, Waltair, India

Manuscript Received by the Secretary of the Society, August 23, 1957